An investigation of PKA phosphorylation gradients and a mechanism for their enhancement

Shane Edward Tillo

A Dissertation

Presented to the Neuroscience Graduate Program
at the Oregon Health & Science University School of Medicine
in partial fulfillment of
the requirements for the degree of
Doctor of Philosophy

July 18, 2014

Certificate of Approval

This is to certify that the PhD dissertation of

Shane Edward Tillo

has been approved

_____

Mentor: Haining Zhong, PhD

_____

Committee Chair: Craig Jahr, PhD

_____

Member: Wolf Almers, PhD

_____

Member: John Adelman, PhD

_____

Member: John Williams, PhD

_____

Member: Larry Trussell, PhD

Table of Contents

List of Figures

Chapter 1. An introduction to the cAMP dependent protein kinase.

Chapter 2. Imaging PKA phosphorylation gradients using probes optimized for 2photon fluorescence lifetime imaging.

Chapter 3. The role of N-terminal myristoylation in the maintenance of PKA phosphorylation gradients at the plasma membrane.

List of Abbreviations

2p	Two-photon
2pFLIM	Two-photon fluorescence lifetime imaging
A	Acceptor
AMPA	a-amino-3-hyroxy-5-methyl-4-isoxazolepropionic acid receptor
AKAP	A-kinase anchoring protein
AKAR	A-kinase phosphorylation reporter
cAMP	Cyclic AMP
CNB	Cyclic nucleotide binding domain
cp	Circular-permuted
cyt	Cytosolic
D	Donor
dsRed	*discoma* red fluorescent protein
ECFP	Enhanced cyan fluorescent protein
EYFP	Enhanced yellow fluorescent protein
EGFP	Enhanced green fluorescent protein
F	Forskolin
FP	Fluorescent protein
FHA	Forkhead-associated domain
Forsk	Forskolin
FRET	Fluorescence resonance energy transfer
GFP	Green fluorescent protein
GluR1	Glutamate receptor type 1
GPCR	G-protein coupled receptor
HEK	Human embryonic kidney
I	IBMX
IQ	inner-quartile
IBMX	3-methyl-1-methylxanthine
MAP2	Microtubule-associated protein type 2

MAPK	Mitogen-activated kinase
mCerulean	Monomeric cerulean fluorescent protein
mCherry	Monomeric cherry fluorescent protein
mEGFP	Monomeric enhanced green fluorescent protein
MPET	Mean photon emission time
NE	Norepinephrine
NMR	Nuclear magnetic resonance
nmPKA-c	Non-myristoylated protein kinase A catalytic subunit
OA	Okadaic acid
PA-GFP	Photoactivatable green fluorescent protein
PKA	Protein Kinase A
PKA-cat	Protein kinase A catalytic subunit
PKA-reg	Protein Kinase A regulatory subunit
pm	Plasma membrane
RIIα	PKA regulatory subunit type II alpha
RIIβ	PKA regulatory subunit type II beta
sREACh	Silent resonance enhancement acceptor chromophore
TA	Threonine to Alanine point mutation
wt	Wild-type

Acknowledgements

This dissertation could not have been completed without the help from a great many people. First among them are my friends and colleagues in the lab. Dr. Brian Long continues to teach me much about the physics of diffusion and optics, as well the Matlab programming language. His instruction was invaluable to my success as a graduate student. Dr. Dale Fortin supported me in ways too numerous to mention. He is a great friend and I consider him a most important mentor and collaborator. A big thanks to Danielle Robinson for always making lab a fun place to be and teaching me about the art and style of science. Thank you to Maozhen Qin and Guang Yang for providing me with excellent cultured slice throughout my time in the lab. Also a big thanks to Tianyi Mao for the enthusiasm and knowledge she brought everyday to the lab.

Thanks to my advisor Haining Zhong. He has taught me all I know about microscopy and image analysis and put up with my stubbornness. I will miss our time building the lab from scratch and our lively debates about how to approach and do science.

A special thanks to my mentors – Wolf Almers, Phil Stork, Craig Jahr, John Williams, John Adelman and Thom Hughes – for always having my best interests in mind and sharing with me their secrets about life and science.

Finally, thanks to Miss Jeannie Hunnicutt for being my best friend. The work described here would not have been possible without her unique intelligence and positive outlook on life.

To my family, for their love and encouragement.

Abstract

The cAMP dependent protein kinase, or protein kinase A (PKA) is an important and ubiquitous intracellular mediator of information transfer in neurons, where it plays critical roles in neurotransmission, cellular excitability, and synaptic plasticity. All of these processes require high specificity in PKA phosphorylation. An abundance of studies have shown that PKA specificity is mediated by a class of proteins called A-kinase anchoring proteins (AKAPs), which target upstream activators, downstream substrates, and inhibitors of PKA to defined subcellular locations, putatively establishing tight gradients of PKA phosphorylation. However, AKAPs directly anchor only the regulatory subunit of PKA. Once bound by cAMP, conformational changes in the PKA holoenzyme result in the release of catalytic subunit of PKA (PKA-cat) whereupon it is free to diffuse. A cytosolic protein of comparable size to PKA-cat is expected to fully sample synaptic compartments, such as dendritic spines, in tens of milliseconds and exit these compartments within hundreds of milliseconds. Considering that these time scales are significantly shorter than both the enzymatic turnover of PKA-cat and the observed time scales of PKA signaling, such diffusion would be expected to break down the PKA specificity established by AKAPs.

Here, we use a variety of imaging and biochemical techniques in both neurons and model cell lines to investigate gradients of PKA phosphorylation and the mechanisms by which they are enhanced in both resting and stimulated conditions. Collectively, the results paint a picture in which both states of PKA phosphorylation preferentially occur in the plasma membrane compartment of cells. In resting states, PKA phosphorylation is largely confined to the plasma membrane. Similar to resting PKA phosphorylation, exogenous stimulation of the PKA holoenzyme also results in a gradient of PKA phosphorylation emanating from the plasma membrane. Furthermore, we have discovered a role for N-terminal myristoylation of PKA-cat in imparting membrane affinity to the freed PKA-cat thereby limiting its mobility and enhancing its phosphorylation in the plasma membrane Such targeting of PKA-cat is a novel mechanism for maintaining AKAP established PKA signaling gradients. As PKA is one of the many promiscuous, yet specific, diffusible proteins involved in signal transduction, we hope that these results will provide a better template

from which to understand the general principles of specificity in neuronal regulatory signaling.

Chapter 1.

An introduction to the cAMP dependent protein kinase

Dissertation Overview

All cells communicate with their environment and their neighbors by sending and receiving signals. In neurons, the signals are carried by a group of molecules collectively know as neurotransmitters. Neurotransmitters convey information regarding the state of neighboring cells (i.e. voltage potential, pH, health, etc.), and may also carry with them commands, a set of instructions if you will, for which to complete a task. In neurons the number of these tasks is vast, and can include the additional recruitment of receptors, re-uptake of receptors, protein degradation, alteration of receptor or channel kinetics, local translation, and gene transcription, to name a few. It is often the case that a single intracellular effector pathway may be activated by multiple extracellular signals and can result in multiple independent responses (see **Figure 1**). To discriminate amongst these possible outcomes and establish some semblance of signaling specificity, the cell must effectively bias the effector response towards an intended outcome.

The overarching goal of this dissertation is to provide a glimpse into the mechanisms by which neurons bias their intracellular signaling and thus encode the information contained in extracellular signals. The focus is placed on the cAMP dependent protein kinase, or protein kinase A (PKA). More specifically, we investigate the ways in cells can utilize gradients of PKA concentration and PKA phosphorylation to effectively bias PKA activity. PKA is an enzymatic mediator of signal transduction in neurons and exemplifies many of the complexities regarding information transfer discussed above. For instance, despite the convergence of many activators onto the cAMP/PKA pathway, PKA is capable of biasing its phosphorylation profile in a manner dependent upon its upstream activator. The mechanisms for attaining this specificity have been investigated since the early 1980s (Buxton and Brunton, 1983) and are thought to rely upon a concept known as compartmentalization. Compartmentalization endows specificity through the spatiotemporal confinement of activators, effectors, and substrate. Shown in **Figure 1** is an illustration of the many neurotransmitters that utilize PKA as an information carrier and a multitude of possible effector pathways that it must discriminate amongst in order to accurately convey that information.

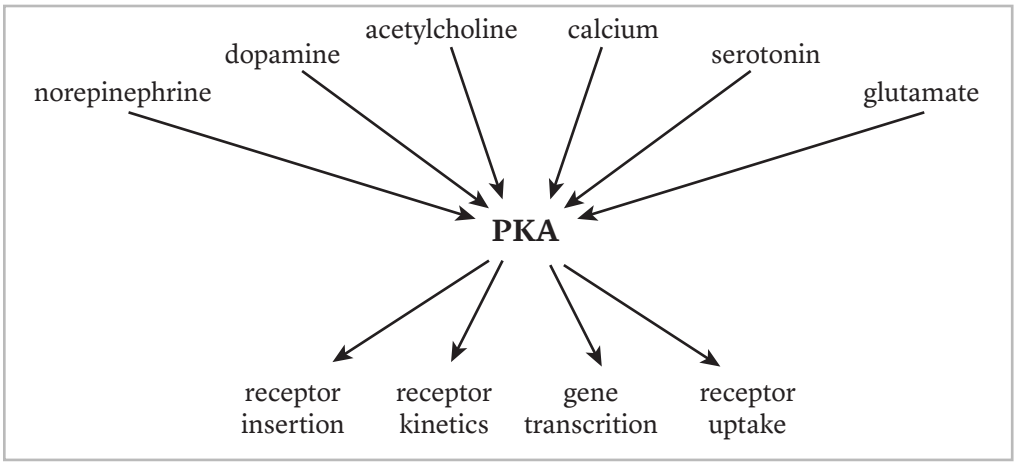

FIGURE 1. CONVERGENCE ONTO THE PKA EFFECTOR PATHWAY.
A wide range of stimuli converge on PKA to regulate diverse cellular function via a wide variety of cellular processes. Note that the figure does not represent the complete pool of PKA activators or targeted processes. (Adapted from the work of Dr. Haining Zhong)

A Rich History

In 1968, DA Walsh in the laboratory of Edwin Krebs at the University of Washington, purified a protein kinase from skeletal muscle who's phosphorylation was completely dependent upon levels of 3',5'-monophosphate, or cyclic adenosine monophosphate (cAMP, see also **Figure 3)** (Walsh et al., 1968) . At the time, it was known that norepinephrine stimulation of adenylyl cyclase, the enzyme that converts ATP into cAMP, activated a *phosphorylase kinase* (Posner et al., 1965). Speculating that they had found the identity of an intermediary in this reaction, they proposed to name the kinase *phosphorylase kinase kinase.* In his 1970 PhD dissertation, Thomas Soderling, also in the laboratory of Edwin Krebs, showed that this same kinase directly acted upon *Glycogen Synthetase* in muscle. This discovery was the first example of enzyme inhibition via phosphorylation (Soderling et al., 1970). Soderling referred to the enzyme as the cAMP dependent protein kinase, or protein kinase A (PKA), names that are used to this day.

The discovery of PKA opened the avenue for the investigation of signaling *cascades* in which one protein kinase activates another, providing cells with a means to greatly amplify signals (Cohen, 2002). Twenty years passed before MAP kinase was discovered providing the second demonstration of a signal transduction cascade. PKA's long history, along with the simplicity of its action, have made it the prototypical protein kinase, and it

remains one of the best understood and most studied (Johnson et al., 2001). Dr. Krebs and Dr. Eddy Fischer received the 1992 Nobel prize in Physiology or Medicine *for their discoveries concerning reversible protein phosphorylation as a biological regulatory mechanism*. Since its initial discovery, PKA has remained at the forefront of efforts aimed at characterizing and discerning the mechanisms by which protein phosphorylation can precisely and efficiently regulate cellular function (see **Figure 2**).

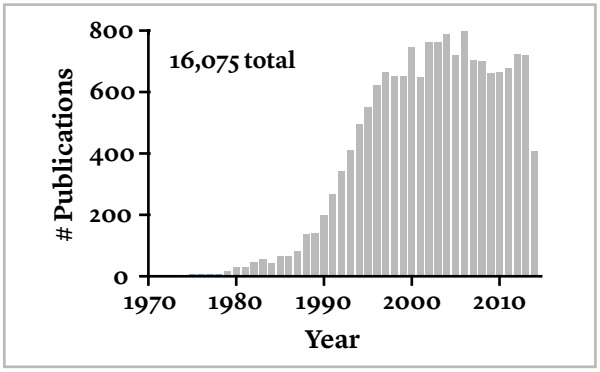

FIGURE 2. PUBLICATIONS MENTIONING CAMP DEPENDENT PROTEIN KINASE OR PKA IN THE TITLE.

Since 1970 there have been 16,075 publications, the number of which rose rapidly in the 1990s.

Diversity and Distribution

PKA is found in a wide variety of animal phyla and all types of mammalian tissues (Kuo and Greengard, 1969; Francis and Corbin, 1994). Moreover, the cyclic nucleotide binding domain (CNB) of the PKA regulatory subunit is a highly conserved structural domain present in all organisms (Johnson et al., 2001). The focus here will be on the PKA subtypes found in the mammalian brain, specifically those found in rodents.

Mammalian PKA is classified on the basis of the regulatory subunit type — type I (RI) and type 2 (RII) — present in the holoenzyme complex (see Figure 3). The regulatory subunits (PKA-reg) are further divided into alpha (α) and beta (β) categories, all of which are products of different genes (Francis and Corbin, 1994). The RII subtypes are highly enriched in the mouse brain and show punctate or non-uniform patterns of subcellular expressions with the relative abundance of alpha and beta subtypes dependent upon the brain region (Brandon et al., 1997). The RI subunits are also expressed abundantly in the brain but show a more ubiquitous and diffuse pattern of subcellular expression. RI subunits are located primarily in the cytosolic fraction of the cell (Brandon et al., 1997), and appear to play a role in compensation for variation in PKA phosphorylation (Amieux and McKnight, 2002). Concomitant with its important role in regulating PKA phosphorylation levels,

knockout of the RI subunits is generally less favorable to mouse viability (Amieux et al., 2002) than knockout of either of the RII subunits (Burton et al., 1997).

The PKA-catalytic subunit (PKA-cat) is categorized into 3 separate isozymes known as Cα, Cβ, and Cγ, all of which can form holoenzyme with either type of PKA-reg. The Cγ form appears to only be expressed in human testes (Foss 1992). The Cα and Cβ isozymes are present in most if not all mammalian tissue, including in neurons (Brandon et al., 1997). Knockout of the Cα subunit in mice results in postnatal lethality (Ska lhegg et al., 2002) whereas knockout of the Cβ subunit only seems to effect basal, or resting levels of PKA phosphorylation (Howe, 2002).

PKA Structure and Function

PKA utilizes an evolutionarily conserved signaling mechanism whereby ligand binding disrupts an established protein-protein interface (Das et al., 2007). In the case of PKA, the ligand is cAMP and the interface disruption occurs between a dimer of PKA regulatory subunits and two PKA catalytic subunits. An illustration depicting the general architecture of an intact PKA holoenzyme is shown in **Figure 3**. The PKA regulatory subunits all share the same general structure, containing two cyclic nucleotide binding domains in series, an inhibitory sequence, a relatively long disordered region, and a dimerization/docking domain (Taylor et al., 2005). The subtle differences in structure, however, lead to different properties and the PKA-reg variants are functionally non-redundant (Taylor et al., 2013). In contrast, the catalytic subunits are very similar and contain little to no functional differences (Uhler et al., 1986).

Though many have worked to elucidate the structure function relationships of PKA, the main body of work reviewed here was done in the laboratory of Dr. Susan Taylor at the University of California, San Diego. Susan's laboratory has provided numerous X-ray crystallography and NMR based structures of free catalytic subunits, free regulatory subunits, and intact holoenzyme structures. Her work has been invaluable to the understanding of the enzymatic function of this ubiquitous kinase.

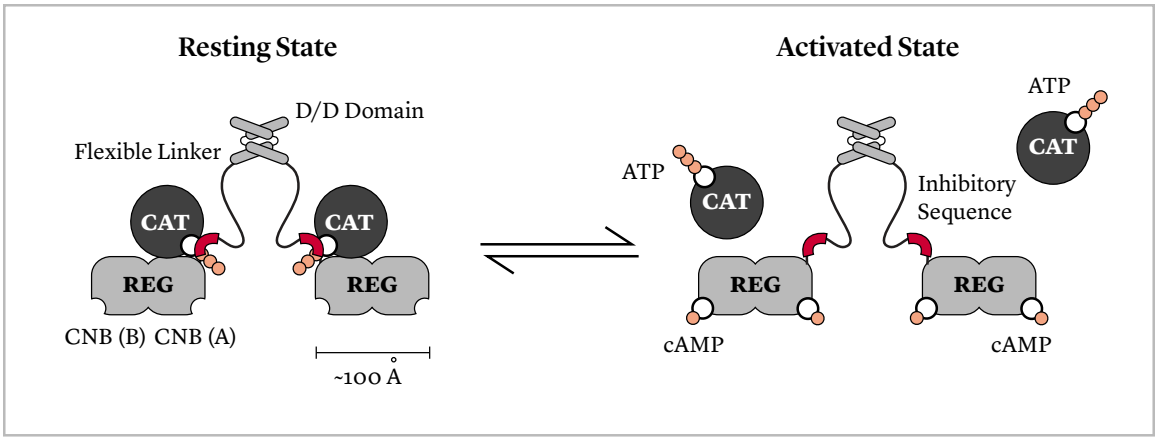

FIGURE 3. CONFORMATIONAL CHANGES IN THE PKA HOLOENZYME INDUCED BY CAMP.
Left, illustration of the PKA holoenzyme in the resting, or non-cAMP bound state. The PKA regulatory subunit (REG, gray) consists of a dimer of subunits. The interface between PKA-reg dimers occurs through the formation a four-helix bundle in the dimerization /docking (DD) domain. The DD domain is connected to the two cyclic nucleotide binding domains (CNB (A) and (B)) via a long disordered linker (Flexible linker, black line). The CNB domain of the regulatory subunit binds to the PKA catalytic subunit (CAT, dark gray) near the active site of the enzyme through a consensus inhibitory sequence (Red noodle) immobilizing and diminishing its ability to phosphorylate nearby substrate, despite it being primed with ATP. Right, illustration of PKA in the activated, cAMP bound state. In conditions of high cAMP, the CNB domains become occupied with cAMP, inducing a conformational change and release of the catalytic subunits. (Illustrations were adapted from the work of Smith & Gonen and Zhang & Taylor).

Regulatory Subunit (PKA-reg)

The function of the CNB domain of PKA-reg is to bind both cAMP and provide docking for the catalytic subunit, thus enabling PKA to mediate biological responses. In the resting holoenzyme, the CNB B site is in an open conformation and is the first to bind cAMP, resulting in a conformational change that opens the A site (Herberg et al., 1996; Vigil et al., 2006). Once bound, the local structure of the CNB prevents degradation of cAMP by phosphodiesterases. Binding of the final 2 cAMP molecules to the CNB A sites in the holoenzyme complex disrupts the ability of the docking regions in the CNB to bind PKA-cat (Kim et al., 2005), and the two catalytic subunits are subsequently released. Binding of cAMP decreases the affinity of PKA-reg for PKA-cat on the order of 10,000 – 100,000 fold (Francis and Corbin, 1994).

Measurements of the activation constants for PKA-reg vary somewhat in the literature but range from ~ 100 nM cAMP for the RIα (Huang and Taylor, 1998; Vigil et al., 2006) and RIIα (Herberg et al., 1996) subunits to ~ 30 nM for the RIβ (Cadd et al., 1990) and ~ 600 nM cAMP for the RIIβ subunit (Zhang et al., 2012). The near order of magnitude higher activation constant for the RIIβ likely plays an important functional role as auto-phosphorylation by PKA-cat significantly reduces the likelihood of holoenzyme formation providing an important site on PKA-reg to regulate overall PKA activity levels (Zhang et al., 2012).

The inhibitory sequence (IS) is found directly upstream of the CNB domain and functions to bind near the active site cleft of the PKA catalytic subunit. A very similar sequence is found on the PKA inhibitor peptide (PKI), and PKI provides an efficient and highly specific way to inhibit PKA phosphorylation in the presence of high cAMP concentrations. The IS region works in concert with 3 -4 other regions on the CNB domain to render the catalytic subunit immobile and relatively inactive.

In the PKA holoenzyme, the dimerization/docking (DD) domain is composed of a four helix bundle, with each PKA-reg contributing 2 helices. The formation of the four helix bundle maintains PKA-reg as a stable homodimer. In addition to stable dimer formation, the four helix bundle in the PKA holoenzyme forms a hydrophobic binding groove to which a single A-kinase anchoring proteins can dock (Newlon et al., 2001). The relevance of AKAP binding to the regulatory subunits will be discussed in the *A-kinase anchoring proteins* section.

In between the DD domain and the CNB domain resides a long (~ 100 amino acid) flexible linker. The linker provides conformational flexibility and also contains multiple phosphorylation sites for increased regulation of the holoenzyme structure (Johnson et al., 2001). Due to its inherent disorder, crystal structure containing this region have remained elusive. However, nuclear magnetic resonance (NMR) studies have elucidated the conformational flexibility of the linker, and have indicated important differences between the RIIα and RIIβ holoenzymes. Both structures are found in an extended conformations in the absence of bound catalytic subunit, giving the PKA-reg protomer a PKA-cat *buffer* radius of ~ 300 angstroms (Newlon et al., 2001; Smith et al., 2013). The difference reveals

itself upon docking of the catalytic subunits. The RIIα subunit remains in an extended conformation giving it a wider radius for which to bind free PKA-cat and to potentially phosphorylate local substrate in a cAMP independent manner (Smith et al., 2013). In contrast, upon PKA-cat binding the RIIβ subunit adopts a globular conformation potentially limiting such cAMP independent phosphorylation (Vigil et al., 2006a). Smith and Gonen have recently confirmed the extended conformation of the RIIα holoenzyme using low resolution electron micrograph structures of the intact RIIα PKA holoenzyme (Smith et al., 2013). The conformational differences have implications regarding both activated and stimulated PKA phosphorylation that will be discussed further in Chapter 2 and the Discussion sections.

Catalytic Subunit (PKA-cat)

The PKA catalytic subunit's function is to transfer the gamma-phosphate of ATP onto substrate. PKA-cat is a general serine/threonine phosphate meaning that the enzyme targets only these residues on substrate. The affinity of the catalytic subunit for ATP is ~ 65 μM (Steinberg et al., 1993), indicating that the mM cellular concentration of ATP is more than enough to populate the vast majority of PKA-cat. Once released from the regulatory subunit and bound by ATP, the catalytic subunit is in position to dock with substrate, a situation that is mediated by a variety of residues in the enzyme (Johnson et al., 2001). Docking with the substrate helps to optimally position the active cleft of the enzyme for efficient phospho-transfer of the gamma phosphate of ATP. The phosphoryl transfer event is fast and occurs at the rate of ~ 500 per second (Adams and Taylor, 1992). The enzymatic turnover rate, however, is considerably slower and on the order of ~ 20 per second reflecting the rate limiting step of ADP dissociation from the active cleft of the enzyme (Zhou and Adams, 1997). An illustration representing some important kinetic parameters of the catalytic subunit is shown in **Figure 4.**

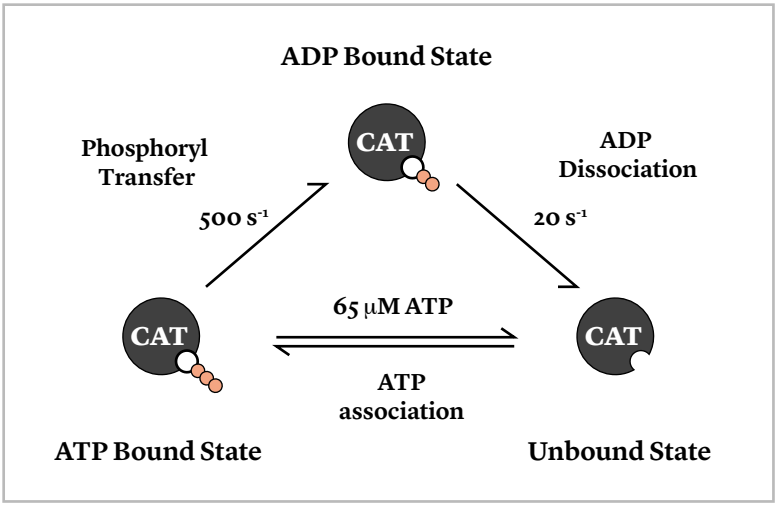

FIGURE 4. PKA-CAT ENZYMATIC TURNOVER.
The turnover rate of the PKA catalytic subunit is reflected by the rate limiting step of ADP dissociation (~20 molecules per second). Note also that in a recent crystal structure for the RIIβ regulatory subunit (Zhang et, al., 2012), PKA-cat is expected to depart the holoenzyme complex in an ADP bound state.

N-terminal myristoylation of the PKA catalytic subunit

The PKA catalytic subunit undergoes a variety of co and post-translational modifications important for its proper function (Cheng et al., 1998, Iyer 2005). Of particular relevance here, is the co-translational addition of a myristic-acid moiety to the N-terminal glycine residue of PKA-cat (Carr et al., 1982). N-terminal myristoylation is carried out by the enzyme N-myristoyl transferase (NMT) (Towler et al., 1988; Boutin, 1997) and leads to the addition of a 14-carbon chain to the N-terminus of PKA-cat. Unlike other cellular constituents where myristoylation clearly results in an increase in membrane affinity, such as the α subunit of G-proteins (Mumby et al., 1990) and the cGMP-dependent protein kinase (Vaandrager et al., 1996; Vaandrager et al., 1998), the physiological consequence of this modification on PKA-cat remains murky.

Structural studies of the free catalytic subunit show the myristoyl moiety tucked into a hydrophobic pocket of the enzyme (Zheng et al., 1993; Bastidas et al., 2012), the immediate functional consequence of which is to convey thermal and structural stability to the enzyme (Yonemoto et al., 1993). This observation has limited the investigation into thephysiological role of myristoylation for the activated catalytic subunit. However, when

separated from the main body of the PKA-cat the myristoylated N-terminal 14 amino acids of PKA-cat exhibits membrane affinity (Struppe et al., 1998), and the myristoylation moiety of PKA-cat has been shown to extend itself into solution and associate with lipid bicells when in conjunction with type RII regulatory subunits (Gangal et al., 1999). These results have hinted at the possibility that myristoylation may impart membrane affinity to the freed PKA-cat, but this phenomenon has yet to demonstrated in living cells.

3'-5'-monophosphate – cyclic AMP

Any discussion of PKA would be incomplete without a discussion of its activator, cyclic adenosine monophosphate, or cAMP. The action of cAMP was discovered by Earl Sutherland shortly before the discovery of its downstream effector, PKA. Like Krebs and Fisher after him, Sutherland was awarded a Nobel Prize *for his discoveries concerning the mechanisms of the action of hormones.*

The levels of cellular cAMP are controlled by the activities of two opposing enzymatic pathways (see **Figure 5**). cAMP is produced in a magnesium dependent manner by the membrane resident adenylyl cyclase, which converts cellular ATP into pyrophosphate and cAMP. Nine isoforms (AC1 - AC9) of adenylyl cyclase exist, with types AC1 and AC2 having prominent roles in neuronal signaling (Hanoune and Defer 2001). The general neurotransmitter mode of activation of adenylyl cyclase is initiated through the agonism of the Gαs subunit and inhibited by agonism of the Gαi subunits. Intracellular calcium can also serve to activate adenylyl cyclase affording the cell an additional mechanism to control the phosphorylation of these enzymes (Cooper et al., 1995). Downstream of the G-protein coupled receptors and calcium signaling are are enzymes known as phosphodiesterases, which convert cAMP into AMP via cleavage of the phosphodiester bond present in the cyclic ring of cAMP.

Throughout this manuscript we control the levels of cellular cAMP using the exogenous application of 3 drugs. To elevate cAMP to its maximal levels we use the cell permeant adenylyl cyclase activator Forskolin in combination with the general phosphodiesterase inhibitor IBMX (Forsk + IBMX or F + I). Norepinephrine (NE) is used as a more endogenous activator of cAMP and works through the binding of endogenous

noradrenergic Gαs coupled receptors in both rat CA1 hippocampal neurons and HEK293 cells.

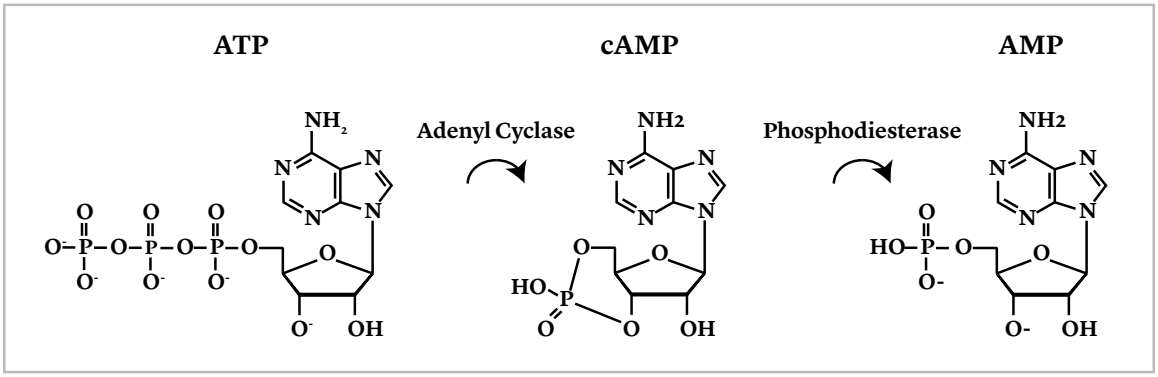

FIGURE 5. THE LIFECYCLE OF CAMP.
The membrane bound enzyme, adenylyl cyclase converts cellular ATP into cAMP and pyrophosphate (not shown). cAMP is negatively regulated by enzymes collectively known as phosphodiesterases which cleave the phosphodiester bond of cAMP producing AMP.

cAMP concentration gradients

It is important to note that because cAMP activates PKA, any specificity in PKA signaling must first arise from the confinement of cAMP in space and time. Measurements of cAMP diffusion constants in cells range from 270 - 780 $\mu m^2 s^{-1}$ (Chen 1999; Bacskai et al., 1993) indicating that cAMP behaves much like an electrolyte in the cytosol. These observations point to the possibility for long-range cAMP action, theoretically in the range of up to ~ 220 μm (Kasai and Petersen, 1994). However, despite the potential for long-range cAMP action, observations in many cell types have indicated the presence of gradients or distinct spatial compartments of cAMP (Hempel et al., 1996; Rich et al., 2000; Rich et al., 2001; Zaccolo and Pozzan 2002; Wong and Scott, 2004; DiPilato et al., 2004; Zaccolo et al., 2006).

In this context, what we mean by a compartment is micron, or sub-micron cellular region in which cAMP concentration is maintained as a gradient, either through regulation of its production, diffusion, or degradation (Neves and Iyengar 2009). The relative rates of these processes will directly influence the steepness and persistence of this gradient over time, and thus the volume of the compartment over time. In neurons, and many other cells, these gradients appear to be largely controlled through the local presence of

phosphodiesterases, which limit the spread of cAMP and confine it near the source of activation (Castro et al., 2010; Gervasi et al., 2010; Oliveira et al., 2010). Other observations indicate that restricted cAMP diffusion, possibly through physical barriers, plays a role in maintaining a cAMP concentration gradient over time (Rich et al,. 2001). Whatever the case, we observe cAMP gradients and compartments and question whether or not these gradients propagate to PKA signaling.

Confining the PKA holoenzyme in space – A-kinase anchoring proteins

In 1984 Suzanne Lohmann found that the microtubule associated protein-2 (MAP2) co-purified with type RII regulatory subunits from calf brain extract (Lohmann et al., 1984). She correctly speculated that such binding could specify the location of the PKA holoenzyme, thereby establishing distinct compartments of PKA in resting conditions. Since their initial discovery, well over 50 of these A-kinase anchoring proteins (AKAPs) have been discovered (Wong and Scott, 2004). Though AKAPs have been shown to bind all subtypes of PKA-reg, in general the RI type subunits bind to AKAPs at ~ 500 fold lower affinity than the RII type subunits (Burton et al., 1997), again pointing to the important role of the RII type subunits in establishing spatially distinct signaling compartments. The relatively low affinity of AKAPs for RI PKA-reg and the relatively low numbers of AKAPs shown to bind RI PKA-reg point to RI PKA-reg existing in a significant part as a soluble holoenzyme, consistent with observations showing its diffuse cytosolic distribution.

Binding of PKA-reg to AKAPs is mediated by the aforementioned dimerization/docking (DD) domain of the PKA holoenzyme and an amphipathic helix of the AKAP (Kinderman et al., 2006; Gold et al., 2006). Type II PKA holoenzymes bind to AKAPs at a high affinity of 1 – 5 nM (Kinderman et al., 2006). AKAPs localize PKA to discrete subcellular compartments through their binding to effector proteins such as MAGUKs (Colledge et al., 2000), to the post synaptic density (Carr et al., 1992; Choi et al., 2002), the mitochondrial membrane (Chen et al., 1997), ion channels (Goldsmith and Abrams, 1992; Chen et al., 2006), membrane receptors (Dell'Acqua et al., 2006; Davare et al., 2001; Joiner et al., 2010), cytoskeletal elements (Lohmann et al., 1984; Glantz et al., 1993; Zhong et al., 2009), to the plasma membrane (Trotter et al., 1999; Burgers et al., 2012), in the nucleus

(Sastri et al., 2005), and many more effectors. The functional relevance of AKAP anchoring in neurons, was first shown by Christian Rosenmund in the laboratory of Gary Westbrook who demonstrated the necessity of AKAPs in the PKA dependent modulation of AMPA and Kainate receptor conductances in CA1 hippocampal neurons (Rosenmund et al., 1994).

In addition to binding the PKA regulatory subunit, AKAPs also function to bind receptors that activate the synthesis of cAMP, enzymes that degrade cAMP, PKA substrates, and counterbalancing PKA phosphatases. In doing so, AKAPs can create distinct PKA signaling hubs that enable the efficient activation of PKA by localizing PKA near the source of cAMP production (Kim et al., 2011) and potentially limit PKA interaction with downstream targets. A general illustration of an AKAP mediated PKA signaling complex is shown below in **Figure 6**.

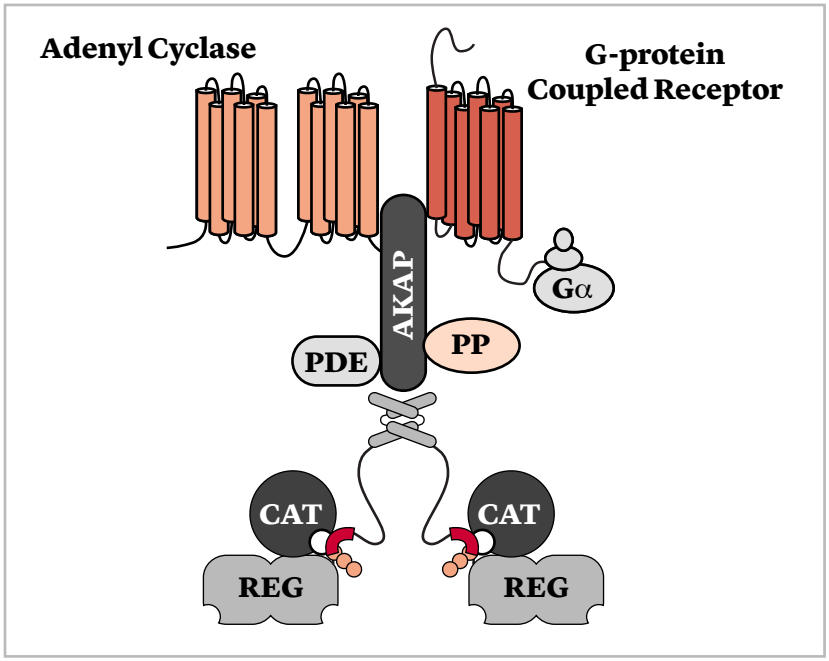

FIGURE 6. AKAP ESTABLISHED PKA SIGNALING HUBS.
Illustration of a generalized PKA signaling hub mediated by the binding of AKAPs to the PKA holoenzyme, PKA activators (G-protein Coupled Receptor & Adenylyl Cyclase), inhibitors of cAMP production (phosphodiesterase (PDE)) and inhibitors of PKA phosphorylation (protein phosphatase (PP)). AKAPs also function to bind PKA substrate (not shown) providing a spatially isolated compartment for PKA phosphorylation.

Considerations for specificity - mobility of PKA-cat

In 3-dimensional cellular space, the activated PKA catalytic subunit is expected to rapidly sample a region significantly greater than the volume of an AKAP established PKA signaling hub (radius ~ 50 nm). This conclusion is based upon assigning PKA-cat with a diffusion constant measured for soluble green fluorescent protein (GFP) in neurons (~35 $\mu m^2 s^{-1}$) (Bloodgood and Sabatini, 2005), followed by correction for the size, or drag, of PKA-cat. The molecular weight of PKA-cat t is ~ 38 kD, or 1.4 times that of GFP (~27 kD). Given the Stokes – Einstein relationship (Einstein 1905) regarding the influence of drag on the diffusion coefficient of a molecule, we conclude that a freely diffusing catalytic subunit should have a diffusion coefficient of ~1.1 times less than GFP, or ~30 $\mu m^2 s^{-1}$ (see **Equation 1** below).

(1) Diffusion coeffient (D) = constant / drag (ζ)
where...

(2) $\zeta = 6\pi nr$, where n = visocity, r = radius
then...

(3) D = constant / $6\pi nr$
if...

(4) Volume sphere = $4/3\pi r^3$
and...

(5) PKAc volume ~ 1.4 * GFP volume
then...

(6) GFP(r) / PKA-cat(r) = $\sqrt[3]{1.4} = 1.1$

EQUATION 1. EXPECTED DIFFUSION COEFFICIENT FOR PKA-CAT.
The diffusion coefficient of a molecule in solution is directly proportional to its drag, which is directly proportional to its molecular radius. Assuming that GFP and PKA-cat adopt roughly spherical conformations then the radius of PKA-cat is ~ 1.1 fold that of GFP. Given GFP's measured diffusion coefficient in neurons (~35 $\mu m^2 s^{-1}$) we expect PKA-cat to have a diffusion coefficient of ~ 30 $\mu m^2 s^{-1}$.

At a diffusion rate of 30 $\mu m^2 s^{-1}$, free PKA-cat would be expected to sample the molecular vicinity of the AKAP established compartment in ~ 10 μs, sample an entire dendritic spine in 1.5 ms, and equilibrate a typical dendritic volume in ~ 20 ms (see **Figure 7** below). As these timescales are much shorter than the known duration of signaling through PKA (Gervasi et al., 2007), it creates the potential for PKA-cat diffusion to break down the compartment established by AKAPs. Furthermore, when we consider the enzymatic turnover rate of PKA-cat (~ 20 per second), and the fact that PKA-cat may exit the holoenzyme complex in an ADP bound state (Zhang et al., 2012), the role of PKA-cat

diffusion becomes even more apparent in the maintenance of AKAP established compartments. How a freely diffusing PKA-cat is capable of maintaining PKA signaling specificity remains largely unknown. **Chapter 3** of this dissertation deals almost exclusively with this problem and considers the role of N-terminal myristoylation of PKA-cat as a mechanism for decreasing PKA-cat mobility and enhancing a phosphorylation gradient at the plasma membrane.

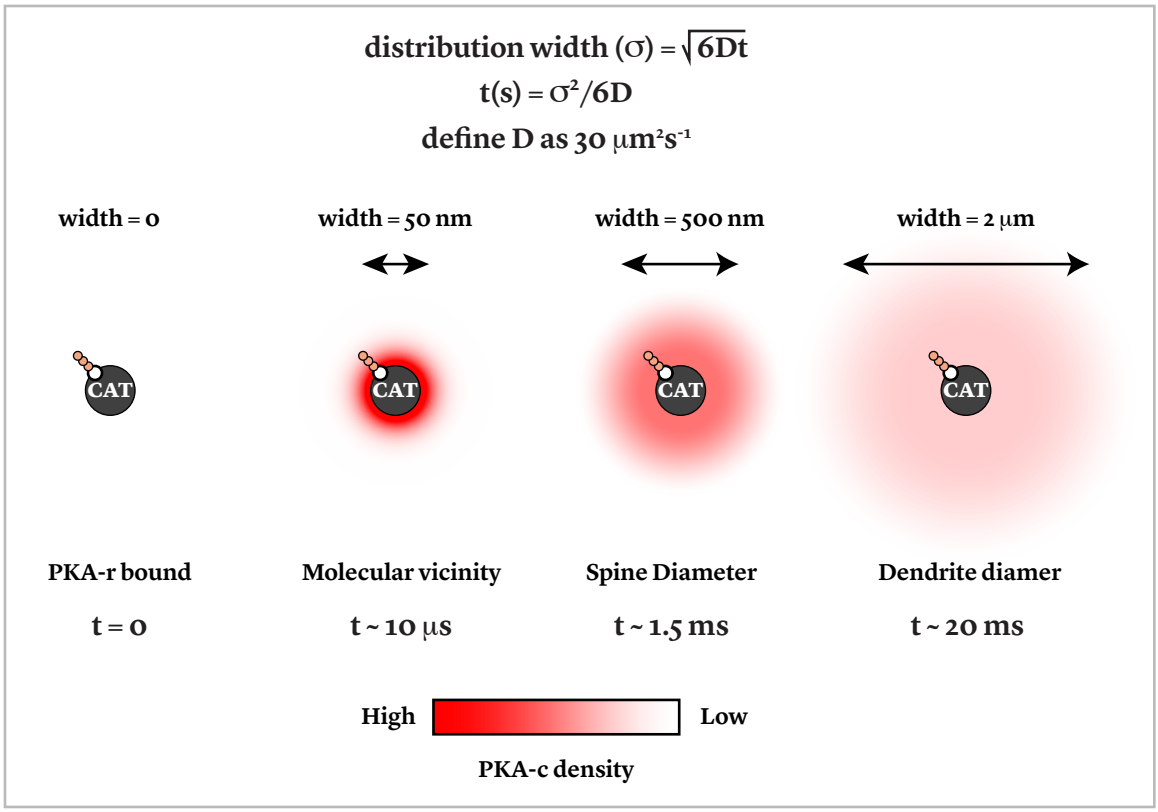

FIGURE 7. PKA-CAT MOBILITY AND POTENTIAL BREAKDOWN OF AKAP ESTABLISHED COMPARTMENTALIZATION.

At time = 0, PKA-c is bound by PKA-r and its distribution width is = 0. After activation of the holoenzyme, PKA-c is released and the width of its probability density function increases with time in accordance with its expected diffusion coefficient (30 $\mu m^2 s^{-1}$). Note that the distribution widths are not drawn to scale.

Imaging PKA in live tissue

Structural, biochemical, and molecular characterization have provided enormous insight into the workings of PKA. These methods, however, provide only a static, and thereby incomplete picture of PKA signaling. The timescales of PKA phosphorylation can

be gleaned from the monitoring of cellular changes it is known to induce. For instance, PKA modulation of the slow after-hyperpolarization potential in neurons provides an electrical readout for the time scales in which PKA acts (Madison and Nicoll, 1986; Pedarzani and Storm, 1993; Gervasi et al., 2010), yet it does not provide information as to the cellular compartments in which this modulation takes place, nor do such methods enable tracking of PKA subcellular distribution and phosphorylation. This type of information was impossible to obtain until the development of fluorescent protein tags (Chalfie et al., 1994), and optical sensors for detecting PKA activation (Adams et al., 1991; Zaccolo et al., 1999) and PKA phosphorylation (Zhang et al., 2001).

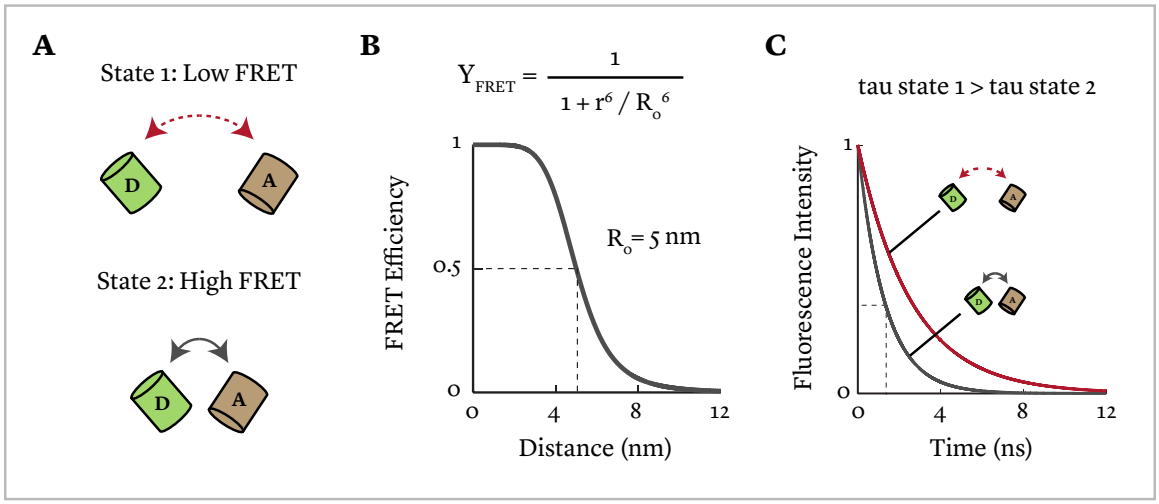

FIGURE 8. 2PFLIM DETECTION OF CHANGES IN FRET EFFICIENCY.
(A) General depiction of the two different conformational arrangements of a donor fluorophore (D) and acceptor fluorophore (A) that 2pFLIM can distinguish between. In state 1 the fluorophores are separated and the FRET efficiency (Y_{FRET}) is low. In state 2 the fluorophores are in proximity and the FRET efficiency is high. **(B)** Dependence of distance on FRET efficiency. For fluorescent proteins, the R_o, or distance for 50% FRET efficiency, is ~ 5 nM. Note also the steep dependence of FRET efficiency on the distance between donor and acceptor fluorophores. **(C)** Changes in FRET efficiency are detected in 2pFLIM as changes in the fluorescence lifetime of the donor. Low FRET efficiency is reflected as a long donor lifetime (tau) and High FRET efficiency is reflected as a short donor lifetime.

Here, we use 2photon imaging of GFP tagged PKA catalytic subunits to track the subcellular distribution and mobility of activated PKA-cat. From these measurements we infer the functional consequences of activated PKA-cat's mobility. To monitor PKA phosphorylation, we developed a novel sensor for PKA phosphorylation based on

intermolecular fluorescence resonance energy transfer (FRET) in a genetically engineered PKA substrate (see **Figure 8**). 2photon fluorescence lifetime (2pFLIM) measurements from this sensor targeted to different subcellular locations inform of relative PKA phosphorylation levels between cellular compartments, and thus gradients of PKA phosphorylation.

Formative Observations and Experiments

A major impetus for the work described here came from the post-doctoral work of Dr. Haining Zhong in the laboratory of Dr. Karel Svoboda (Zhong et al., 2009). In his paper, on the *Subcellular Dynamics of Type II PKA in Neurons*, Dr. Zhong used over-expression of both type I and type II PKA holoenzymes to map their distribution in the soma and dendrites of cortical and hippocampal neurons. He found enrichment of type II PKA in dendrites and a much more uniform distribution of type I PKA, consistent with previous observations showing non-uniform, more discrete distribution of RII subunits and a more diffuse, homogenous distribution of RI subunits. Perhaps more interestingly, he found that type II PKA is largely excluded from spines in resting conditions through the binding to the AKAP MAP2. Upon activation of the PKA holoenzyme by Forskolin + IBMX, the catalytic subunits redistributes to become enriched in dendritic spines, establishing a gradient of PKA-cat concentration from the spine to its parent dendrite. It is important to note that these measurements were performed in conditions where an equilibrium should have been reached between the spine head and dendrite, indicating the existence of mechanisms for confining PKA-cat in dendritic spines and establishing the observed gradient of PKA-cat concentration.

Dr. Zhong's results were confirmed in the early years of the laboratory (see panels B and C of **Figure 9**) and later extended to include information about the state of the catalytic subunit. Using the PKA sensor described in panel A of **Figure 9**, we demonstrated that the redistributed catalytic subunit exists in large part as a free protomer, ruling out rebinding to regulatory subunits as a mechanism to confine over-expressed PKA-cat to spines upon stimulation. The goal of the work presented here has been to investigate such mechanisms using CA1 hippocampal neurons and more reduced systems using a variety of imaging and biochemical approaches.

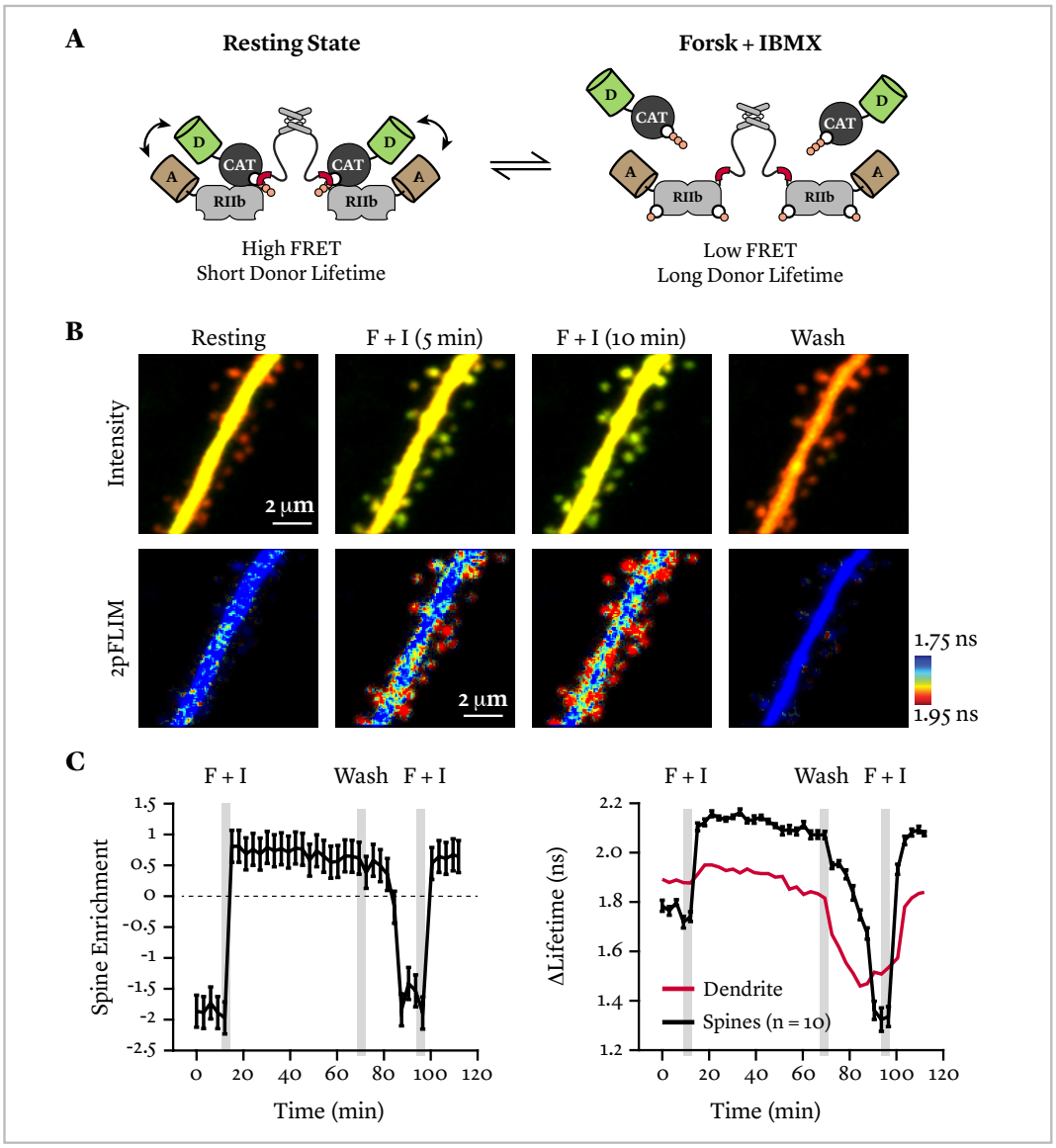

FIGURE 9. PKA-CAT SPINE ENRICHMENT LEADS TO AN INCREASE OF FREE PKA-CAT IN SPINES.

(A) Illustration of the PKA sensor used in the experiments. **(B)** Top row, fluorescent intensity image series depicting of the redistribution of PKA-cat from the parent dendrite to the spines after F + I stimulation. Bottom row, 2pFLIM image series depicting the presence of free-catalytic subunit in spines following stimulation. Note the higher percentage of PKA-cat (red pseudo-color) in the spines compared to the dendrite (blue pseudo-color). **(C)** Left, quantification of the spine enrichment index over time where spine enrichment = PKA-cat:Red_{spine} / PKA-cat : Red $_{dendrite}$ Note that a spine enrichment = 0 indicates equal distribution between the spine and dendrite; a value < 0 indicates dendritic enrichment and a value > 0 indicates spine enrichment. Right, quantification of the fluorescence lifetime of the GFP tagged catalytic subunit over time in the dendrite (red line) and spines (black line).

Rationale

An important consequence of compartmentalization is that it establishes a molecular vicinity in which the concentration of the compartment constituents is high relative to the surround. For the anchored constituents — often the activators (i.e. GPCRs and adenylyl cyclase) and substrates — this concentration gradient should be maintained stably over time. In contrast, the mobile compartment constituents — often the effectors (i.e. cAMP or PKA-cat) — have the potential to dissipate this concentration gradient over time. In the case of cAMP, and as stated before, the persistence of a cAMP gradient will depend upon its relative rates of production, diffusion, and degradation. It is important to note, however, that a gradient of cAMP originating at the plasma membrane will inevitably result from its production at the membrane and degradation in the cytosol. with regulated diffusion serving to enhance this gradient over time. A main question investigated here is whether or not the expected gradient of cAMP concentration is transmitted to its downstream effector PKA. Such a gradient would provide an effective means for which to achieve signal biasing and thus specificity in PKA signaling.

A PKA concentration gradient mirroring the expected cAMP gradient is not inevitable. For one, PKA-cat is not produced in the same manner a cAMP, which in the presence of continued stimulation (i.e. GPCR mediated stimulation of adenylyl cyclase) should also be continuously produced, further establishing and maintaining its gradient. PKA-cat, on the other hand, exists in a finite amount, the concentration of which is fixed over time. In conditions of finite PKA-cat concentration, the time scales in which a PKA-cat concentration gradient persists upon cAMP mediated holoenzyme activation will be completely dependent upon PKA-cat mobility. High mobility will result in a relatively fast dissipation of the concentration gradient whereas slow mobility will lead to its relative persistence. In its simplest sense, a persistent gradient of PKA-cat concentration should allow for the biasing of its phosphorylation.

Here, we have developed novel optical sensors capable of reporting PKA phosphorylation across cellular compartments. We use the sensors, to investigate whether or not a gradient of PKA phosphorylation results from the expected gradient of cAMP concentration at the plasma membrane. We further investigate a role for N-terminal

myristoylation of PKA-cat to target it to the plasma membrane, limit its mobility, and enhance its concentration and phosphorylation gradient over time.

Chapter 2.

Imaging PKA phosphorylation gradients using probes optimized for two-photon fluorescence lifetime imaging.

Shane E. Tillo[1,2], Maho Takahashi[1,2], Philip J.S. Stork[1], & Haining Zhong[1]

1. Vollum Institute, Oregon Health & Science University, Portland, OR USA

2. These authors contributed equally to this work

Foreword

This work was done in close conjunction with Dr. Maho Takahashi and she was instrumental in obtaining the data found in this chapter. Maho subcloned the new AKAR5 sensors presented here, collected the data for the cp-sREACh AKAR5 sensor found in Supplementary Figure 4, and collected the data for the folding and maturation experiments found in Supplementary Figure 1 at my direction. In addition, Maho collected ~ 50% of the data for the AKAR4 dose response curve (orange line, Figure 1d and Supplementary Figure 2), performed the okadaic acid experiments found in Figure 3f, the Ht31 AKAP inhibition experiments found in Figure 5, at my direction. Maho also collected the western blot data found in Supplementary Figure 7. The remaining experiments, all data analysis and figure preparation were done by me. Maho, Dr. Phil Stork, and Dr. Wolf Almers edited and reviewed this manuscript.

Abstract

The cAMP dependent protein kinase, or protein kinase A (PKA), is a major mediator of biochemical signaling cascades in a multitude of cell types. Often, PKA modulates multiple cellular processes in the same cell. In these cases, PKA specificity can arise from the subcellular source of PKA activation such that a given activator can lead to the preferential phosphorylation of a distinct set of PKA substrates. The mechanisms for establishing and maintaining this signal biasing have long been thought to arise from the compartmentalization of PKA phosphorylation in space and time. Thus, measuring dynamic PKA phosphorylation profiles amongst different cellular compartments is essential for understanding PKA specificity. The development of genetically encodable reporters of PKA phosphorylation make it possible to track these dynamics in the context of live cells. Here we report the development of a novel PKA phosphorylation reporter that has been optimized for 2photon fluorescence lifetime imaging. The new sensor is called AKAR5, and it offers several advantages over its predecessor including an increased sensitivity and signal to noise ratio. We use AKAR5 to investigate and compare unstimulated, or resting, PKA phosphorylation gradients in the cytosol and plasma membrane compartment of HEK293 cells. We find that resting PKA phosphorylation is largely confined to the plasma membrane compartment of cells, indicative of a steep gradient of PKA phosphorylation emanating from the plasma membrane. In the future, AKAR5 should be especially useful for interrogating PKA phosphorylation gradients in highly light scattering tissue such as in neuronal slice.

Introduction

The recent explosion in the development of optically based biosensors has allowed for the detection and measurement of biochemical signaling cascades in live tissue (Miyawaki, 2011). Compared to traditional biochemical methods, these sensors have enabled the probing of signaling events in live cells, over a wide range of cell types, cellular compartments, and time scales, giving insight into the mechanisms that establish specificity in cell signaling. Such probes have been especially fruitful for imaging the cAMP dependent protein kinase (PKA) phosphorylation profiles, whose compartmentalization in time and space is thought to provide a mechanistic explanation for specificity (Lohmann et al., 1984; Wong and Scott, 2004). Two prototypic versions of PKA phosphorylation reporters have been developed. The first PKA sensor used intermolecular fluorescence resonance energy (FRET) to detect PKA catalytic subunit (PKA-cat) dissociation from the PKA regulatory subunit (Adams et al., 1991; Zaccolo et al., 1999). Here, the relative amount of free PKA-cat is used as a surrogate for the amount of PKA phosphorylation. However, because the sensor scaffold is based upon the PKA holoenzyme, use of this sensor results in the artificial over-expression of PKA in the cell. As such, saturation of the available binding sites for PKA, excess buffering of cAMP, and excess phosphorylation of substrates, are all potential problems of this sensor (Rich et al., 2014) and its use has been fairly limited.

To overcome the problems of traditional PKA sensors, a new class of PKA phosphorylation reporters — named A-kinase phosphorylation reporters (AKARs) — were developed and subsequently modified and improved (Zhang et al., 2001; Zhang et al., 2005; Allen and Zhang, 2006; Depry et al., 2011). Though the standard architecture of the original AKAR probe has undergone modification, collectively they work via a intramolecular FRET-detected change in probe conformation resulting from PKA phosphorylation (see **Figure 1a**). The most recent version in the AKAR probe series is called AKAR4 which uses mCerulean (Rizzo et al., 2004) as the donor fluorophore and circular-permuted mVenus (cp-mVenus) as the acceptor (Depry et al., 2011). AKAR4 is suggested to have the best signal-to-noise ratio of all the AKAR probes developed thus far.

AKAR probes have been used extensively in the investigation of subcellular PKA phosphorylation profiles and the compartmentalization of those signals. For instance,

AKAR probes have been used to compare PKA phosphorylation profiles in the plasma membrane and cytosol of model cells (Saucerman et al., 2006; Allen and Zhang, 2006; Depry et al., 2011) to investigate the role of A-kinase anchoring proteins (AKAPs) in compartmentalizing PKA phosphorylation (Zhang et al., 2001; Dodge-Kafka et al., 2005; Zhang et al., 2005), to investigate time course of PKA phosphorylation in different subcellular compartments within neurons (Gervasi et al., 2007), and more recently to assess the functional role of flexibility within the PKA regulatory subunit (Smith et al., 2013), to name a few.

To date, the use of AKAR probes has been almost exclusively limited to the intensity-based, or ratiometric method of measuring FRET, in which the ratio of donor to acceptor emission intensity is used as a readout for PKA phosphorylation. Here, we sought to develop PKA probes more suitable for measuring FRET using 2photon fluorescence lifetime imaging (2pFLIM). which can offer several advantages over intensity based methods. These include an insensitivity to wavelength-dependent light scattering which can be of great importance when imaging in thicker tissues, and the possibility that the acceptor fluorophore can be non-fluorescent thereby opening up a channel for additional imaging. For a nice review see Yasuda et al., 2006. Here we present the development of a PKA phosphorylation reporter optimized for 2pFLIM that we have named AKAR5. We compare the response properties of AKAR5 to AKAR4 in 2pFLIM and then further characterize the sensor's response as a function of both the reported resting PKA phosphorylation (resting lifetime) and relative amount of sensor expression across cells.

Because adenylyl cyclase, the enzyme that converts cellular ATP into cAMP, is predominantly a membrane bound enzyme cAMP should be predominantly produced there. By contrast, its conversion into AMP occurs by via cytosolic enzymes known as phosphodiesterases. This should generate a standing [cAMP] gradient wherein [cAMP] declines with distance from the plasma membrane. In turn, the [cAMP] gradient should establish a similar gradient in which activation of the PKA holoenzyme occurs. However, in contrast to cAMP, the PKA holoenzyme exists in a finite amount, and thus upon its activation and subsequent release of PKA-cat, it is not immediately apparent that a gradient of cAMP mediated PKA holoenzyme activation will propagate to PKA phosphorylation.

Here, our aim is to use the newly developed AKAR5 sensor in an attempt to identify whether or not a gradient of PKA phosphorylation exists from the plasma membrane to the cytosol. The presence of such a gradient is expected to provide a means for cells to bias their PKA signaling and thus establish signaling specificity.

Results

AKAR5 sensor construction and characterization

The backbone of AKAR5 is identical in sequence to AKAR4, containing the forkhead associated domain (FHA) (Durocher et al., 1999) and pseudo-PKA substrate domain (Durocher et al., 2000) in series (see **Figure 1a**). To optimize the probe for 2pFLIM, we replaced the donor fluorophore mCerulean with the brighter and more photostable mEGFP (Zacharias et al., 2002; Shaner et al., 2005). For the acceptor fluorophore, we replaced cp-mVenus with the dark acceptor sREACh (Ganesan et al., 2006; Murakoshi et al., 2008). The left panel of **Figure 1a** depicts the sensor in its non-phosphorylated state. In this configuration the donor (mEGFP,D) and acceptor fluorophore (sREACh, A) are relatively far apart, the FRET efficiency is low, and the donor lifetime is long. In 2pFLIM measurements, the long donor lifetime is detected as a relatively long average delay of fluorescence emission from the arrival of 2photon excitation at the sample (see Methods) (Yasuda 2006, Lakowicz 2007). The right panel illustrates the sensor in its phosphorylated state in which the FHA domain exhibits affinity for the phosphorylated pseudo-PKA substrate domain. In this configuration the donor and acceptor are relatively close, the FRET efficiency is high, the donor lifetime is short, and the detected average delay in fluorescence emission is relatively short. Because previous reports indicate that circular permutation of the acceptor fluorophore in AKAR probes can improve their performance, we also constructed a version of AKAR5 containing circular permuted sREACh (cp-sREACh) as the acceptor (see Methods) (Allen and Zhang, 2006).

In lifetime imaging, fluorescence from the acceptor fluorophore can pollute measurements of donor lifetime. Much of this can be mitigated by using sREACh which is *dark* in the sense that it has a low quantum yield of fluorescence. However, given the short lifetime of sREACh (~0.35 ns) (Murakoshi et al., 2008) compared to EGFP (~2.6 ns) even a small amount of acceptor fluorescence bleed-through into the green detection channel can influence measurements of donor lifetime. We therefore, characterized the fluorescence bleed-through of the acceptors into our green detection channel using methods established by Murakoshi et al. Under 960 nm 2photon excitation, sREACh has a bleed-through of 2.8% and cp-sREACh a bleed-through of 2.1% into the EGFP detection channel. These low values

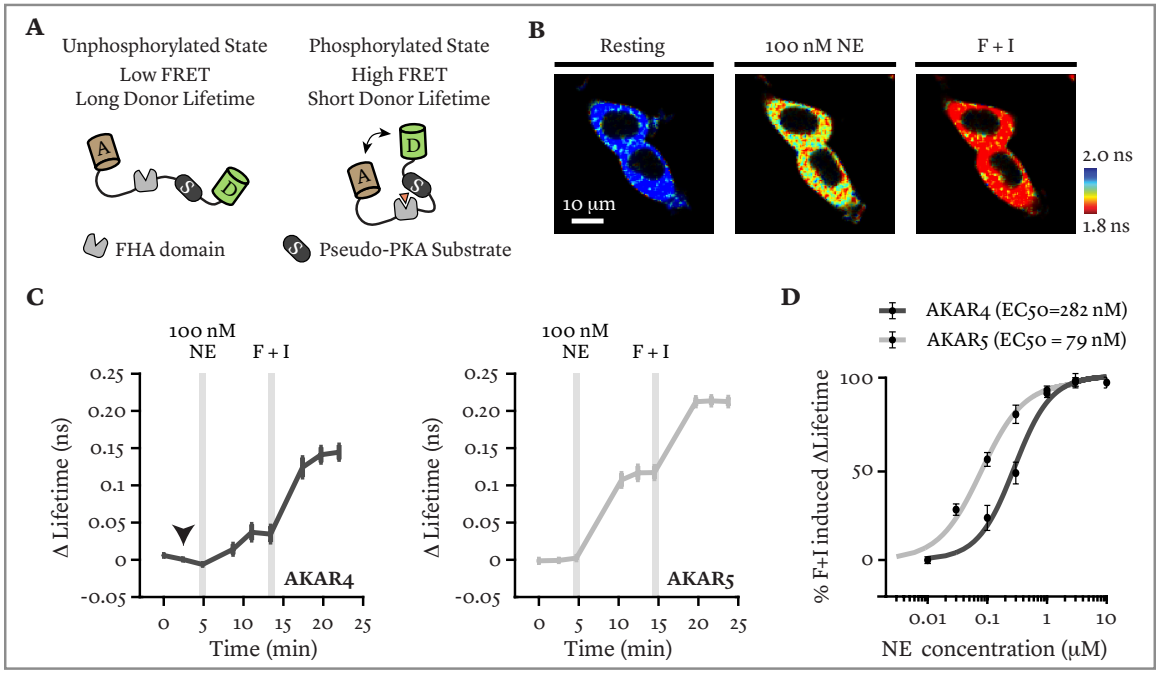

FIGURE 1. AKAR5 SENSOR CONSTRUCTION AND COMPARISON TO AKAR4 IN 2PFLIM

(A) Schematic of the cyt-AKAR5 PKA phosphorylation reporter in its unphosphorylated state (left panel) and phosphorylated state (right panel). A = acceptor fluorophore; D = donor fluorophore; FHA = Forkhead Associated Domain; S = pseudo-PKA substrate (B) 2photon fluorescence intensity (left panel) and 2pFLIM images of cyt-AKAR5 in the unstimulated resting state, upon the addition of 100 nM norepinephrine, and 20 µM Forskolin + 100 µM IBMX (F + I). The images are pseudo-colored based on the calculated donor lifetime in each pixel. Lifetime color bar found to the lower right of last panel. (C) Sensor responses (mean, s.e.m.) expressed in Δlifetimes (ns) of AKAR4 (left panel, n = 20) and cyt-AKAR5 (middle panel, n = 37) in response to the PKA activators 100 nM NE (NE) and 20 µM Forskolin / 100 µM IBMX (F + I). Arrowhead in AKAR4 panel points to the decreasing Δlifetimes in the sensor. (D) Plot of the ratio of the norepinephrine (NE) to F + I response as a function of NE concentration for AKAR4 (orange/black) and AKAR5(cyan/red). Data are presented as mean and s.e.m. Solid lines are fits to the data using the Hill equation. AKAR4 has an EC50 of 282 nM and cyt-AKAR5 an EC50 of 79 nM.

indicate that the intrinsic fluorescence of the acceptor should have little effect on our measurements of donor lifetime (**Supplementary Figure 1** and Methods).

We next measured the folding and maturation of our acceptor fluorophores using again methods established by Murakoshi et al (See **Supplementary Figure 1b** and Methods). sREACh has a median folding efficiency of 53% and cp-sREACh a median folding efficiency of 68%. A comparison of the sensor responses to PKA activators showed no detectable difference (see **Supplementary Figure 1c**), and for further experiments we

chose to use the non-circular permuted version of the sensor. For future use of the sensor we appended a nuclear export sequence (NES) sequence (Fukuda et al., 1996) to prevent its nuclear entry and refer to it as cyt-AKAR5. A more thorough characterization of AKAR4 and the sREACh and cp-sREACh versions of the AKAR5 sensor is shown in **Supplementary Figures 2 – 4**.

Here, we consider two modes of PKA phosphorylation. The first, which we explore in depth in this chapter using the AKAR5 sensor, is termed resting PKA phosphorylation. By resting we mean in the absence of exogenous stimulation (i.e. bath application of norepinephrine or Forsk + IBMX), and not in the absence of PKA holoenzyme activation as endogenous cAMP production is expected to occur even in resting states. The other mode we consider is stimulated PKA phosphorylation, which we achieve through the bath application of the PKA activators norepinephrine or Forsk + IBMX. Due to the nature of our sensor (see Methods, p.46), we cannot use the measured response from the sensor (lifetimes) as a measure of absolute sensor phosphorylation, and instead can only infer of relative levels of phosphorylation between cells or between different cellular compartments.

Strictly speaking, we can also not assign the measured response from the sensors as a direct product of PKA activity as phosphatases are also expected to influence the sensor lifetimes. Only through extensive literature on norepinephrine and cAMP action can we attribute changes in sensor response to changes in the state of the PKA holoenzyme and thus changes in PKA activity. We therefore refer to the differences in sensor response across cells and between cellular compartments as differences in net PKA phosphorylation, which we refer to simply as PKA phosphorylation.

AKAR5 comparison to AKAR4 in 2pFLIM

In HEK293 cells norepinephrine (NE) induces activation of the PKA holoenzyme through the binding of β-noradrenergic G-protein coupled receptors (GPCRs) and their subsequent activation of adenylyl cyclases and synthesis of cAMP. To compare the response properties of AKAR4 and AKAR5 in 2pFLIM we performed NE-mediated dose response experiments in HEK293 cells. AKAR4 was imaged at 860 nm, near the peak 2photon

excitation of mCerulean (Tillo et al., 2010; Drobizhev et al., 2011). Individual applications of NE were followed by the addition of 20 μM Forskolin and 100 μM IBMX (F + I) for a measure of the maximal achievable responses in individual cells. Forskolin is a cell-permeant activator of adenylyl cyclases and IBMX is a general phosphodiesterase inhibitor. Both work in concert to elevate cAMP levels to maximal levels throughout the cell. Note that all experiments involving F + I are performed at 20 μM Forskolin and 100 μM IBMX, unless noted otherwise. **Figure 1b** is a series of representative 2pFLIM images of cells expressing AKAR5. The images are pseudo-colored based on the calculated average lifetime of each pixel (see Methods). Because AKAR4 and AKAR5 contain different donor fluorophores their resting, or unstimulated, lifetimes will be different. In addition to the differences in resting lifetimes between the sensors, there is cell to cell variability in resting lifetimes amongst cells expressing the same sensor. Therefore, to compare PKA phosphorylation between sensors and amongst individual cells, the lifetimes from individual cells are presented as difference between the mean resting lifetime and the recorded lifetimes at any given time point. In the text and figures, we refer to this value as Δlifetime, where larger Δlifetimes in a given sensor are indicative of greater PKA phosphorylation (see Methods).

Figure 1c shows the response of AKAR4 (left panel) and cyt-AKAR5 (right panel) represented as Δlifetime (ns) to 100 nM NE and the subsequent application of F + I. The signal to noise ratio of cyt-AKAR5 was significantly better than AKAR4 as indicated by the larger F + I induced response, with cyt-AKAR5 having an mean Δlifetime of -0.21 ns and AKAR4 a mean Δlifetime of -0.14 ns. The unstimulated, or resting, Δlifetimes of AKAR5 were also more stable than that of AKAR4. The arrowhead in the left panel of **Figure 1c** points to the decreasing Δlifetimes of the AKAR4 sensor present in resting conditions. This decrease in lifetimes was consistent across NE doses (data not shown). This instability has been observed in previous ratiometric measurements of AKAR sensors, and is presumed to be an artifact of the cp-mVenus acceptor in the sensor (Valentin et al., 2005). We created NE dose response curves by ratioing the NE induced response in each cell to the F + I response, to control for cell to cell differences in PKA availability. Somewhat surprisingly, the cyt-AKAR5 probe was about 3.5 fold more sensitive as a reporter for PKA phosphorylation

induced by NE with an EC50 of 79 nM (light gray, Hill Coefficient = 1.21) compared to an EC50 of 282 nM (dark gray, Hill coefficient = 1.41) for AKAR4 (**Figure 1d**). We do not know whether this apparent increase in sensitivity to NE induced activation of the PKA holoenzyme is the result of increased sensitivity to PKA phosphorylation or reduced sensitivity to phosphatase activity.

AKAR5 sensor response characterization

The folding efficiency of the acceptor fluorophore in the AKAR5 sensor is expected to influence measured fluorescence lifetime in both resting and stimulated conditions. To simplify, consider two cells, each expressing 100 sensor molecules. Now consider the first cell containing 100 fully function sensors (i.e. 100 folded acceptors) and the second cell containing 50 fully functional sensors (i.e. 50 folded acceptors). (Note that folding efficiency of the donor does not matter in lifetime imaging as we do not detect sensors lacking a functional donor fluorophore). Under the same resting conditions, the first cell will report a shorter lifetime and thus report more PKA phosphorylation than the second due to the presence of more acceptors for the donor to FRET with. Upon stimulation, cell 1 will also report a higher amount of sensor phosphorylation (greater Δlifetime) for the same reason. Therefore, under ostensibly the same conditions (i.e. same plating of HEK293 cells) variation in acceptor folding efficiency across cells is expected to influence both the reported resting and stimulated PKA phosphorylation levels.

Figure 2 is dedicated to exploring the relationship between the inherent cell to cell variability in acceptor folding efficiency — inferred from measurements of resting lifetimes across cells — and the amplitude of the sensor response. Unexpectedly, we found a slight correlation between the amount of sensor expressed in individual cells and the resting lifetime of those cells. We quantify sensor expression from individual cells as the mean number of donor photons collected from the cytosolic region of the cell (mean photon counts). Because we use the same power to image all cells, this value provides a measure of the relative amount of sensor expression across cells (see Methods). Over the course of the experiments we observed that both the resting lifetimes and the F + I induced Δlifetimes of

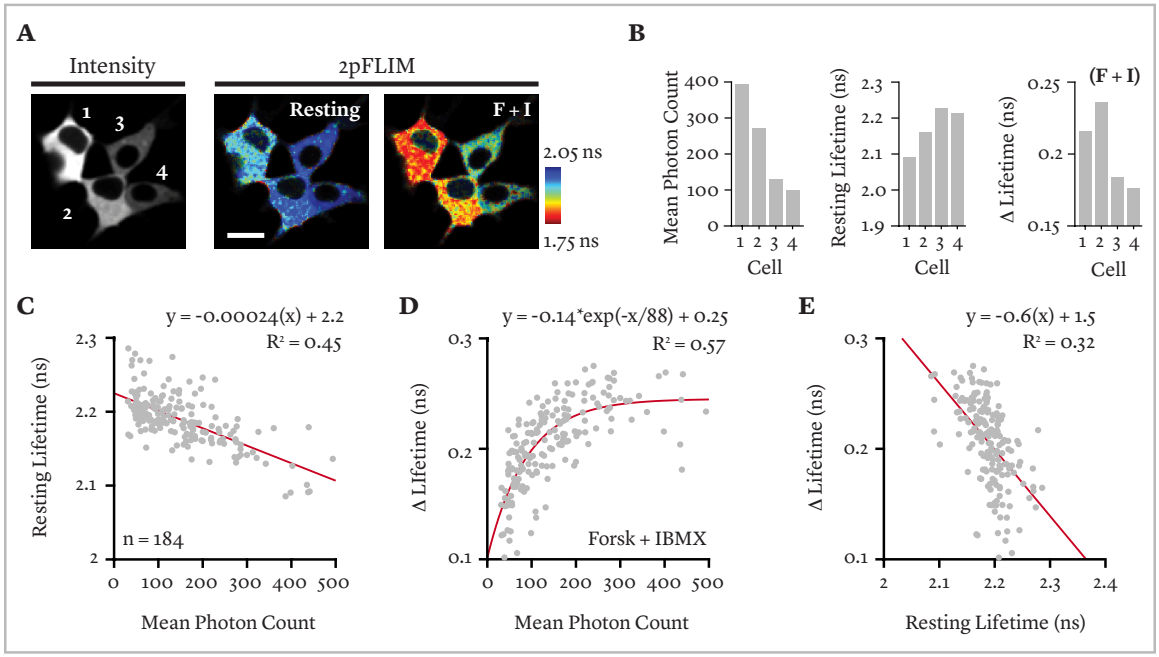

FIGURE 2. AKAR5 SENSOR RESPONSE CHARACTERIZATION.

(A) Left panel, 2photon fluorescence intensity image of a group of 4 cells expressing varying levels of sensor. Right panels, 2pFLIM images of the cells found to the left. Scale bar is 20 μm. Lifetime color bar found to the right of the last image in the panel. **(B)** Quantification of the mean photon count (sensor expression), resting lifetime (ns) and 20 μM Forskolin +100 μM IBMX responses (Δlifetime) of the 4 cells found in panel A**. (C)** Population data comparing the amount of sensor expression (mean photon count) to resting lifetime, **(D)** the amount of sensor expression to the F + I induced Δlifetime, and **(E)** the resting lifetime to the F + I induced response. Gray dots represent individual cells (n = 184) and the red lines are the data fitted with the equation found above each sub-panel.

the sensors correlated with the amount of sensor expressed in the cell (see also **Supplementary Figures 2 – 4**). The left panel of **Figure 2a** is a 2photon fluorescence intensity image of a group of 4 cells expressing varying levels of cyt-AKAR5. The middle and rights panels of **Figure 2a** are the corresponding 2pFLIM images of the cells in the non-stimulated resting (middle) and the F + I stimulated states (right). Note that in the brightest cell, (cell 1, top left) we detect both a high level of resting PKA phosphorylation (short lifetime), and a high level of F + I stimulated PKA phosphorylation (large Δlifetime) relative to the other cells in the image. **Figure 2b** is the quantification of the sensor expression, resting lifetimes, and the F + I induced Δlifetimes of the cells found in **Figure 2a**. The population data (n = 184 cells) comparing the relative levels of sensor expression to resting

PKA phosphorylation for individual cells is shown in **Figure 2c**. **Figure 2d** shows the comparison between mean photon counts and the F + I induced PKA phosphorylation (Δlifetime) for individual cells. **Figure 2e** relates Δlifetime to the unstimulated, or resting, lifetimes of individual cells.

We next investigated whether or not the level of F + I induced PKA phosphorylation depended upon prior PKA activation via NE. Shown in supplementary **Supplementary Figure 5a** is the F + I induced Δlifetime as a function of prior doses of NE. **Supplementary Figure 5b** plots the F + I induced responses as corrected for using the exponential fit found in the middle panel (see Methods). No significant differences were found in the F + I induced response across NE treatments. We conclude that the maximal induced PKA phosphorylation is independent of prior induction of PKA phosphorylation via NE.

Comparing PKA phosphorylation between the plasma membrane and cytosol

We next sought to utilize the AKAR5 sensor to test the prediction that, among two otherwise identical substrates, that near the membrane is phosphorylated in preference. To measure PKA phosphorylation in the plasma membrane we appended AKAR5 with the membrane targeting C-terminal tail of Kras (Hancock et al., 1989). We refer to this sensor as pm-AKAR5 and compared it to the purely cytosolic cyt-AKAR5 probe (see Methods). To help control for variability we see in resting lifetimes across distinct platings of HEK293 cells, we co-plated cells expressing either pm-AKAR5 plus the nuclear marker mCherry-histone2b or cyt-AKAR5 alone. The left panel of **Figure 3a** is an example 2photon image of two cells used for such experiments. Note the distinct membrane labeling and red nucleus of the lower cell expressing pm-AKAR5, and the uniform cytosolic labeling of the upper cell expressing cyt-AKAR5. In cells expressing pm-AKAR5 we also detected a fraction of sensor located in the cell interior, in addition to that found on the plasma membrane. We do not know whether this fraction of the sensor is soluble, bound to internal membrane components, or both. The average resting lifetime of the intracellular component of pm-AKAR5 expressing cells is 1.77 ns, which is similar to PKA phosphorylation measured in the cytosol, but due to our uncertainty of its identity we exclude it from further analysis and analyze only the sensor located on the plasma membrane. (**Supplementary Figure 6**)**.** The

right panels of **Figure 3a** show a series of 2pFLIM images of the cells in the left panel stimulated with 100 nM NE and F + I. At rest, the lifetime of the pm-AKAR5 expressing cell is shorter than that of cyt-AKAR5 expressing cell indicating that in unstimulated conditions, PKA phosphorylation is higher in the membrane compartment of cells. (see also **Supplementary Figure 6**). **Figure 3b** shows the population data of resting PKA phosphorylation for pm-AKAR5 (n = 105 cells) and cyt-AKAR5 (n = 105 cells). The plasma membrane component of HEK293 cells has on average, a resting lifetime of 1.58 ns whereas cytosolic compartment has a mean resting lifetime of 1.84 ns.

In addition to the resting PKA phosphorylation, the average NE stimulated responses indicate that PKA located in the plasma membrane (pm-AKAR5, n = 13) responds more robustly to NE than PKA located within the cytosol (cyt-AKAR5, n = 9) with mean Δlifetimes of 0.18 ns and 0.07 ns, respectively (**Figure 3c**). In other works, in the cytosol, NE and F+I cause additive changes, whereas near the plasma membrane the change in F+I is nearly abolished. This suggests that at the plasma membrane, but not in the cytosol, NE causes almost complete phosphorylation of AKAR5. This result may be expected given the fact that NE mediated stimulation of adenylyl cyclase is expected to result in a cAMP concentration gradient very near to the plasma membrane. However, given the correlation between resting lifetimes and the amplitude of the stimulated response (Δlifetime) found in the middle panel of **Figure 2c**, we were concerned that some of the difference merely reflected the shorter resting lifetime of the pm-AKAR5 sensor. To help rule out this possibility we stimulated cells on the same coverslip expressing either cyt-AKAR5 or pm-AKAR5 to sensor saturation with 20 μM Forskolin and then added increasing doses of the competitive inhibitor of PKA phosphorylation H89 (**Figure 3d**). If NE stimulated PKA phosphorylation occurs more readily at the plasma membrane it should require larger doses of H89 to recover the F + I induced Δlifetimes of the saturated pm-AKAR5 sensors. Indeed, the pm-AKAR5 expressing cell (light gray) required 5-fold more H89 (50 μM) to induce recovery back to resting levels compared to the cyt-AKAR5 expressing cell (dark gray). However, given the limited number of cells for the experiment (n= 1), and the fact that we are dealing with sensors in the saturated state, we take these results with a grain of salt. We also cannot rule out H89 as having a diminished ability to work at the plasma membrane

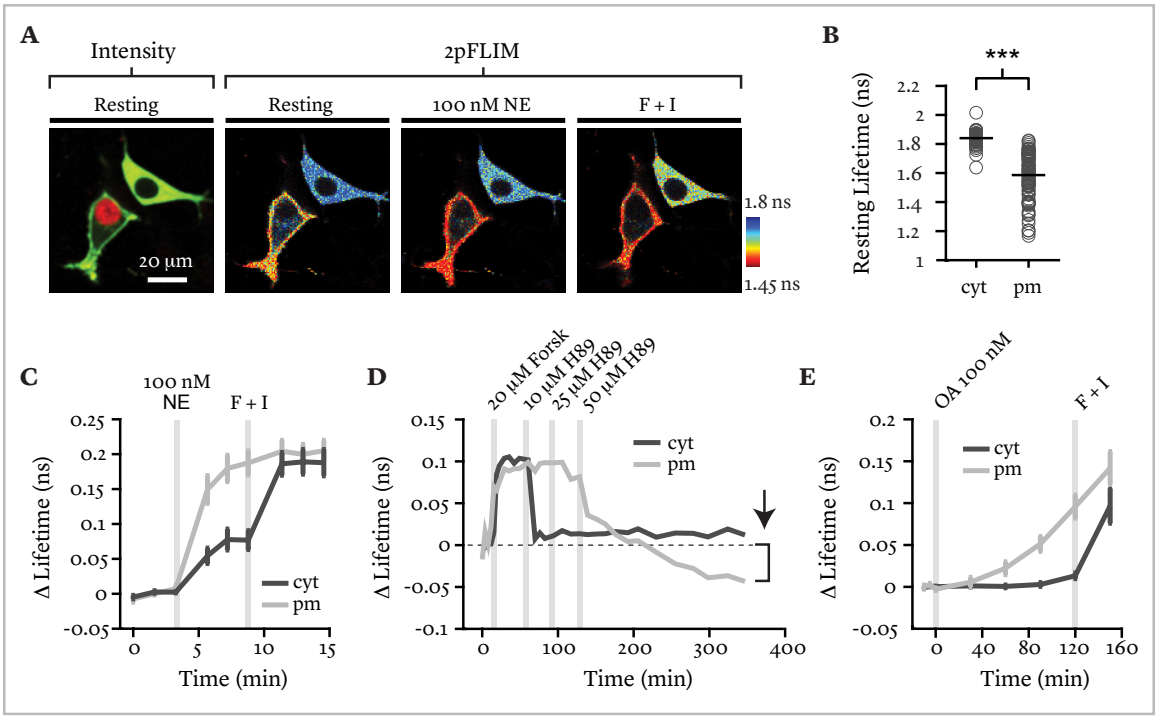

FIGURE 3. GRADIENTS OF PKA PHOSPHORYLATION AT THE PLASMA MEMBRANE OF HEK293 CELLS.

(A) Representative 2photon fluorescence intensity image (left) and 2pFLIM image series of an HEK293 cell expressing the pm-AKAR5 sensor (red nucleus) and the cyt-AKAR sensor (upper right) in resting conditions and after NE and F + I treatment. **(B)** Population data of the resting lifetimes (ns) for the cytosolic cellular compartments (cyt, mean = 1.84 ns, n = 105) and for the plasma membrane (pm, mean = 1.58 ns, n = 105) of HEK293 cells. Gray open circles represent individual cells. Black line represents the mean. *** = $p < 0.0001$ using Student's t-test. **(C)** Summary of the responses of the pm-AKAR5 sensor (pm, light gray, n = 13, mean + s.e.m.) and the cyt-AKAR5 sensor (cyt, dark gray, n = 9, mean + s.e.m.) to 100 nM NE and F+I. **(D)** Plot of Δlifetime over time for cyt-AKAR5 (cyt, dark gray, n = 1) and pm-AKAR5 (pm, light gray, n = 1) in response to 20 µM Forskolin and subsequent treatment with the PKA competitive phosphorylation inhibitor H89 (10 µM, 25 µM, 50 µM). Time of drug application is indicated by the gray bars. The arrow indicates the amount of recovery from F = I induced PKA phosphorylation below resting conditions for the pm-AKAR5 expressing cell. n = 1. **(E)** Time course of Δlifetimes for cells expressing cyt-AKAR5 (dark gray, n=20) and pm-AKAR5 (light gray, n=20) after treatment with 100 nM okadaic acid. Cells were treated with F + I to test the functionality of the sensors. Gray bars indicate time of drug application.

compared to the cytosol. Despite these caveats, it is worth noting that H89 inhibition of PKA phosphorylation in the pm-AKAR5 cell led to inhibition to a level below resting values, consistent with the notion that shorter resting lifetime values reflect higher phosphorylation in that compartment (**Figure 3d**, arrow).

To further test our observation that resting PKA phosphorylation is higher at the plasma membrane we treated cells expressing either cyt-AKAR5 or pm-AKAR5 with 100 nM okadaic acid. Okadaic acid is an inhibitor of serine/threonine phosphatases 1 and 2a both of which are known to counteract PKA mediated phosphorylation in many cells, including in HEK293 cells (**Figure 3e**) (Bialojan and Takai, 1988; Reinhart et al., 1991). 100 nM Okadaic acid increased the phosphorylation in the plasma membrane compartment indicated by the increase in Δlifetimes in pm-AKAR5 expressing cells (cyan, n = 20) compared to the stable Δlifetimes found in cytosolic AKAR5 expressing cells (orange, n = 20). Treatment with F + I confirmed the functionality of the sensors. These results are consistent with the observation that resting PKA phosphorylation is at the least higher, if not confined, in plasma membrane of HEK293 cells.

Comparing the resting lifetimes of functional and phospho-deficient AKAR5 probes

The differences in resting lifetimes of the pm-AKAR5 and cyt-AKAR5 sensors — which are putatively identical PKA substrates — support the idea that PKA phosphorylation is higher close to the membrane than far from it. However, given the slight differences in sensor makeup resulting from the NES and CAAX signaling motifs, the results presented thus far cannot rule out the possibility that pm-AKAR5 is simply a better substrate for PKA phosphorylation than cyt-AKAR5. In an attempt to mitigate this concern, we compared the resting lifetimes of cyt-AKAR5 and pm-AKAR5 to their phospho-deficient counterparts, cyt-AKAR5^{TA} and pm-AKAR5^{TA}, respectively (see Methods) (Zhang et al., 2001). In the phospho-deficient sensors, the threonine within the pseudo-PKA substrate domain is converted to alanine (TA), and they can no longer be phosphorylated by PKA as indicated by both 2pFLIM and western blot measures (**Figure 4a** and **Supplementary Figure 7**). The lifetimes of these phospho-deficient sensors should thus define that which would be measured in the absence of PKA phosphorylation (Zhang et al., 2005). Any variation in the measured resting lifetimes of cyt-AKAR5^{TA} or pm-AKAR5^{TA} will be attributable to factors that effect donor lifetime independent of PKA phosphorylation such as those presented in **Figure 2**. Again, in an attempt to reduce the variability in measured lifetimes, we co-plated cells expressing either the functional or phospho-deficient sensors co-expressing the

mCherry nuclear marker. We predict that in resting conditions the cyt-AKAR5 sensor and its phospho-deficient counterpart will have nearly the same lifetimes whereas the pm-AKAR5 will have a shorter resting lifetime (more PKA phosphorylation) than its phospho-deficient counterpart.

The leftmost column of **Figure 4a** shows example 2photon fluorescence intensity images of cells used in the experiment. On the top are images of cyt-AKAR5 expressing cells. The lower two cells contain red nuclei and thus represent cells expressing the phospho-deficient cyt-AKAR5^{TA} probe. On the bottom is an image of two pm-AKAR5 expressing cells. The lower cell within the bottom row is expressing the phospho-deficient pm-AKAR5^{TA} as indicated by its red nucleus. The right three columns of **Figure 4a** are a series of 2pFLIM images of the cells represented in the left column. At rest, the lifetime of the cyt-AKAR5 sensor matches that of cyt-AKAR5^{TA} with mean lifetimes of 1.81 ns for each. As expected, the cyt-AKAR5^{TA} sensor does not respond to the addition of 100 nM NE and subsequent F + I. In contrast to the cyt-AKAR5 sensor, the lifetime of the pm-AKAR5 is slightly shorter than that of pm-AKAR5^{TA}, as evidenced by the mean resting lifetimes of 1.76 ns for pm-AKAR5^{TA} and 1.51 ns for the functional pm-AKAR5 sensor (**Figure 4b**). As with the cyt-AKAR5^{TA} sensor, the pm-AKAR5^{TA} sensor is sensitive neither to NE nor F + I treatment.

Notably, the resting lifetime of the pm-AKAR5^{TA} sensor is shorter than that of the phospho-deficient cyt-AKAR5^{TA} sensor, indicating that insertion of the sensor into the plasma membrane alone results in a shorter lifetime for the donor fluorophore. Though not investigated further, a possible explanation for this phenomenon is that insertion into the membrane anchors the acceptor in space, thereby increasing the probability for interaction with the donor. Another explanation is that membrane anchoring could select for acceptors with a preferred dipole orientation to the donor, thus causing the observed decrease in fluorescence lifetime. Yet another explanation is that membrane insertion concentrates the sensor into 2-dimensional space increasing the likelihood for intermolecular FRET between the sensors. However, the comparison of the functional sensors to their phospho-deficient counterparts provides a nice control demonstration as to whether or not PKA phosphorylation levels are on average above zero in either of the two investigated

subcellular compartments. These results also help to alleviate the concern that the detected higher PKA phosphorylation at the plasma membrane is the result of pm-AKAR5 simply being a better substrate than cyt-AKAR5.

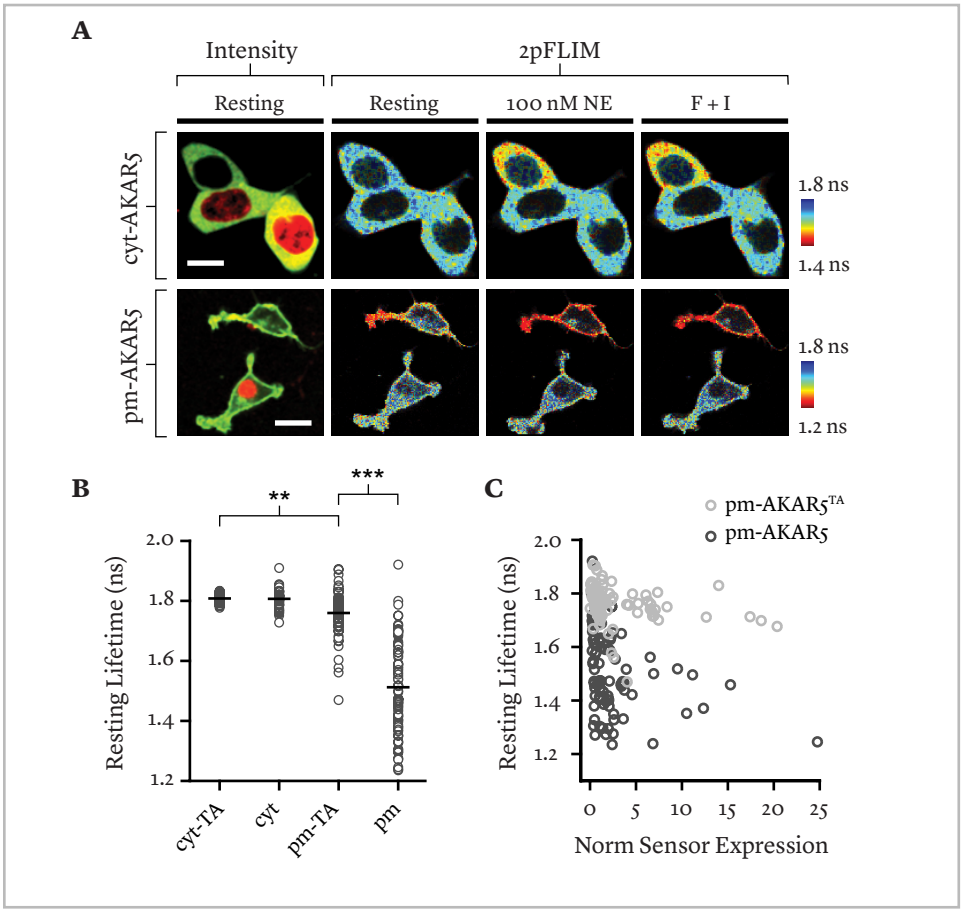

FIGURE 4. RESTING PKA PHOSPHORYLATION IS CONFINED TO THE PLASMA MEMBRANE.

(A) 2photon fluorescence intensity (left column) and 2pFLIM image series (3 right columns) for cyt-AKAR5 and cyt-AKAR5^{TA} (top row) and pm-AKAR5 and pm-AKAR5^{TA} (bottom row). Lifetime color bar found on lower right of both rows. Scale bar = 20 μm. **(B)** cyt-AKAR5 lifetimes for the functional (cyt, mean = 1.81ns, n = 80) and phospho-deficient (cyt-TA, mean = 1.81ns, n = 80) sensors, and the lifetimes for the functional (pm, mean = 1.51 ns, n = 90), phospho-deficient (pm-TA, mean = 1.76 ns, n = 90) pm-AKAR5 sensors. Gray open circles represent individual cells. Black line represents the mean. ** = $p < 0.005$ and *** = $p < 0.0001$ as determined by 1-way ANOVA and Turkey's post hoc test. **(C)** Comparison of the sensor expression to the resting lifetimes of the functional (dark gray dots) and phospho-deficient (light gray dots) pm-AKAR5 probes.

Discussion

Overview of the newly developed sensor

In this manuscript we presented the development and characterization of a new class of PKA phosphorylation reporters that we have named AKAR5. These sensors should provide considerable advantages over previous probes, especially for use in 2pFLIM. For one, the donor fluorophore in AKAR5 is mEGFP instead of mCerulean or another cyan based fluorescent protein. mEGFP is brighter and more photostable than mCerulean (Shaner et al., 2008), and more suitable for 2photon imaging owing to its larger two photon cross section (Tillo et al., 2010; Drobizhev et al., 2011). In addition, it can be imaged at longer wavelengths thereby lessening degradation of the point spread function in tissue. For the acceptor fluorophore we have used sREACh from the Yasuda laboratory which is *dark* in the sense that it has limited bleed-through into the mEGFP channel (Murakoshi et al., 2008), as shown here as well (**Supplementary Figure 1a**). Owing to its low intrinsic fluorescence, and the fact that lifetime measurements depend only on the donor fluorophore, the use of sREACh should allow for simultaneous imaging of other cellular constituents in the red detection channel. For instance, one can imagine simultaneously imaging PKA phosphorylation and calcium transients using AKAR5 and the recently developed calcium sensitive R-GECOs (Zhao et al., 2011; Tewson et al., 2012).

In terms of response properties, AKAR5 offers several advantages over AKAR4 in 2pFLIM. First, AKAR5 is ~ 3.5 times more sensitive for detecting NE induced PKA phosphorylation as indicated by the NE dose response experiments in **Figure 1d**. This sensitivity can be especially important for monitoring conditions of low PKA phosphorylation such as that seen under unstimulated, or resting, conditions. Second, the signal to noise ratio of the AKAR5 sensor is better than AKAR4 as reported by the ~25% larger Δlifetime induced by F + I (**Figure 1c**). The lower response amplitude of AKAR4 may be due to the fact that its acceptor, cp-mVenus, like other YFP species, photo-converts to a CFP like species during prolonged imaging thereby reducing the available pool of functional sensors over time (Valentin et al., 2005). Third, the lifetime of AKAR5 in resting conditions is much more stable than that reported by AKAR4 (**Figure 1c**). Like the lower

response amplitude, the shortening lifetime of AKAR4 over time may be explained by photo-conversion of cp-mVenus as described above. The steady resting measurements provided by AKAR5 will be important for interpreting resting PKA phosphorylation profiles across cellular compartments and for maintaining sensor efficacy during long-term imaging experiments.

As documented in **Figure 2**, both the resting and stimulated PKA phosphorylation reported by AKAR5 are correlated with the relative amount of sensor expression. Specifically, the higher the expression of the sensor the more phosphorylation it reports both in resting and stimulated conditions. The resting lifetime of cyt-AKAR5 also showed some correlation with the amplitude of the F + I stimulated response (**Figure 2C**, right panel), while the cytosolic cp-sREACh version of AKAR5 demonstrated an even stronger correlation between resting lifetimes and the amplitude of the F + I induced Δlifetime (**Supplementary Figure 4**, panel C, right). At least two possible scenarios could lead to this result: 1) the variation in resting lifetimes, which correlate with sensor expression, represent actual variation in resting PKA phosphorylation levels, and that cells experiencing slightly higher resting PKA phosphorylation are able to mount a more robust response to exogenous stimulus. In this sense, active resting cells may be 'primed' to respond to activators of PKA signaling. 2) The variation in resting lifetimes simply reflects variations in the ratio of donor to acceptor folding in the AKAR5 probes across cells. In this scenario, cells that have a lower donor to acceptor folding ratio will also have a shorter resting lifetime as more acceptor is present for the donor to transfer energy to. Upon the addition of exogenous PKA activators, these cells should also have higher reported phosphorylation for the same reason. The data presented here point to the occurrence of both scenarios. For the cyt-AKAR5 sensor, the average resting lifetimes of the functional and phospho-deficient sensors are nearly identical with mean and median lifetimes of 1.81 ns for both sensors. The standard deviation of the resting lifetime distributions, however, are significantly different with the functional sensor displaying roughly twice the variability (**Figure 2c**). The cyt-AKAR5 has a standard deviation of resting lifetime values of 0.027 ns whereas the cyt-AKAR5^{TA} sensor has a standard deviation of about half, or 0.013 ns, indicating that roughly half the variability in reported PKA phosphorylation can be explained by variability in acceptor

folding and half by PKA dynamics. Similar profiles were seen for the pm-AKAR5 sensors (**Figure 4c**).

Resting PKA phosphorylation in the cytosol and plasma membrane of HEK293 cells

There have been few studies investigating the resting phosphorylation of PKA in cells (Depry et al., 2011; Smith et al., 2013). Using AKAR4 probes, Depry et al. used H89 treatment in resting HEK293 cells to test for PKA phosphorylation in non-lipid raft plasma membrane or lipid-raft containing plasma membrane using the KRas (AKAR4-KRas) and Lyn kinase (Lyn-AKAR4) membrane targeting sequences, respectively. They found that H89 only had an effect on Lyn-AKAR4 expressing cells and thus concluded that resting PKA phosphorylation occurred largely in lipid rafts of the plasma membrane. This study, however, failed to compare the resting FRET values of the functional sensors to their corresponding phospho-deficient counterparts. In addition, the authors looked only at H89 effects over relatively short time scales (~ 5 min.).

Here we aimed to detect a plasma membrane gradient of resting PKA phosphorylation by comparing PKA phosphorylation levels in the cytosolic and plasma membrane compartment of HEK293 cells using the AKAR5 sensor. For the cytosolic compartment we used an NES tagged AKAR5, that we refer to as cyt-AKAR5. Cells expressing this sensor had uniform green emission from the cytosol that was excluded from the nucleus (**Figures 1b & 2a**). For the plasma membrane fraction we also used a KRas targeting sequence appended to the C-terminal tail of the sensor and refer to it as pm-AKAR5. Cells expressing pm-AKAR5 had robust plasma membrane labeling with a fraction sensor located in the cell interior, which we did not include in our analysis (**Figures 3a, 4a,** and **Supplementary Figure 3**).

We used a three pronged approach in combination with the differentially subcellular targeted sensors to compare resting PKA phosphorylation between the plasma membrane and cytosolic compartment. First, we treated Forskolin stimulated cells with the competitive inhibitor of PKA phosphorylation, H89. In the presence of H89, sensor recovery to the unphosphorylated state will be mediated by phosphatase activity. If resting PKA phosphorylation is indeed present in either compartment, H89 treatment should result in

the recovery of PKA phosphorylation to levels below those found at rest. We saw a robust and relatively rapid effect of 10 μM H89 on cyt-AKAR5 expressing cells. Cells expressing pm-AKAR5 required a 5-fold higher dose of H89 and much longer time to recover the Forskolin stimulated PKA phosphorylation (**Figure 3e**). However, in contrast to the cytosol, PKA phosphorylation at the membrane was inhibited to a level exceeding that found at rest. Presumably, this additional inhibition represents resting PKA phosphorylation occurring at the plasma membrane. The fact that the pm-AKAR5 sensor required larger doses of H89 to rescue the Forskolin induced PKA phosphorylation is difficult to interpret. H89 diffusion to the plasma membrane may be impeded, or phosphatases activity may be lower in that compartment. Alternatively, we could be looking at sensor saturation, and fewer molecules of PKA-cat are required to saturate the sensor at the plasma membrane than in the cytosol. This result would be consistent with more efficient phosphorylation at the plasma membrane, but given our uncertainty, we resolve to not interpret these results further.

We next tested the effects of okadaic acid, a potent inhibitor of the protein phosphatases 1 and 2a, on resting PKA phosphorylation in the plasma membrane and cytosol (Bialojan and Takai, 1988). We reasoned that okadaic acid should only exert its effects in the plasma membrane compartments where PKA phosphorylation is confined. Over the time course of our experiments (~120 min.), okadaic acid significantly increased PKA phosphorylation in the plasma membrane. We saw very little effect in the cytosolic compartment (**Figure 3f**). These results are consistent with the observation the resting PKA phosphorylation is present in the plasma membrane but sequestered from the cytosol in HEK293 cells.

To further confirm the gradient of PKA phosphorylation that we see between the cytosol and plasma membrane we compared each sensors reported resting phosphorylation to that of its phospho-deficient counterpart (**Figure 4**). We assume that the lifetimes of the mutant sensors (cyt-AKAR5^{TA} and pm-AKAR5^{TA}) represent that which we would measure in a cell experiencing zero PKA phosphorylation. Our results with H89 and okadaic acid predict that the resting lifetimes of cyt-AKAR5 and cyt-AKAR5^{TA} should be equal to one another and that the resting lifetimes of pm-AKAR5 should be shorter than pm-AKAR5^{TA}. **Figure 4c** shows the population data for these experiments. As predicted, cyt-AKAR5 and

cyt-AKAR5^{TA} report the same average resting PKA phosphorylation whereas pm-AKAR5 reports a higher level of phosphorylation than pm-AKAR5^{TA}. Taken together, these experiments paint a picture of relatively high resting PKA phosphorylation at the plasma membrane that is excluded from the cytosol. In other words, the expected gradient of cAMP production at the plasma membrane is mirrored by a gradient of PKA phosphorylation.

Our comparison of the functional pm-AKAR5 probe to the phospho-deficient pm-AKAR5 probe also suggests that resting PKA phosphorylation at the plasma membrane represents a substantial amount of total achievable PKA phoshorylation (**Figure 4c**). Clearly, some proteins (i.e AMPA type glutamate receptors) located at the plasma membrane of cells, manage to remain unphosphorylated by PKA during resting states in order to maintain the ability of PKA to alter ð43their function. Our data thus point to cellular mechanisms for keeping PKA phosphorylation in check, such as sequestration of PKA substrates by AKAP anchored phosphatases and phosphodiesterases (Coghlan et al., 1995). Alternatively, the relatively high resting PKA phosphorylation detected here could be due the recently described cAMP independent PKA phosphorylation mediated by the type RIIα PKA-reg (Smith et al., 2013). As HEK293 cells express relatively high levels of the Gαi coupled dopamine D2 and D4 receptors, and little to no Gαs coupled dopamine receptors (Atwood et al., 2011), one could imagine using dopamine application to reduce cAMP concentration to near zero values, performing the same experiments, and seeing if, and to what levels, the high-resting PKA phosphorylation persists. Alternatively, heterologous expression of Gαi coupled DREADDs (Alexander et al., 2009; Ferguson et al., 2011) could be used to clamp down resting cAMP levels throughout the cell. These and other possibilities warrant further investigation.

Materials and Methods

Assembly of AKAR5 sensors

AKAR5 was constructed from the backbone of the published AKAR4 sequence (Depry et al., 2011). We first replaced the donor mCerulean (Rizzo et al., 2004) with mEGFP (Zacharias et al., 2002). mEGFP was amplified by PCR to add the restriction sites BamH1 and BsrG1 which were used for the removal of mCerulean and subsequent in-frame insertion of mEGFP. Our acceptor sREACh (Murakoshi et al., 2008)was amplified by PCR to add the restriction sites SgrA1 and EcoR1 which used for the removal of cp-mVenus and in-frame insertion of sREACh. The lucine-rich nuclear export sequence of MEK (ALQKKLEELELDE) (Fukuda et al., 1996) or the membrane targeted farnesylation lipid modification sequence from KRas (KKKKKKSKTKCVIM) (Hancock et al., 1989; Depry et al., 2011) were introduced at the 3' terminus of sREACh within AKAR5 using oligo synthesis and subcloning to generate cyt-AKAR5 and pm-AKAR5. The phospho-deficient mutant of AKAR5 was generated by site-directed mutagenesis. A circular-permutated version of AKAR5 (cp-AKAR5) was produced by replacing the sREACh sequence with the corresponding circularly permuted version. PCR primers were designed to generate a new start methionine followed by the amino acids 174 to 238, followed in frame with amino acids 1-172 of sREACh.

cDNA constructs

mEGFP-mKeima and sREACh-mKeima were kindly provided by Ryohei Yasuda. The tandem constructs mVenus-mKeima and cp-sREACh-mKeima were generated by subcloning mVenus or cp-sREACh PCR product into the original mEGFP-mKeima construct. For generating mEGFP-Reach constructs, mEGFP was subcloned into the mCherryC1 vector, replacing mCherry with mEGFP. Subsequently, the PCR products of mVenus, sREACh or cp-Reach were subcloned in frame downstream of the mEGFP sequence. The cDNA for mCherry-Histone 2b was purchased from Addgene.

HEK293 cell culture

HEK293 cells were cultured in DMEM plus 10% fetal calf serum, penicillin-streptomycin and L-glutamine at 37°C and 5% CO_2. Cells were plated on coverslips coated with Poly-D-Lysine, and transient transfections were performed using Lipofectamine 2000 (Invitrogen, Carlsbad, CA), according to the manufacturer's instructions. Cells were serum starved for 2 – 4 hours prior to imaging.

To compare two cell populations transfected with different reporter constructs, cells were transiently transfected individually. In general, one group received mCherry-Histone2b as a nuclear marker in addition to the reporter constructs. 16 hours later, cells were detached using trypsin and resuspended in complete medium. Equal numbers of cells from the two groups were mixed and re-plated onto coated cover slips and imaged the next day.

Two-photon fluorescence lifetime imaging

We used a custom built Olympus 2photon microscope, with a Ti:sapphire laser (MaiTai) steered down the optical path for 2photon excitation. Excitation intensity was controlled by a Pockel's cell (Conotpics). The laser was tuned to 960 nm to excite the donor mEGFP in the AKAR5 probes. mEGFP and sREACh (or cp-sREACh) emission were initially separated using a 565 LP dichroic mirror (Chroma) and mEGFP emission was collected through a 500/40 barrier filter (Chroma). sREACh and cp-sREACh and mCherry histone-2b fluorescence were collected through a 630/92 barrier filter (Semrock). For imaging AKAR4, the laser was tuned to the peak excitation of its donor fluorophore mCerulean (860 nm) whose emission was initially separated from cp-mVenus with a 511 LP dichroic mirror (Semrock) and later collected through a 483/32 barrier filter (Semrock). cp-mVenus fluorescence emission was collected with a 550/49 barrier filter (Semrock). Laser scanning was controlled by ScanImage software (Pologruto et al., 2003). Fluorescence decay curves were measured in the time domain by comparing the arrival of the laser pulses detected by photodiode to the arrival of donor emitted photons detected by a fast photomultiplier tube using a time-correlated single photon counting board Data acquisition and analysis were performed by custom software in Matlab written and kindly provided by Ryohei Yasuda.

2pFLIM data analysis

To quantify AKAR5 phosphorylation from individual cells we used methods established previously (Lakowicz, 2007; Yasuda et al., 2006). Briefly, we assume PKA phosphorylation to be directly correlated to the mEGFP and mCerulean fluorescence lifetimes in both the AKAR5 and AKAR4 sensors. To measure the fluorescence lifetimes we calculate the mean photon emission time (lifetimes) from a region of interest (ROI) encompassing the cytosolic fraction of individual cells for cyt-AKAR5 and AKAR4 expressing cells and from and ROI encompassing plasma membrane compartment of pm-AKAR5 expressing cells (Lakowicz, 2007; Yasuda et al., 2006). Because multiple populations of binding states exist within our sensor (i.e. resting state with low FRET, resting/activated state with no FRET due unfolded acceptor, and the activated state with high FRET) we cannot adequately determine a binding fraction of our sensor as the donor decay will be represented by >2 exponents and we are not collecting the requisite amount of photons. We therefore report the mean photon arrival time of the donor and acknowledge the fact that it will deviate from the actual fluorescence lifetime of the donors.

Definition of resting and Δlifetimes

We define resting lifetimes as the average lifetime of individual cells prior to the addition of exogenous stimulus. In some experiments we did not add PKA activators, such as when only measuring resting PKA phosphorylation (see **Figures 3 & 4)**. In these cases, resting lifetime is determined on a cell to cell basis from single 2pFLIM images. Delta lifetimes were determined by subtracting the average resting lifetime (determined as the mean of all data points prior to drug application) from every individual data point. In this case larger Δlifetimes are indicative of greater net PKA phosphorylation.

Acceptor bleed-through and folding measurements

As stated in the results section, fluorescence from the acceptor fluorophore can influence the measured lifetime in the donor detection channel. The amount of this influence will depend upon what fraction of the detected fluorescence in the green lifetime is represented by the acceptor. Because the fluorescence emission of EGFP overlaps with

sREACh, some of this contamination will be unavoidable. We therefore sought to quantify the contribution of acceptor fluorescence to the total signal detected in the donor lifetime channel. To measure this contribution we used methods established by Murakoshi et al, 2008. Briefly, we created tandem constructs containing sREACh or cp-sREACh fused to the fluorescent protein mKeima (Kogure et al., 2008) via the long linker sequence (SGLRSRAQASNSAVDGTAGPGSG). The tandem constructs provide a fluorescent ratio to control for differences in absolute expression of sREACh and cp-sREACh. mKeima was specifically used because of its long (~180 mm) stokes shift, allowing us simultaneously excited the sREACh variants and mKeima with 960 nm excitation and detect sREACh fluorescence in the green channel and mKeima almost solely in the red channel (mKeima fluorescence maximum = 620 nm). The green to red fluorescence ratio of these constructs measured across many cells (n > 150) was then normalized to the green to red fluorescence ratio of an mEGFP—mKeima tandem construct (n = 205 cells) containing the same linker sequence (note that mEGFP bleed-through into the red detection channel (~0.3%) was corrected for). This value provides us with a normalized measure (to mEGFP) of the contribution of sREACh and cp-sREACh fluorescence into the green detection channel which we refer to as relative fluorescence intensities in Supplementary Figure 1a.

For folding efficiency measurements we transfected cells with the tandem construct mEGFP-sREACh or mEGFP-cp-SREACh. We used the short linker sequence (VDGTAGPGSG) found in Murakoshi et al. 2pFLIM images of cells transfected with the tandem constructs and the weights from double exponential fits of the lifetime decay from individual cells were used to determine the binding fraction (i.e. % of mEGFP coupled with a functional sREACh or cp-sREACh) as described in Murakoshi et al.

Determining relative level of sensor expression across cells

To determine the level of sensor expression across cells we measured the average green fluorescence emission (mean photon counts) in the cytosolic portion of the cell for cyt-AKAR5 and in the plasma membrane region of the cell for pm-AKAR5. For the cyt-AKAR5 expressing cells we used the same power (measured daily at the back focal plane) and thus variation in average cell intensity will be directly proportional to the amount of

sensor with a functional donor fluorophore. The pm-AKAR5 experiments were carried out with varying amounts of power at the back focal plane of the objective. In these conditions measurements of mean photon counts from cells across distinct platings were normalized to one another by assuming a quadratic power dependence of emission on the intensity of excitation at the back focal plane. In the text and figures we refer to this value at normalized sensor expression (norm sensor expression).

Cyt-AKAR5 Forskolin + IBMX induced Δlifetime correction

In **Supplementary Figure 5** we corrected the amplitude of the F + I induced Δlifetimes for variations in the relative levels of sensor expression using the exponential fit shown in the middle panel of **Figure 2c**. To do so we took the ratio of the mean Δlifetime of the exponential fit (0.1923) to the Δlifetime at any given value of mean photon counts as predicted by the fit. On average, this ratio will be > 1 for cells expressing relatively low levels of sensor and < 1 for cells expressing relatively high levels of sensor. We then take the product of this ratio and the measured Δlifetime from each cell as a measure of the adjusted Δlifetime.

Chapter 2. Supplementary Information

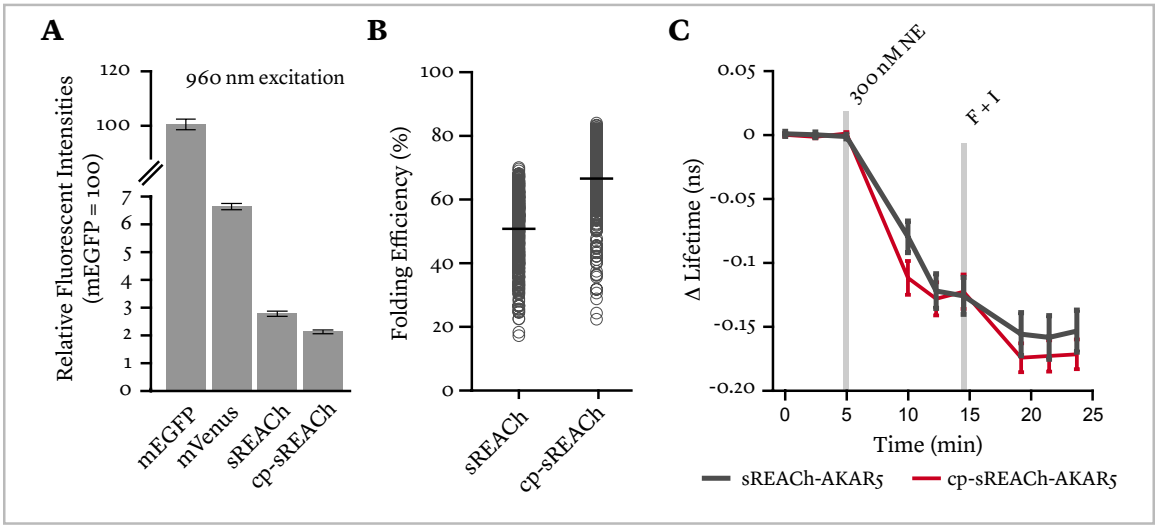

SUPPLEMENTARY FIGURE 1. COMPARISON OF SREACH AND CP-SREACH FOR USE AS THE ACCEPTOR IN AKAR5.

(A) Quantification of the relative fluorescence intensities (bleed-through into green FLIM channel) for mVenus (6.6%, n = 193), sREACh (2.8%, n = 183 cells) and cp-sREACh. (2.1%, n = 2005 cells) All data are normalized to bleed-through corrected mEGFP (n = 226) fluorescence intensity. Data are represented as mean +/- s.e.m. **(B)** Comparison of folding efficiency for sREACh and cp-sREACh. sREACh (n = 361 cells) has a median folding efficiency of ~53% and cp-sREACh (n = 316 cells) a median folding efficiency of ~68%. Open gray circles represent individual cells. Black line represents the mean. **(C)** Time course of sREACh-AKAR5 (dark gray, n = 22 cells) and cp-sREACh-AKAR5 (red, n = 29 cells) responses to 300 nM NE and 20 μM forsk + 100 μM IBMX. Data are represented as the mean and s.e.m. of the Δlifetime (ns) of the sensors.

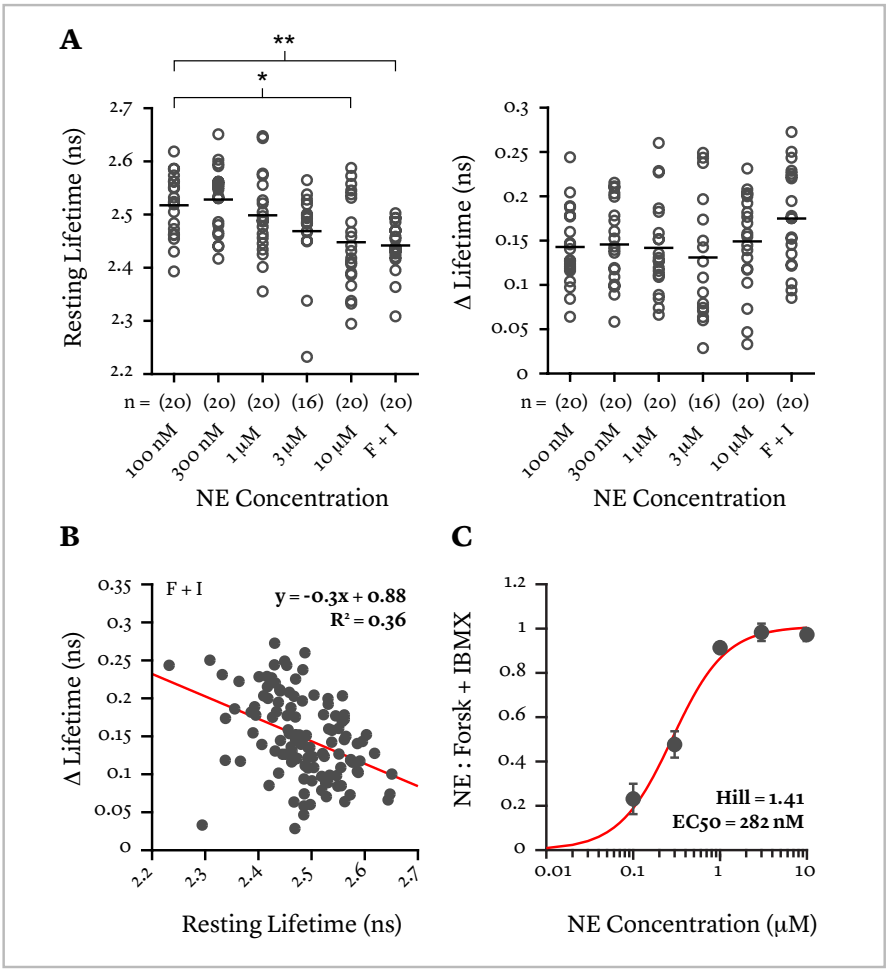

SUPPLEMENTARY FIGURE 2. AKAR4 SUMMARY.

(A) Left panel, boxplot of resting lifetimes as a function of individual doses of NE. F + I indicates Forskolin + IBMX alone treatment (n = 20, 20, 20, 20, 20, 16). Right panel, boxplot of the F + I induced response as a function of individual does of NE. No significant differences exist between doses (n = 20, 20, 20, 20, 20, 16). Gray circles represent individual cells. Black line represents the mean. * = $p < 0.05$ and ** = $p < 0.01$ as determined by 1-way ANOVA and Turkey's post hoc test. **(B)** Scatter plot of the F + I induced Δlifetime as a function of the resting lifetimes. Dark gray dots represent individual cells and red line is a linear fit to the data (n = 116) **(C)** Plot of the ratio of NE to Forskolin/IBMX induced response as a function of NE concentration. Dark gray dots represent mean +/- s.e.m. (n= 20 cells / NE dose). Red line is the data fitted with the Hill equation.

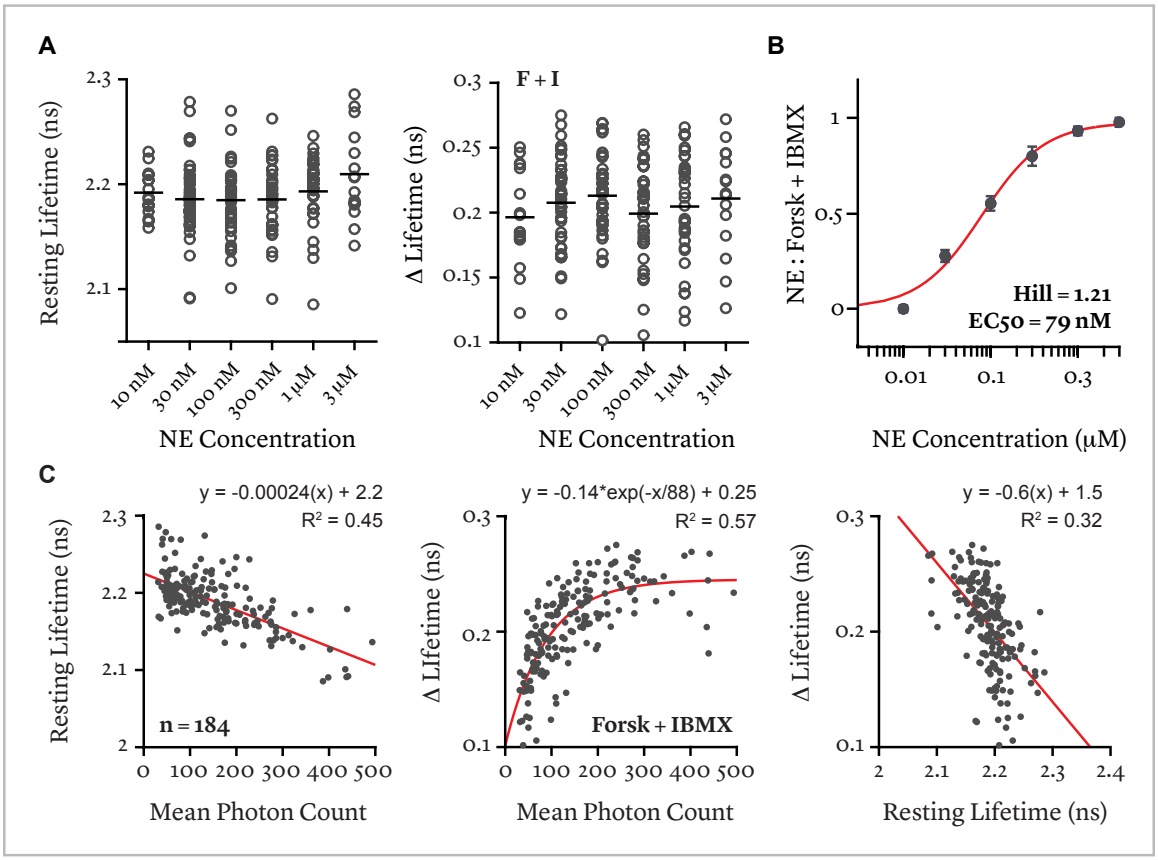

SUPPLEMENTARY FIGURE 3. SREACH-AKAR5 SUMMARY.

(A) Left panel, resting lifetimes as a function of individual doses of NE (n = 17, 45, 37, 37, 33, 15). No significant difference exists between groups. Right panel, F + I induced response (Δlifetime) as a function of individual doses of NE. No significant difference exists between doses (n = 17, 45, 37, 37, 33, 15). Gray circles represent individual cells. Black line represents the mean. **(B)** Plot of the ratio of NE to F + I induced response as a function of NE concentration. Dark gray dots represent mean +/- s.e.m. Red line is the data fitted with the Hill equation. **(C)** Same data as presented in Figure 2 for additional comparison.

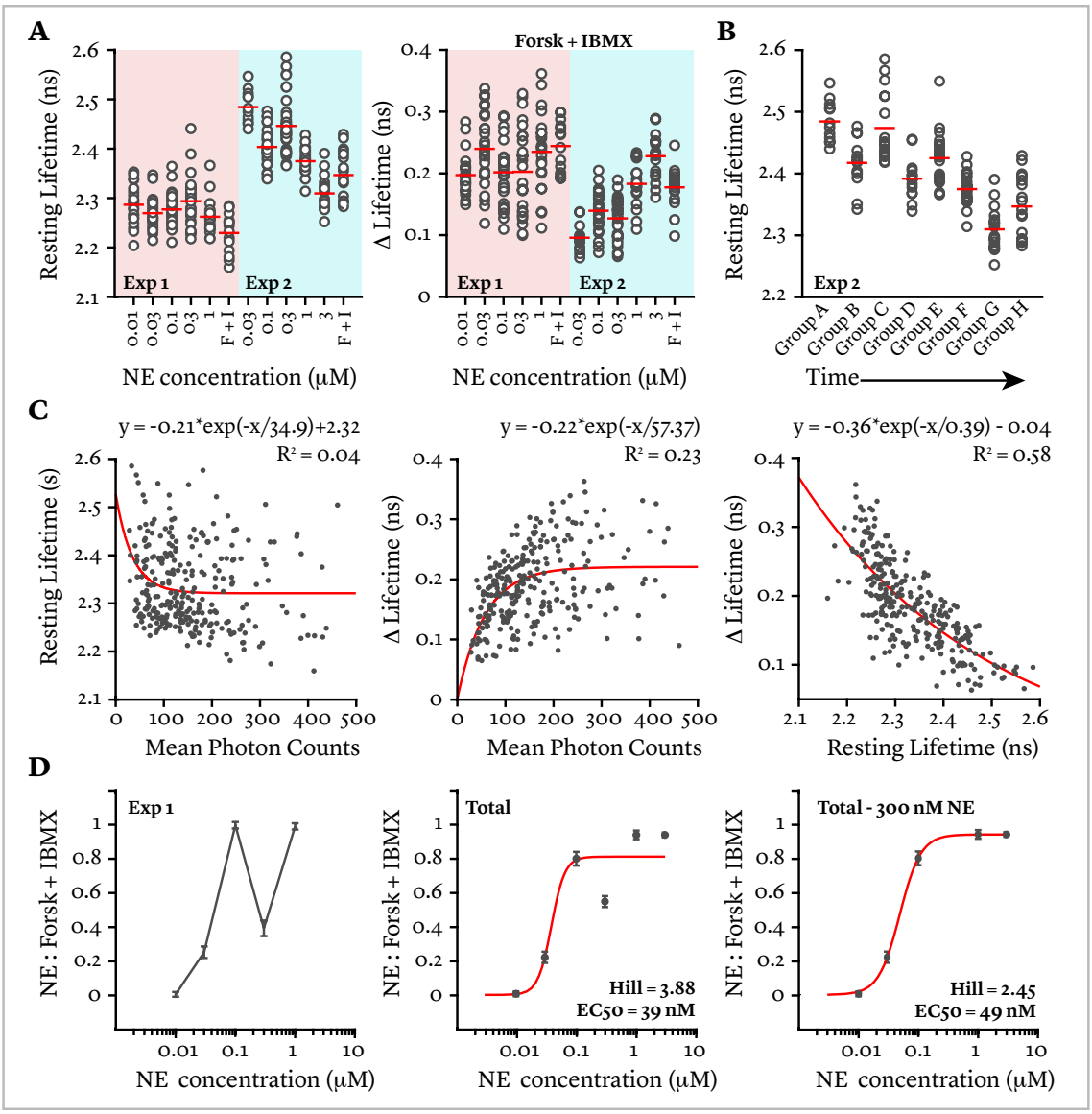

Supplementary Figure 4. cp-sREACh-AKAR5 summary.

(A) Left, resting lifetimes as a function of NE doses across 2 days of experiments. The resting lifetimes of the 1st day were consistent with a mean and standard deviation of 2.27 +/- 0.02 ns. The 2nd day lifetimes were higher in absolute value (mean & s.d. = 2.39 +/- 0.06 ns) and more variable throughout the day. Right, amplitude of the F + I induced responses. The 2nd day's (mean & s.d. = 0.16 +/- 0.05 ns) were much shorter and more variable than the first day (mean & s.d. = 0.22 +/- 0.02 ns) **(B)** Plot of the resting lifetimes for the 2nd day experiments as a function of time. The lifetimes decrease over time may be indicative of continued folding and maturation the acceptor. **(C)** Plots of resting lifetimes as a function of Mean Photon Counts (MPC, left), F + I response v. MPC (middle), and the F + I induced Δlifetimes as a function of resting lifetimes. Red line is exponential fit. n = 276 cells. **(D)** NE:F + I dose response curves for Exp 1 (left panel), total cells (middle) and total cells w/out the 300 nM NE response (Hill coefficient = 2.45, EC50 = 49 nM).

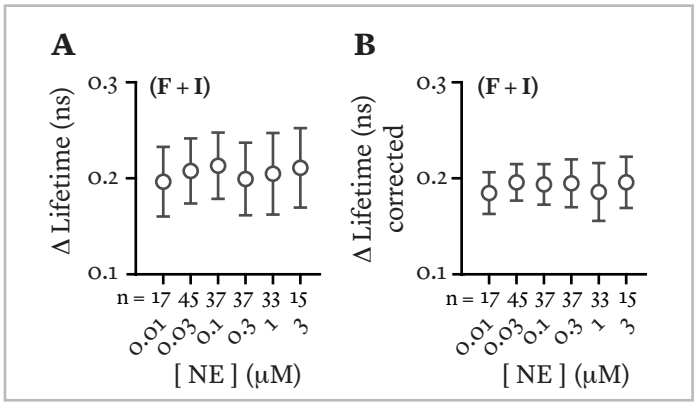

SUPPLEMENTARY FIGURE 5. FORSKOLIN + IBMX INDUCED PKA PHOSPHORYLATION IS INDEPENDENT OF PRIOR NE EXPOSURE.

(A) Comparison of the F + I induced Δlifetimes of the cyt-AKAR5 sensor across prior doses of NE. Open circles represent the means. Whiskers represent the standard deviation No significant differences exist across NE treatments **(B)** Comparison of F + I induced Δlifetimes adjusted for differences in sensor expression using the exponential fit in the middle panel of **Figure 2c** (see Methods). No significant differences exist amongst the group. Note that the width of the standard deviations are decreased upon adjustment.

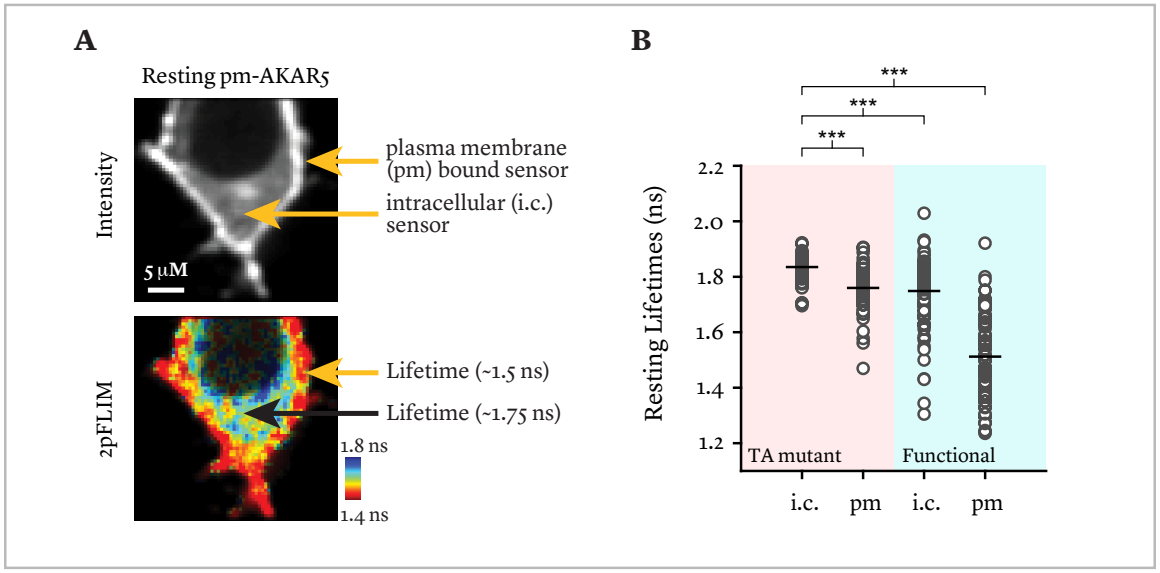

SUPPLEMENTARY FIGURE 6. COMPARING RESTING PHOSPHORYLATION PROFILES OF THE FUNCTION AND PHOSPHOR DEFICIENT PM-AKAR5 SENSORS.

(A) Top panel, 2photon fluorescence intensity image of a cell expressing the functional pm-AKAR5 sensor. Top arrow points to sensor found in the plasma membrane compartment of the cell. Bottom arrow points to sensor located in the interior of the cell. The relative brightness of the 2 components indicates that the highest concentration of sensor is found on the plasma membrane. Lower panel, 2pFLIM image of the cell found in the upper panel. Lifetime color bar found in lower right hand corner. The lifetime of the plasma membrane component of the example cells is ~ 1.5 ns and the intracellular component is ~ 1.75 ns. **(B)** Population data for the intracellular (i.c.) and plasma membrane (pm) components for the phospho-deficient pm-AKAR5^{TA} (TA mutant, n = 90) and the functional pm-AKAR5 (Functional, n = 90) sensors. Open gray circles represent individual cells. Black line represents the mean. *** = $p < 0.001$ based on ANOVA-1 and Turkey's post hoc test.

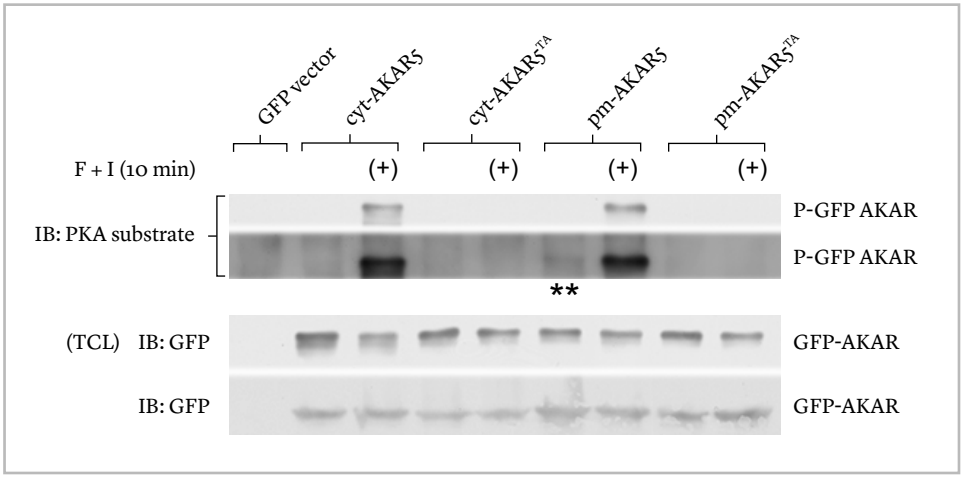

SUPPLEMENTARY FIGURE 7. WESTERN BLOTS CONFIRM THE RESTING PHOSPHORYLATION REPORTED BY THE PM-AKAR5 SENSOR.

Western blot of GFP immunoprecipitated cyt-AKAR5 and pm-AKAR5 sensors from HEK293 cells untreated or treated for 10 min with F + I (+). Top two rows are the GFP immunoprecipitated product probed with the general PKA phopho-substrate antibody. The 2nd, higher exposed, row shows PKA phosphorylation in untreated pm-AKAR5 expressing cells (**). No phosphorylation was detected in untreated cyt-AKAR5 expressing cells. Both sensors responded to F + I whereas the phospho-deficient (TA) sensors did not. The bottom two rows show the GFP blot for total sensor amount in each condition, with total cell lysate (TCL) on top and the immunoprecipitated product on bottom. The left most column of all rows represents the GFP vector only control.

Chapter 3.

The role of N-terminal myristoylation in the maintenance of PKA phosphorylation gradients at the plasma membrane

Shane E. Tillo[1,], Maho Takahashi[1,], Maozhen Qin[1], Philip J.S. Stork[1], & Haining Zhong[1]

1. Vollum Institute, Oregon Health & Science University, Portland, OR USA

Foreword

The PKA sensor work used in this chapter was performed using sensors developed by Dr. Maho Takahashi and Dr. Phil Stork. Dr. Adriana Andrade assisted in gathering the preliminary AKAR5 data in neurons. Dr. John Adelman recommended the majority of the western blot experiments presented in Figure 2. All hippocampal slice preparations were done by Dr. Maozhen Qin and Dr. Guan Yang. The rest of the experiments, all data analysis and figure preparation were done by me.

Abstract

The cAMP protein dependent kinase A (PKA) is ubiquitous enzymatic mediator of cellular signaling. Despite its many targets, PKA phosphorylation exhibits a remarkable level of specificity. In neurons, PKA activation by a given neuromodulator can lead to the biasing of phosphorylation to a distinct set of PKA's potential targets. This specificity is established at least in part by A-kinase anchoring proteins (AKAPs), which target the PKA holoenzyme, its upstream activators, and downstream targets, within the same molecular vicinity. Upon elevations in cAMP concentration, a subset of PKA catalytic molecules are released, and must diffuse short distances to phosphorylate their target. Though greatly beneficial, AKAP targeting of PKA alone cannot fully explain signaling specificity, as a fraction of activated PKA molecules will rapidly vacate the established molecular vicinity. Here we confirm the existence of a PKA signaling compartment in the plasma membrane of HEK293 cells and in CA1 hippocampal neurons. We investigate the role that N-terminal myristoylation of the PKA catalytic subunit plays in biasing PKA phosphorylation to toward that compartment. We find that myristoylation imparts plasma membrane affinity to the activated PKA catalytic subunit, targeting it to the plasma membrane, thereby hindering its mobility and increasing local PKA phosphorylation in the plasma membrane subcellular compartment.

Introduction

At rest, the cAMP dependent protein kinase A (PKA) exists as a holoenzyme and consists of a dimer of regulatory subunits (PKA-reg), that bind and render immobile, two PKA catalytic subunits (PKA-cat) (Gill and Garren, 1971; Kim et al., 2005). Upon elevations in cellular cAMP, the regulatory subunits are bound by cAMP resulting in the release of the catalytic subunit. Subcellular targeting of the PKA holoenzyme is mediated by A-kinase anchoring proteins (AKAPs), which bind to and distribute PKA regulatory subunits in a non-random manner throughout the cell through their binding to various effector proteins such as ion channels, membrane receptors, or cytoskeletal elements, to name a few (Wong and Scott, 2004). In addition to anchoring the regulatory subunit, AKAPs also function to anchor PKA activators such as GPCRs, PKA substrate, and PKA inhibitors, and in doing so, create spatially distinct PKA signaling hubs (Beene and Scott 2007). For instance, neurotransmitters that initiate PKA signaling — i.e. norepinephrine (NE), dopamine, calcium, etc — impinging on these hubs has been shown to lead to the local production of cAMP (Dodge-Kafka et al., 2005), the subsequent local activation of PKA holoenzyme, and the efficient phosphorylation of local targets potentially at the expense of phosphorylation in other AKAP established compartments. Abound in the literature are examples of AKAP-mediated PKA signaling complexes, in a myriad of cell types, whose function is necessary for the efficient phosphorylation of downstream targets (Colledge et al., 2000, Davare et al., 2001, Few et al., 2007).

The abundance of literature on AKAPs strongly indicates that they play an integral role in confining PKA phosphorylation over space and time. However, given the diffusive nature of the catalytic subunit (Kopperud et al., 2002), AKAPs alone cannot explain PKA signal biasing, and their primary function may be to place PKA in the vicinity of cAMP microdomains (Kim et al., 2011) thereby ensuring efficient activation of the PKA holoenzyme. Such diffusion may have profound implications on PKA specificity, especially in synaptic compartments where the length scale is small, such as in neuronal dendrites and spines (~1 μm). Consider, for instance, that a freely diffusing protein of comparable size to PKA-cat will equilibrate within dendritic spines on the order of a 100 ms (Sabatini et al.,

2002) and exit spines in 0.2–0.4 s (Svoboda et al., 1996; Bloodgood and Sabatini, 2005), much faster than what is thought to be a relevant timescale for PKA signaling (Zhang et al., 2001; Lancaster et al., 2006; Gervasi et al., 2007). Such rapid equilibration would be expected to break down the AKAP established PKA specificity and additional mechanisms must be present to maintain that specificity (Kim et al., 2011; Oliveira et al., 2012).

One potential mechanism to limit PKA phosphorylation, and provide the necessary additional brakes on the system, would be a decreased mobility of the activated catalytic subunit. Constraining the mobility of PKA-cat would serve to increase local compartment phosphorylation at the expense of phosphorylation in neighboring AKAP-established PKA signaling hubs. Notably, the N-terminus of the PKA catalytic subunit in myristoylated (Carr et al., 1982), providing a potential mechanism for insertion into membranes (Boutin, 1997). Membrane insertion would limit catalytic diffusion to the two-dimensional surface of membranes and slow down diffusion due to the higher viscosity of membranes compared to the cytosol. However, structural investigations of the PKA catalytic subunit reveal the N-terminal myristoylation domain tucked into a hydrophobic core of the enzyme. Denaturing studies suggest that the function of this arrangement is to increase the thermal stability of the catalytic subunit (Zheng et al., 1993; Yonemoto et al., 1993). In another study, N-terminal myristoylation was shown to increase the affinity of only the RIIβ holoenzyme as shown through a FRET-based liposomal binding assays (Gangal et al., 1999). These observations have limited the investigation for the role of myristoylation in compartmentalizing the activated PKA catalytic subunit, and the focus has remained primarily on the study of AKAPs role in establishing PKA compartmentalization through its interaction with the regulatory subunit.

Recently, it has been shown the N-terminal myristoylation can enhance the membrane affinity for the freed PKA catalytic subunit, indicating that in the presence of membranes, the N-terminal domain is exposed to and binds the hydrophobic pockets of membranes (Gaffarogullari et al., 2011). This observation offers several predictions for the behavior of the activated PKA catalytic subunit. First, myristoylation should target PKA to the plasma membrane in cells and serve to enhance phosphorylation in membrane

compartments. Second, PKA should diffuse slower than expected for a protein of its size and loss of myristoylation should increase its mobility. Here we confirm the establishment and maintenance of a PKA signaling hub in the plasma membrane compartment of HEK293 cells using a variety of approaches. Furthermore, we show that in dendritic spines of rat CA1 hippocampal neuron, the activated catalytic subunit moves significantly slower than expected given its prediction as a soluble protein, and that this slow mobility is partly due to N-terminal myristoylation.

Results

Gradients of PKA phosphorylation in CA1 hippocampal neurons

In previous studies (see Chapter 2) we used optical reporters of PKA phosphorylation to establish the idea that a gradient of PKA phosphorylation emanates from the plasma membrane of HEK293 cells. We wondered —given the stark differences in HEK293 and neuronal morphology — if and to what extent the PKA plasma membrane phosphorylation gradient existed in the dendrites of CA1 hippocampal neurons. We confirmed the presence of this gradient using 2pFLIM measurements from the PKA phosphorylation sensors described in Chapter 2**.** The left panel of **Figure 1a** is an example 2p fluorescence intensity image of a rat CA1 hippocampal neuron co-expressing the pm-AKAR5 sensor and the soluble marker dsRed. On the right is a fluorescence intensity profile for the dashed white line crossing the major apical dendrite. The majority of pm-AKAR5 is located on the plasma membrane and has a membrane index of ~ 3 (see Methods and **Figure 4**). **Figure 1b** is the corresponding example 2pFLIM images of the neuron found in panel A during resting conditions and after treatment with 300 nM NE and Forsk + IBMX. Note that the plasma membrane experiences higher PKA phosphorylation than the interior of the apical dendrite as indicated by the darker red pseudo-coloring. The lifetime color bar is found on the lower right of the last image. An example 2pFLIM image series for a cyt-AKAR5 expressing CA1 neuron is found in **Figure 1c**.

The summary results comparing the NE and Forsk + IBMX induced Δlifetimes of the sensors across the different neuronal compartments are shown in **Figure 1d**. On the left is the response of the cyt-AKAR5 sensor (n = 3, data shown as mean +/- s.d.). The time of drug application is indicated by the grey bars. On the right is the response of the pm-AKAR5 sensor in the same neuronal compartments (n = 3, data shown as mean +/- s.d.). Like in HEK293 cells, NE induced PKA phosphorylation is higher at the plasma membrane as indicated by the larger NE induced Δlifetime for the pm-AKAR5 sensor (0.17 +/- 0.02 ns) compared to the cyt-AKAR5 sensor (0.064 +/- 0.012 ns).

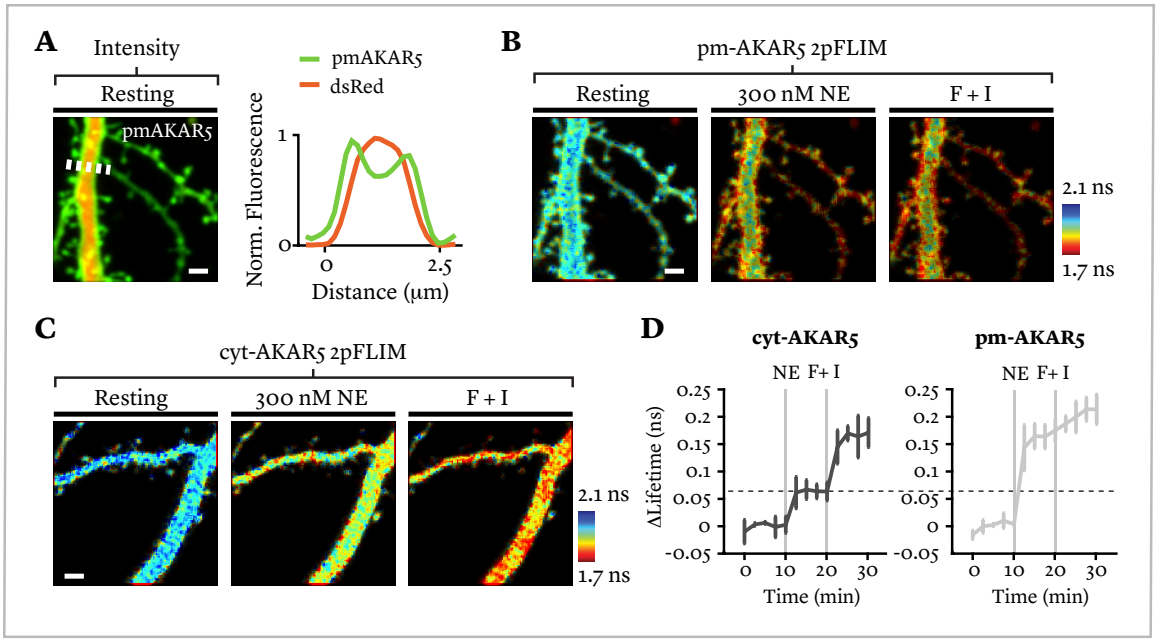

FIGURE 1. PKA PHOSPHORYLATION GRADIENTS IN CA1 HIPPOCAMPAL NEURONS.

(A) Left, 2photon fluorescence intensity image of a neuron co-expressing the pm-AKAR5 sensor and the soluble marker dsRed. Scale bar = 2 μm. Right, pm-AKAR5 (green) and dsRed (red) fluorescence intensity profiles from the dashed white line found in the image. **(B)** 2pFLIM image series of the neuron found in panel A, in resting conditions and after treatment with 300 nM NE and F + I. Lifetime color bar found to the right. **(C)** 2pFLIM image series of a CA1 neuron expressing the cyt-AKAR5 sensor in resting conditions and after treatment with 300 nM NE and F + I. Lifetime color bar found to the right. **(D)** Summary data of the Δlifetime response of the indicated sensor (cyt_AKAR5 left, pm-AKAR5 right). Data are shown as mean +/- s.d. Grey bars indicate time and type of drug application. The gray dashed line is placed at the response amplitude of the cyt-AKAR5 sensor to NE for easy comparison to the pm-AKAR5 sensor NE induced response. The cyt-AKAR5 sensor (n = 3) has a Δlifetime response of 0.064 +/- 0.012 ns to NE and an F + I induced Δlifetime response of 0.169 +/-0.03 ns. The pm-AKAR5 sensor (n = 3) reports NE induced Δlifetimes of 0.17 +/- 0.02 ns in spines. and an F + I induced Δlifetimes response of 0.21 +/- 0.02 ns. All scale bars = 2 μm.

Verification of PKA phosphorylation gradients using biochemical approaches

In the previous section we the AKAR5 sensor to confirm the existence of a plasma membrane gradient of PKA phosphorylation in CA1 hippocampal neurons. We next aimed to investigate the the same phenomenon using another set of otherwise identical substrates with well described PKA phosphorylation sites and phospho-specific antibodies. For the plasma membrane target we used the full-length AMPA subtype glutamate receptor (GluR1) and its intracellular C-terminal tail (GluR1-c) alone as a cytosolic target. In neurons, PKA

phosphorylation of GluR1 on its C-terminal tail at a serine residue at position 845 (S845) influences channel open time, trafficking, and synaptic strength. GluR1 S845 has also been shown to be phosphorylated in an AKAP dependent manner when heterologously expressed in COS7 cells (Colledge et al., 2000). We also created a tandem construct in which GluR1-c is tethered to membranes via its genetic fusing to the hCD4 single transmembrane domain (Zhong et al., 2003). All constructs were tagged with EGFP for visualization of their cellular distribution.

To detect the amount of expression of each construct, we used an antibody directed to the C-terminal tail of GluR1 that is present in each construct. To detect GluR1 and GlurR1-c phosphorylation we use an antibody directed to the phosphorylated S845 residue, which is also present in each construct. The constructs and antibodies used are illustrated in the upper panel of **Figure 2a**. The lower panel of **Figure 2a** is a series of 2photon fluorescence intensity images of cells expressing the constructs found above each image. EGFP-GluR1 is distributed to the plasma membrane and to the interior of the cells, where it is presumably located on intracellular membrane compartments. EGFP-GluR1-c is distributed uniformly throughout the cytosol and also resides in the nucleus. hCD4-EGFP-GluR1-c is primarily located on the plasma membrane, with a small fraction located in the cell interior. **Figure 2b** shows example western blots of control (unstimulated) cells, cells treated with 1 μM NE, Forsk + IBMX, and cells treated with Forsk + IBMX and 10 μM of the ATP competitive PKA phosphorylation inhibitor H89 (Hidaka and Kobayashi, 1992). Whereas the membrane bound full-length GluR1 construct shows robust phosphorylation of S845 (left), the purely cytosolic C-terminal tail does not (middle). In fact, we could only detect phosphorylation of GluR1-c in conditions of over-expression of the PKA holoenzyme (see **Figure 3**), suggesting the presence of mechanisms to restrict PKA phosphorylation to the membrane. Tethering GluR1-c to the plasma membrane via the hCD4 single transmembrane domain (right) rescues the S845 phosphorylation. **Figure 2c** shows the population data for our western blot experiments, quantified as the ratio of the integrated fluorescence intensity of the S845 phosphorylation band to the integrated fluorescence intensity of the total GluR1-c band (see Materials and Methods). Data are presented as mean +/- s.e.m.

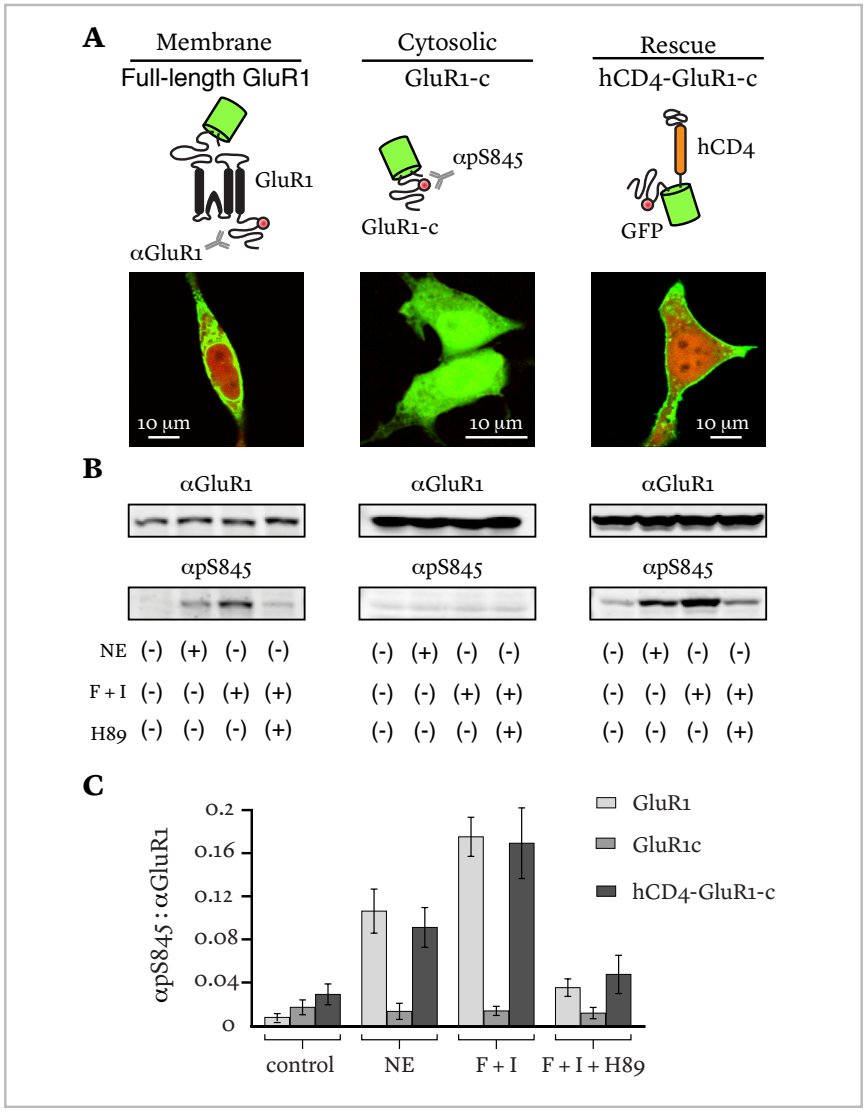

FIGURE 2. PKA PREFERENTIALLY PHOSPHORYLATES MEMBRANE BOUND SUBSTRATE.

(A) Upper row, illustrations of the constructs and antibodies used in the experiment. All constructs contain EGFP in the indicated position. Lower row, 2photon fluorescence images of HEK293 cells expressing the constructs found directly above them. Cells expressing full-length GluR1 and hCD4-GluR1-c also co-expressed tdTomato-GluR1-c as a soluble marker for comparison. **(B)** Example western blots from cell lysates of the conditions found in A. Total GluR1 is detected via an antibody targeting the GluR1 C-terminal tail found in all constructs (αGluR1). Phosphorylated GluR1 is detected via an antibody that recognizes a PKA specific phosphorylation on GluR1-c (αpS845). Cells were either untreated, treated with 1 µM NE, F + I or F + I + 10 µM H89. **(C)** Summary data for GluR1 (n = 5), GluR1-c (n = 4) and hCD4-GluR1c (n = 5). Data are presented as mean +/- s.e.m.

The following supplemental figures are associated with Figure 2.

SUPPLEMENT FIGURE 1: DISTRIBUTION OF GLUR1 CONSTRUCTS IN HEK293 CELLS

N-terminal myristoylation of PKA-cat enhances the plasma membrane gradient of PKA phosphorylation

The differences in PKA phosphorylation between the plasma membrane and cytosol — detected optically with the AKAR5 sensor (see also Chapter 2) and biochemically using modified GluR1 constructs — indicate that PKA phosphorylation is more probable close to the plasma membrane than away from it. This result may be somewhat unexpected given the mobility of PKA-cat. We therefore wondered if N-terminal myristoylation of PKA-cat could provide a mechanism, independent of AKAPs, for the maintenance of the observed PKA phosphorylation gradient. Though crystal structures of the purified catalytic subunit show the myristoylation domain tucked into a hydrophobic pocket of the enzyme (Yonemoto et al., 1993; Yang et al., 2004), recent studies have hinted that it may play a role in imparting membrane affinity to the activated catalytic subunit (Gaffarogullari et al., 2011), as it does with other known signaling molecules (Vaandrager et al., 1998; Tzingounis et al., 2007). Conversion of the N-terminal glycine residue to alanine prevents myristoylation of the catalytic subunit without affecting its catalytic potency or its ability to associate with the PKA regulatory subunit (Clegg et al., 1989). We utilized this mutation to compare the membrane phosphorylation capabilities of myristoylated PKA-cat (wtPKA-cat) and non-myristoylated PKA-cat (nmPKA-cat).

HEK293 cells were transfected with cDNA encoding wtPKA-cat or nmPKA-cat along with a two fold excess of the RIIβ PKA regulatory subunit (PKA-reg) cDNA, membrane bound full-length Glur1 (EGFP-GluR1) cDNA, and the purely cytosolic GluR1-c (EGFP-GluR1-c) cDNA. Illustrations of the constructs and antibodies used are shown in **Figure 3a**. We treated the cells with either 1 μM NE or F + I for 5 minutes, lysed the cells, and probed for total GluR1 and GluR1 S845 phosphorylation. We compared the results to untreated cells expressing the same constructs. **Figure 3b** shows 2 example western blot experiments for the conditions described above. On the left is two separate transfections for wtPKA-cat (first 6 lanes) and on the right is two separate transfections for cells expressing nmPKA-cat (last 6 lanes). Note that we also probed for levels of endogenous and over-

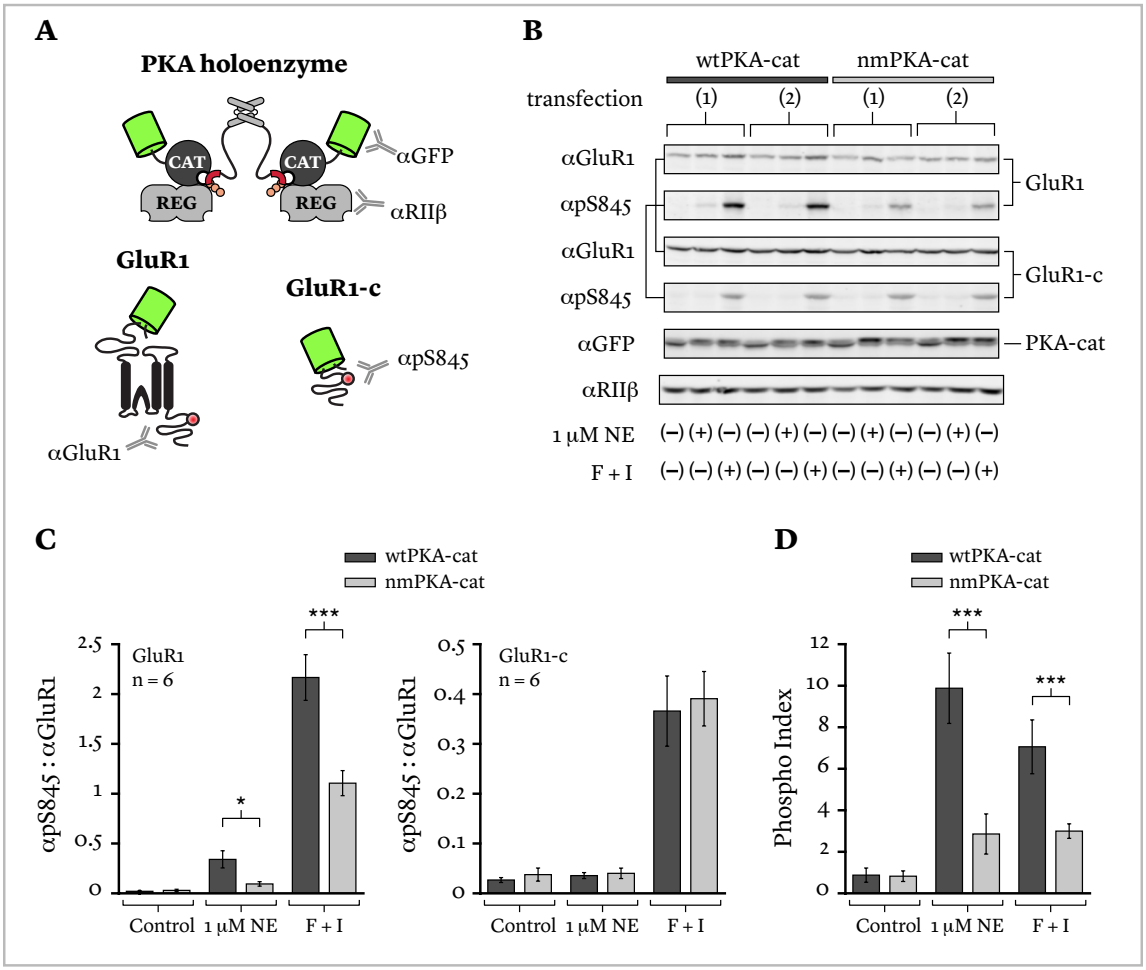

FIGURE 3. N-TERMINAL MYRISTOYLATION OF PKA-CAT CONTRIBUTES TO THE MAINTENANCE OF A PKA PHOSPHORYLATION GRADIENT.

(A) Illustration of the constructs and antibodies used in the experiment. HEK293 cells were transiently transfected with the PKA-r RIIb subunit (REG), a GFP tagged PKA-cat (CAT), full-length GFP tagged GluR1, and the C-terminal tail of GluR1 tagged with GFP (GluR1-c). **(B)** Example western blots from HEK293 cells expressing the constructs in panel A for control cells, cells treated with 1 μM NE or F + I. The left portions of the gels represent 2 separate wtPKA-cat transfections (lanes 1 – 6).The right represents 2 separate nmPKA-cat transfections. The antibodies used are shown to the left of each gel. **(C)** Summary data of the pS845 (αpS845) levels normalized to total GluR1 (αGluR1), for GluR1 (left) and the GluR1-C fragment (right). Data for wtPKA-cat are shown in dark gray and nmPKA-cat are shown in light gray. Data are represented as mean +/- s.e.m. * = $p < .01$ and *** = $p < 0.001$ as determined by Student's T-test. **(D)** Phospho-indexes for wtPKA-cat and nmPKA-cat in control, 1 μM NE, and F + I treatment conditions. *** = $p < 0.001$ as determined by Students T-test.

expressed PKA-reg (αReg), and for levels of over-expressed PKA-cat using an anti-GFP antibody (αGFP) targeted to the GFP label on the over expressed PKA-cat.

Levels of phosphorylated S845 for the soluble C-terminal fragment of GluR1 (GluR1-c) were nearly identical for both wtPKA-cat and nmPKA-cat. This observed phosphorylation of GluR1-c is in contrast to Figure 2 where we observed little to no phosphorylation. Presumably, this gain-of-function results from the overexpression of the PKA-cat holoenzymes and their saturation of regulatory mechanisms that prevent phosphorylation of GluR1-c in non-overexpression conditions. In contrast to the C-terminal fragment, wtPKA-cat was significantly more effective at phosphorylating the membrane bound full-length GluR1 (GluR1, see arrowheads **Figure 3b**) than nmPKA-cat. **Figure 3c** shows the summary results of the experiment for 6 separate transfections for wtPKA-cat and nmPKA-cat. All data are presented as mean +/- s.e.m. The left panel shows the amount of S845 phosphorylation normalized to total full-length GluR1 in control, untreated conditions, 1 μM NE stimulation, and F + I stimulation for wtPKA-cat (light blue) and nmPKA-cat (dark blue). S845 phosphorylation levels were greater for both NE stimulated and F + I stimulated PKA phosphorylation. The right panel of Figure 3c shows the amount of S845 phosphorylation for the soluble C-terminal fragment of GluR1 (GluR1-c). No difference was detected in s845 phosphorylation levels. To get a measure of the membrane phosphorylation preference relative to the cytosol we take the ratio of normalized GluR1 phosphorylation to normalized GluR1-c phosphorylation and define this ratio at the phospho-index. **Figure 3d** shows the phospho-index for wtPKA-cat and nmPKA-cat in control and NE and F + I stimulated cells. The phospho-indexes indicate that wtPKA-cat has roughly a 10-fold preference for membrane phosphorylation during NE stimulation and a 7-fold preference during F + I stimulation. The membrane phosphorylation preference for nmPKA-cat is significantly lower for both NE and F + I stimulation (~ 3-fold for both).

N-terminal myristoylation imparts membrane affinity to PKA-cat

To investigate the ability of N-terminal myristoylation to target PKA-cat to the plasma membrane in neurons, we imaged the spatial distribution of wtPKA-cat and nmPKA-cat tagged with EGFP in larger caliber (~ 2 μm in diameter) apical dendrites of CA1

hippocampal neurons prior to activation of the PKA holoenzyme (resting conditions) and after activation via F + I in the same cells. Again, in an attempt to buffer the over-expression of EGFP-PKA-cat we co-expressed a two-fold excess of the RIIb PKA regulatory subunit along with the soluble fluorophore dsRed as a label of neuronal morphology. To quantify the relative distributions of PKA-cat in dendrites, we first determined the plasma membrane location on a dendrite with a diameter of 2 μm given the width of our imaging beam point spread function (PSF, 450 nm, see **Supplementary Figure 2**). In the images, we approximate the plasma membrane to be at 30% the value of the maximal dsRed fluorescence. Upon activation of the PKA holoenzyme, membrane targeting of PKA-cat should be reflected as an increase in the green (EGFP-PKA-cat) to red (soluble dsRed) fluorescence ratio at the membrane ($GR_{membrane}$) and a decrease of that ratio in the center (GR_{center}) of the dendrite. We therefore, measure the ratio of $GR_{membrane}$ to GR_{center} in both the resting and F+I induced states and use the change in this ratio to compare the abilities of wtPKA-cat and nmPKA-cat to target the membrane upon activation. We define this value as the plasma membrane index, where a value of 1 indicates uniform PKA-cat distribution in the cytosol, a value < 1 indicates anchoring in the interior of the dendrite, and a value > 1 indicates preferential distribution at the plasma membrane (**Figure 4b**, top). At rest, dendritic PKA holoeynzyme is anchored to the underlying cyto-architecture via the AKAP MAP2 (Lohmann et al., 1984; Davare et al., 1999; Zhong et al., 2009). This anchoring is reflected in the membrane index value of < 1 for both the wtPKA-cat (0.89 +/- 0.02) and nmPKA-cat (0.94 +/- 0.03) in resting dendrites (left column, **Figure 4a**). Upon stimulation by F + I, both wtPKA-cat and nmPKA-cat redistribute from the center to fill the dendritic volume. However, a greater percentage of wtPKA-cat (n = 6) redistributes to the plasma membrane as indicated by its higher plasma membrane index value relative to nmPKA-cat (n = 6). **Figure 4b** shows the summary data for the plasma membrane index experiments. wtPKA-cat has an average F + I stimulated plasma membrane index of 1.41+/- 0.05 and nmPKA-cat has an average of 1.08 +/- 0.02. These results confirm observations from another laboratory that myristoylation increases the membrane affinity of the freed PKA catalytic subunit (Gaffarogullari et al., 2011) and is the first hint of such a phenomenon in living cells.

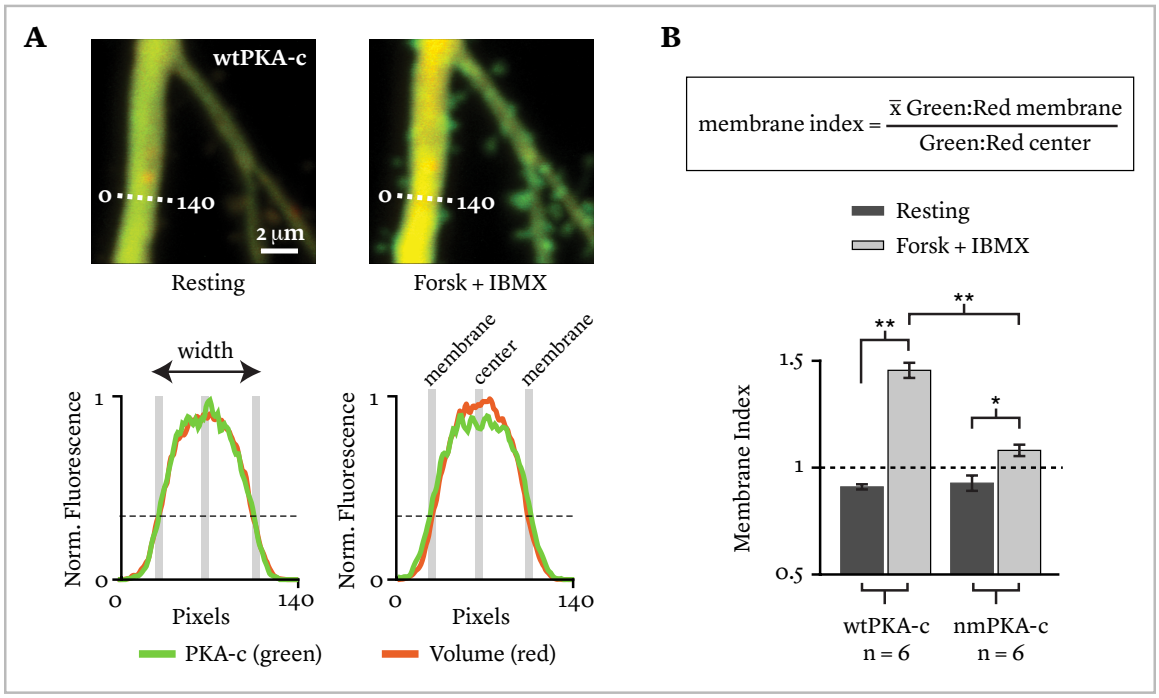

FIGURE 4. N-TERMINAL MYRISTOYLATION TARGETS A FRACTION OF PKA-CAT TO THE PLASMA MEMBRANE IN NEURONS.

(A) Top, example images of wtPKA-c distribution at rest and after the addition of F + I in the major apical dendrite of a CA1 hippocampal neuron**.** The white dashed line in each image indicates a single line profile from with the PKA-c EGFP and dsRed volume. Bottom, fluorescence intensity profiles from the white dashed lines in each image for PKA-c (green) and the dendrite morphology (red) taken from single z-planes in the images. The dashed line marks a level of 30% of the maximum dsRed fluorescence. The gray bars, from right to left indicate the positions at which the PKA-c to Volume ratios were measured. The membrane measures fall at 30% of the max dsRed fluorescence and the center falls at the maximum dsRed fluorescence intensity. All measures are binned at the 3 pixel level (see **Methods**). **(B)** Top, formula used to calculate the membrane index values for wtPKA-c and nmPKA-c. Bottom, summary plot of the membrane index values for wtPKA-c (n = 6) and nmPKA-c (n = 6) before and after F + I treatment. ** = $p < 0.001$ and * = $p < 0.01$ as determined by 2-way ANOVA and Turkey's post hoc test.

N-terminal myristoylation decreases the mobility of PKA-cat in dendritic spines

Given the high viscosity of membranes compared to the cytosol, and given the high plasma membrane to volume ratio of dendritic spines and their necks (Wilson et al., 1983; Harris and Stevens, 1989) we expect the myristoylation moiety to significantly influence the spine mobility of activated PKA-cat. To test this prediction, we used spine localized 2photon photoactivation of activated wtPKA-cat and non-myristoylated PKA-cat versions tagged

with photoactivatable GFP (PA-GFP) and PA-GFP alone as a soluble control (Patterson and Lippincott-Schwartz, 2002; Bloodgood and Sabatini, 2005). We used CA1 neurons in cultured rat hippocampal slice co-transfected with dsRed as a cytosolic marker and the wtPKA and nmPKA-PA-GFP tagged catalytic subunits. **Figure 5a** is a panel of representative 2photon images of the experiment involving wtPKA-cat. At rest (t = -2 s) we image the spine and parent dendrite morphology using 960 nm excitation of dsRed. At t = 0 s we scan the spine head (~ 20 ms dwell time) with 810 nm excitation with a 2nd laser to photoactivate PAGFP-wtPKA-cat in the spine head while simultaneously imaging its fluorescent state with the 960 nm excitation used to image neuronal morphology. 810 nm photoactivation results in a near instantaneous increase in the green fluorescence emission from the spine head. At t = 2 s the fluorescence intensity in the spine has decreased as activated PKA-cat molecules continue to exit the spine. At 4 s the majority of PKA-cat has left the spine. The decay in fluorescence intensity from the spine is well-fit by a single exponential, and we refer to the time-constant of this exponential decay as spine residency. **Figure 5b** shows representative spine fluorescence decay traces of PAGFP-wtPKA-cat, PAGFP-nmPKA-cat, and PAGFP alone. **Figure 5c** shows the population data for the spine residencies of PAGFP and the listed PAGFP tagged PKA-cat variants. The soluble PA-GFP control has a mean spine residency of 0.36s (n = 24 spines, 2 cells). wtPKA-cat has a mean spine residency of 2.56 s (n = 99 spines, 10 cells) and nmPKA-cat and has a mean spine residency of 1.2 s (n = 49 spines, 4 cells). To test whether N-terminal myristoylation is sufficient to decrease the spine mobility of PKA-cat we also measured the spine residency of the myristoylated N-terminal 47 amino acids of PKA-cat tagged again with PA-GFP (Struppe et al., 1998). The myristoylated N-terminal fragment (wtΔPKA-cat) has a mean spine residency of 1.97 s (n = 40 spines, 4 cells). The same construct containing the N-terminal glycine to alanine point mutation (nmΔPKA-cat) that prevents myristoylation has a mean spine residency of 0.37 s (n = 50 spines, 5 cells).

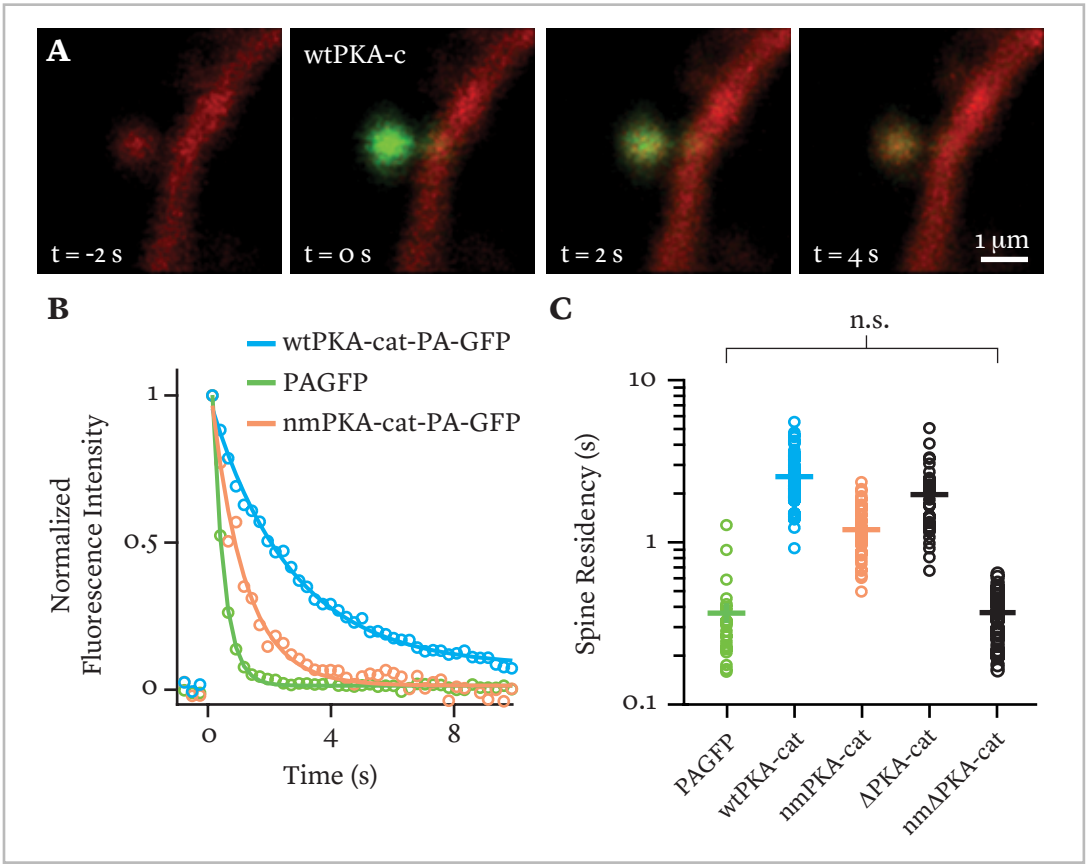

FIGURE 5. N-TERMINAL MYRISTOYLATION IS PARTIALLY RESPONSIBLE FOR THE LONG SPINE RESIDENCY OF PKA-CAT.

(A) Example 2photon photoactivation of wtPKA-cat-PAGFP in a CA1 hippocampal dendritic spine. Prior to the experiment F+I is added to the bath to activate the PKA holoenzyme. At t = 0 s a photoactivation scan is delivered to the spine head. The fluorescence decays from the spine head as wtPKA-cat exits the spine (t = 2 – 4 s). **(B)** Representative spine fluorescence decays for cells expressing the indicated constructs. Spine residency is defined as the time constant of those decays. **(C)** Groups data showing the spine residencies for the indicated constructs. Open circles are individual spines and solid line indicates the mean. PA-GFP (n = 24, 2 cells) has a spine residency of 0.36s +/- 0.05 s. wtPKA-cat (n = 99, 10 cells, 2.56 +/- 0.9 s), nmPKA-cat (n = 49 spines, 4 cells, 1.19 +/- 0.05 s), ΔPKA-cat (n = 40 spines, 4 cells, 1.96s +/- 0.14s), and nmΔPKA-cat (n = 50 spines, 5 cells, 0.36 +/- 0.02 s) All data indicated as mean +/- s.e.m. Only PAGFP and nm(n-term) are not statistically different from one another. All other data are statistically different from one another to a level of < 0.001 as determined by 1-way ANOVA and Turkey's post hoc test.

Discussion

Here we use optical and biochemical approaches to investigate plasma membrane concentration and phosphorylation gradients of the activated PKA catalytic subunit (PKA-cat) in HEK293 cells and in CA1 neurons from rat cultured hippocampal slice. We find that a gradient of stimulated PKA phosphorylation exists in the plasma membrane of both cell types. Furthermore, we present evidence that N-terminal myristoylation of PKA-cat imparts membrane affinity to the freed enzyme. The functional significance of this targeting appears to be two fold. First myristoylation enhances phosphorylation in the plasma membrane compartment of both HEK293 cells and in CA1 hippocampal neurons. Second, myristoylation decreases the mobility of the free PKA catalytic subunit, enhancing its concentration gradient in dendritic spines and potentially limiting spillover of PKA-cat to nearby AKAP established PKA signaling hubs in the dendrite.

PKA's preferential phosphorylation at the plasma membrane and a role for N-terminal myristoylation in HEK293 cells

In the previous chapter, we demonstrated the existence of a PKA phosphorylation gradient emanating from the plasma membrane of HEK293 cells in both resting conditions and upon exogenous stimulation using FRET based reporters of PKA phosphorylation (see Chapter 1 Figures 3 & 4). Here, we confirmed the existence of this gradient upon stimulation of PKA using a biochemical approach combined with the transient over-expression of a known neuronal PKA target, the AMPA type glutamate receptor GluR1. GluR1 is phosphorylated by PKA on a serine residue at position 845, resulting in changes in receptor trafficking (Esteban et al., 2003), channel open time (Banke et al., 2000), and is necessary for the expression of long-term potentiation (Frey et al., 1993). As GluR1 is an obligate membrane protein, we used the full-length version of the receptor to biochemically assay PKA phosphorylation in membrane compartments. In the HEK293 cells, GluR1 expression was not solely confined to the plasma membrane and a significant portion of it was located on intracellular membranes (**Figure 2a** and **Supplementary Figure 1**). We therefore refer to the GluR1 compartment as a general membrane compartment and not solely a plasma membrane compartment. To establish a parallel biochemical assay for PKA phosphorylation in the

cytosol, we used the cytosolic C-terminal fragment of GluR1 alone (GluR1-c) which itself contains the consensus PKA phosphorylation site S845 and the antigen used for detecting total GluR1. Upon stimulation of the PKA pathway, full-length GluR1 was readily phosphorylated. In stark contrast, we could not detect any phosphorylation of the C-terminal fragment (GluR1-c). The lack of detectable phosphorylation is not the result of an obstructed antigen as we detect phosphorylation of GluR1-c in conditions of PKA overexpression (**Figure 3**).

Perhaps the lack of GluR1-c phosphorylation is somewhat surprising considering that the purely cytosolic AKAR5 sensor undergoes a considerable increase in phosphorylation upon stimulation with either NE or F + I in both HEK293 cells and neurons. Though not investigated further, this discrepancy is potentially explained by a greater accessibility of phosphatases to the S845 site in GluR1-c compared to the PKA phospho site in AKAR5. We next asked if PKA phosphorylation of GluR1-c could be rescued by targeting it to the plasma membrane in an alternative manner. Indeed, GluR1-c insertion into the plasma membrane via the hCD4 single transmembrane domain recovered its ability to be phosphorylated. This result strongly indicates that stimulated PKA phosphorylation is more likely to occur in the plasma membrane when compared to the cytosol.

The experiments described above do not discern the mechanisms by which PKA phosphorylation is largely confined to the plasma membrane. To tease apart the roles that AKAPs and N-terminal myristoylation of PKA-cat may play in establishing this preference we measured and compared the membrane phosphorylation preference of over-expressed wtPKA-cat and nmPKA-cat (**Figure 3**). Consistent with a role for myristoylation in directing PKA-cat to the plasma membrane, the fully functional non-myristoylated mutant exhibited significantly less membrane phosphorylation preference than wtPKA-cat. Interestingly, nmPKA-cat still exhibited a 3-fold preference for membrane phosphorylation indicating that the expected gradient of cAMP concentration is sufficient to establish a gradient of PKA phosphorylation emanating from the plasma membrane.

The preferential phosphorylation of PKA at the plasma membrane and a role for N-terminal myristoylation in neurons

Though the mechanisms that establish a gradient of PKA phosphorylation at the plasma membrane in HEK293 cells are likely present in neurons, the morphology and makeup of the two cells are vastly different. This fact warranted investigation into whether a similar compartment existed in neurons. Again using the targeted expression of AKAR5 sensors and 2pFLIM we were able to visualize a downhill gradient of PKA phosphorylation from the plasma membrane into the cytosol (**Figure 4**). Given that this gradient is present in both these essentially disparate cells, it is likely to be present in a wide variety of cells.

To infer the role of N-terminal myristoylation in the maintenance of the PKA phosphorylation gradient we imaged and compared the spatial distribution of wtPKA-cat and nmPKA-cat in CA1 dendrites before and after activation with F + I in the same cells. If myristoylation plays a role, we expect it to assist in targeting activated PKA-cat to the plasma membrane. Consistent with this notion we find that compared to nmPKA-cat, wtPKA-cat exhibits a greater ability to redistribute from its site of anchoring to the plasma membrane. This finding confirms the recent observation that myristoylation is capable of imparting membrane affinity to the free catalytic subunit (Gaffarogullari et al., 2011), and is the first hint of such a phenomenon for PKA-cat in any cell type.

The role of myristoylation in the mobility of PKA-cat in neurons

The fact that myristoylation can indeed functionally target at least a fraction of PKA-cat to the plasma membrane hints to an alluring mechanism for enhancing and maintaining AKAP established PKA signaling gradients. Membrane insertion of PKA-cat should not only augment phosphorylation in that compartment as discussed previously, but also limit the mobility and spread of activated PKA-cat due to the high viscosity of membrane environments relative to the cytosol. Given their high surface area to volume ratio, this mechanism may be especially important in the synaptic compartments of neurons. To investigate this possibility further, we used 2photon localized photoactivation of PAGFP tagged PKA-cat to compare the mobility of wtPKA-cat and nmPKA-cat in dendritic spines of CA1 hippocampal neurons. In accordance with our previous observations, myristoylation enables activated wtPKA-cat to reside in spines for greater than twice the duration of nmPKA-cat, or about 1.3 – 1.4 seconds longer. Given the

enzymatic turnover of PKA-cat (~20 s^{-1}) (see Chapter 1 Figure 4) (Zhou and Adams, 1997), N-terminal myristoylation could potentially spare the cell from greater than 20 unintended phosphorylation events thereby limiting spillover of PKA phosphorylation to neighboring PKA compartments. In the future we plan to further investigate the physiological role of N-myristoylation in preventing crosstalk between AKAP established PKA signaling gradients. It is presently clear however, that myristoylation affords PKA with another mechanism for maintaining a concentration and phosphorylation gradients that are independent of A-kinase anchoring proteins.

Materials and Methods

cDNA constructs

cDNA for the cyt-AKAR5 and pm-AKAR5 constructs were identical to those used and described **Chapter 2**. The non-myristoylated PKA catalytic subunit was made using site-directed mutagenesis to replace the glutamine in the second amino acid position with alanine, which prevents myristoylation. The PKA-c-mEGFP and PKA-cat-PA-mEGFP were identical constructs to those used and described in Zhong et al. 2009 (Zhong et al., 2009).

Hippocampal Slice Cultures and Transfection

Rat hippocampal slice cultures were prepared from P6 – P7 pups using established methods [Stoppini 1991, Zhong 2009] and in accordance with the animal care and use guidelines of the Oregon Health & Science university. Experiments were performed after 2 – 3 weeks in vitro. PKA and FP constructs were introduced to the slice cultures via biolistic gene transfer using the Helios gene gun and 1.6 μm gold beads.

Western blots

HEK293 cells grown on 10 cm dishes were transiently transfected using Lipofectamine 2000 (Invitrogen) with a combination of the following constructs depending on the indicated experiment. 5 μg EGFP-GluR1, 0.5 μg EGFP-GluR1c, 1 μg EGFP-hCD4-GluR1-c, 2 μg EGFP-nmPKA-c, 2 μg EGFP-wtPKA-c, 4 μg RIIβ. The cells were harvested 24 hours post transfection and were lysed and sonicated in ice cold lysis buffer containing in mM 150 NaC l, 50 NaF, 10 NaH_2PO_4, 5 EDTA,5 EGTA, 10 sodium pyrophosphate,1 sodium vanadate, plus 10 U/ml aprotinin and 1 % M okadaic acid and then centrifuged. The pellet was then resuspended in sample buffer containing 2% glycerol and beta-mercaptoethanol, 2% SDS in Tris-HCl buffer and boiled for 5 min. The samples were then run on polyacrylamide gel composed of an 7 – 10% resolving section and 4% stacking section. The gels were then transferred overnight to PVDF membranes, followed by incubation in blocking buffer.

2photon Imaging and 2photon photoactivation

We use a custom built Olympus microscope and scan setup for 2photon imaging. The setup is well described in the methods section of **Chapter 2**. For the photoactivation experiments we use 810 nm 2photon excitation to photoactivate PAGFP and 990 nm 2 photon excitation from a separate laser to simultaneously image the photoactivated state of PAGFP and the soluble dsRed marker of neuronal morphology. Spines are images for 80 – 120 frames at 8 Hz, with a pixel size of ~ 100 nm and a field of view of ~ 6 μm. Power for photoactivation was determined empirically at the time of individual experiments.

2photon fluorescence lifetime imaging (2pFLIM) and analysis

See Chapter 2.

Image Analysis

Image analysis was done using custom software written in Matlab by Dr. Haining Zhong. For plasma membrane index measurement, line profiles of single pixel width were manually drawn across regions of the apical dendrites > 1.8 μm in diameter that were smooth on both sides containing no spines. The profiles were obtained from a single z stack (0.8 μm) centered along the middle z-plane of the dendrite. The background subtracted fluorescence intensity of the dsRed soluble marker and the GFP tagged PKA catalytic subunits along the profiles were then used to calculate the membrane index values (M.I). M.I. is defined as the ratio of the Green:Red signal at the membrane to the Green:Red signal at the center of the dendrite as described in the text.

Photoactivation experiments were analyzed by manually drawing ROIs over the x – y projection of the spines of interest. The green fluorescence emission from the ROI over the course of the experiment was then averaged after background subtraction for three consecutive z slices with the middle z slice giving the highest integrated green signal among all z slices in the image. The green fluorescence intensity decay post photoactivation was then averaged across 3 separate trials and subsequently fit with a single exponential, the time constant of which we define as the spine residency.

Chapter 3: Supplementary Information

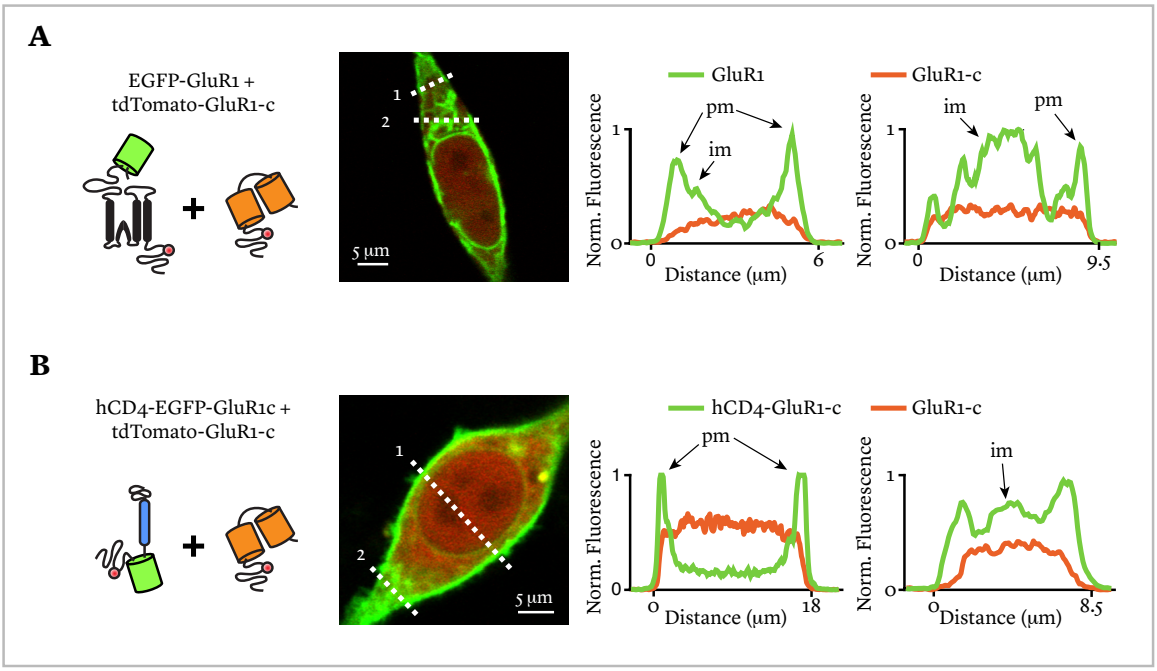

SUPPLEMENTAL FIGURE 1: DISTRIBUTION OF EGFP-GLUR1 AND HCD4-EGFP-GLUR1-C IN HEK293 CELLS.

(A) Left, Illustration of EGFP-GluR1 construct and the tdTomato-GluR1-c construct. The latter was used to get a measure of the distribution of a cytosolic construct for comparison. Middle, representative 2photon image of the an HEK293 cells expressing the constructs shown on the left. Right, fluorescent intensity profiles from the white dashed lines found in the image. **(B)** Same as panel A except for the hCD4-EGFP-GluR1-c construct shown on the left.

Chapter 4.

Discussion of key findings, considerations, & future directions

Key Findings

1. A gradient of PKA phosphorylation exists at the plasma membrane wherein phosphorylation is more probable near the plasma membrane than far from it.

2. N-terminal myristoylation of the PKA catalytic subunit provides a mechanism for enhancement of the observed PKA phosphorylation gradients.

Discussion

Gradients of resting PKA phosphorylation in HEK293 cells

In Chapter 2, we consider a mode of PKA action in HEK293 cells that we define as resting PKA phosphorylation. By resting, we mean in the absence of exogenous stimulation on our part, that is not to say unstimulated PKA phosphorylation. When in culture, HEK293 cells are undoubtedly receiving information in the form of extracellular cues that have the potential to activate the cAMP pathway. However, resting conditions also favor the type of cAMP independent phosphorylation mediated by the RIIα type recently described by Smith & Gonen (Smith et al., 2013). The conformational landscape of the RIIα subunit would seemingly favor this type of action as the holoenzyme structure is capable of adopting an extended conformation, which is in contrast to the RIIβ subunit whose holoenzyme structure adopts a more globular conformation thereby limiting the radius of cAMP independent phosphorylation. Here, we do not discriminate between cAMP dependent and independent PKA action, though the experiment should be fairly straightforward as outlined in the discussion section of Chapter 2.

What we do show quite convincingly, through a series of controlled PKA sensor experiments, is that resting PKA phosphorylation is confined in space to the plasma membrane of HEK293 cells. We detect little to no PKA phosphorylation in the cytosolic compartment. Again this observations supports the idea that the expected gradient of [cAMP] production at the plasma membrane is propagated through PKA phosphorylation. Also of particular interest, is the fact that our measurements indicate that resting PKA plasma membrane phosphorylation accounts for a significant amount of the total achievable PKA phosphorylation. This result certainly needs to be substantiated using other methods (i.e. immunoblots), but if true, points to some interesting biology concerning the regulation of PKA phosphorylation. For instance, a high resting PKA phosphorylation could serve to prime the cell to respond to a more direct stimulus, or provide an easy way to increase PKA phosphorylation through down regulation of PKA phosphatases. On the other hand, the result may indicate the presence of sub micron regions of high and low PKA phosphorylation in resting conditions. Regions of high PKA phosphorylation may be

required for efficient and continual transport of cell essentials such as water delivery through aquaporins. Compartments of low resting PKA phosphorylation may be maintained through the concerted action of phosphodiesterases and phosphatases and be reserved for PKA activators such as GPCRs that must respond more acutely to external stimuli. High resolution imaging methods are required to investigate such a possibility and it warrants further investigation.

Gradients of stimulated PKA phosphorylation and a role for N-terminal myristoylation

In Chapter 3, we further to consider the role of the PKA catalytic subunit in maintaining its phosphorylation gradient upon its activation and subsequent release from the regulatory subunit. Our theoretical predictions suggest that simple diffusion of the catalytic subunit has the potential to carry PKA-c well out of range of a AKAP established compartment and rapidly dissipate a phosphorylation gradient Such a model would hamper and limit the cells ability to maintain signaling specificity. As we consistently observe sustained gradients PKA signaling, there must be mechanisms in place to limit the potential spillover of PKA phosphorylation. These mechanisms could include the presence of excess local regulatory subunit that serves to corral activated catalytic subunit, the presence of local phosphatases that serve to limit PKA phosphorylation profiles, or some form of restricted diffusion that has in a similar fashion been invoked to explain the compartmentalized phosphorylation of cAMP. Here we investigated the latter possibility and have discovered a novel role for N-terminal myristoylation of PKA-c to target PKA-c to the plasma membrane. This targeting not only enhances PKA mediated phosphorylation in the plasma membrane, it also serves to limit its mobility. Myristoylation of PKA-cat thus serves to enhance the effectiveness of AKAP established PKA membrane compartments through the amplification of local phosphorylation at the expense of targets located outside the intended signaling hub.

Over-expression of the PKA holoenzyme

Many of the experiments described here involve the over-expression of a variety of constructs, most notably that of the PKA holoenzyme itself. The potential for artifacts is

high in such conditions, especially for a kinase with the broad reach of PKA. We have observed that neurons will not tolerate over-expression of the PKA catalytic subunit itself, and to compensate we must also over-express a 2-fold excess of PKA regulatory subunit. We are not naïve enough to believe that this level will not affect the ability of cells to regulate the cAMP/PKA pathway, as the additional holoenzyme will inevitably lead to increased buffering of cAMP, a higher rate of binding to AKAPs, and higher phosphorylation rates in general. Certainly the cell has homeostatic mechanisms to compensate for this insult, but we can never be sure we are dealing with a wild type cell.

Here however, when using PKA over-expression paradigms, we are not necessarily investigating the biology of the cell. We are instead investigating a much more reduced system, specifically the molecular biology of N-terminal myristoylation of the PKA catalytic subunit. If myristoylation imparts membrane affinity to activated, but over-expressed PKA-cat then surely it has the ability to do the same with endogenous PKA-cat. If myristoylation reduces the mobility of activated, but over-expressed PKA-cat then surely too does it have the ability reduce the mobility of endogenous PKA-cat. Though this logic is not foolproof and we certainly have to be wary of the over-expression used here, we remain confident that our results are not the product of over-expression artifacts.

Future Directions

What the neuronal PKA signaling field would really like to have is a comprehensive atlas of PKA distribution and phosphorylation profiles across the subcellular compartments of a neuron. An ideal atlas would contain the following information: (1) a list of all potential PKA targets and their absolute numbers in a given compartment. (2) a high resolution (~ 50 nm) map of the spatial distribution and absolute numbers of both PKA-r and PKA-c in the resting and activated states. This map could be used to infer about the location and number of AKAPs present in a given compartment (3) a high resolution map of the sites of PKA activation and what type of PKA stimulation is likely to occur there (4) the timescales in which PKA-c resides in a given synaptic compartment (5) the average number of sustained phosphorylation events in a given compartment. From this we can infer about the presence and effectiveness of phosphatases.

With this type of atlas one could make a reasonable estimate of the likelihood of a particular target being phosphorylated in a given compartment under a given stimulation paradigm. We are not far off from obtaining the information found in (1), (2), and (3). The advancement of super resolution imaging techniques and laboratories interested in PKA signaling will soon lead to an ever more quantitative picture of the distribution of PKA activators, PKA itself, and PKA targets. Parallel advancements in mass spectrometry and sequencing will soon allow the characterization of the abundance and type of target present in the smallest synaptic compartments such as spines and terminals. Such an atlas would inevitably render the work presented here obsolete. Such is science.

References Cited

Adams, J.A., and Taylor, S.S. (1992). Energetic limits of phosphotransfer in the catalytic subunit of cAMP-dependent protein kinase as measured by viscosity experiments. Biochemistry 31, 8516-522.

Adams, S.R., Harootunian, A.T., Buechler, Y.J., Taylor, S.S., and Tsien, R.Y. (1991). Fluorescence ratio imaging of cyclic AMP in single cells. Nature 349, 694-97.

Alexander, G.M., Rogan, S.C., Abbas, A.I., Armbruster, B.N., Pei, Y., Allen, J.A., Nonneman, R.J., Hartmann, J., Moy, S.S., and Nicolelis, M.A. (2009). Remote control of neuronal phosphorylation in transgenic mice expressing evolved G protein-coupled receptors. Neuron 63, 27-39.

Allen, M.D., and Zhang, J. (2006). Subcellular dynamics of protein kinase A phosphorylation visualized by FRET-based reporters. Biochem Biophys Res Commun 348, 716-721.

Amieux, P.S., and McKnight, G.S. (2002). The essential role of RI alpha in the maintenance of regulated PKA phosphorylation. Ann N Y Acad Sci 968, 75-95.

Amieux, P.S., Howe, D.G., Knickerbocker, H., Lee, D.C., Su, T., Laszlo, G.S., Idzerda, R.L., and McKnight, G.S. (2002). Increased basal cAMP-dependent protein kinase phosphorylation inhibits the formation of mesoderm-derived structures in the developing mouse embryo. J Biol Chem 277, 27294-7304.

Atwood, B.K., Lopez, J., Wager-Miller, J., Mackie, K., and Straiker, A. (2011). Expression of G protein-coupled receptors and related proteins in HEK293, AtT20, BV2, and N18 cell lines as revealed by microarray analysis. BMC Genomics 12, 14.

Bacskai, B.J., Hochner, B., Mahaut-Smith, M., Kaang, B.K., Kandel, E.R., and Tsien, R.Y. (1993). Spatially resolved dynamics of cAMP and protein kinase A subunits in Aplysia sensory neurons. Science *260*, 222-26.

Banke, T.G., Bowie, D., Lee, H.-K., Huganir, R.L., Schousboe, A., and Traynelis, S.F. (2000). Control of GluR1 AMPA receptor function by cAMP-dependent protein kinase. The Journal of neuroscience 20, 89-102.

Bastidas, A.C., Deal, M.S., Steichen, J.M., Keshwani, M.M., Guo, Y., and Taylor, S.S. (2012). Role of N-terminal myristylation in the structure and regulation of cAMP-dependent protein kinase. J Mol Biol 422, 215-229.

Bauman, A.L., Soughayer, J., Nguyen, B.T., Willoughby, D., Carnegie, G.K., Wong, W., Hoshi, N., Langeberg, L.K., Cooper, D.M., and Dessauer, C.W. (2006). Dynamic regulation of cAMP synthesis through anchored PKA-adenylylyl cyclase V/VI complexes. Mol Cell 23, 925-931.

Beene, D.L., and Scott, J.D. (2007). A-kinase anchoring proteins take shape. Curr Opin Cell Biol 19, 192-98.

Bialojan, C., and Takai, A. (1988). Inhibitory effect of a marine-sponge toxin, okadaic acid, on protein phosphatases. Specificity and kinetics. Biochem. J 256, 283-290.

Bloodgood, B.L., and Sabatini, B.L. (2005). Neuronal phosphorylation regulates diffusion across the neck of dendritic spines. Science 310, 866-69.

Boutin, J.A. (1997). Myristoylation. Cellular signalling 9, 15-35.

Brandon, E.P., Idzerda, R.L., and McKnight, G.S. (1997). PKA isoforms, neural pathways, and behaviour: making

the connection. Curr Opin Neurobiol 7, 397-403.

Brandon, E.P., Logue, S.F., Adams, M.R., Qi, M., Sullivan, S.P., Matsumoto, A.M., Dorsa, D.M., Wehner, J.M., McKnight, G.S., and Idzerda, R.L. (1998). Defective motor behavior and neural gene expression in RIIβ-protein kinase A mutant mice. The Journal of neuroscience 18, 3639-649.

Burgers, P.P., Ma, Y., Margarucci, L., Mackey, M., van der Heyden, M.A., Ellisman, M., Scholten, A., Taylor, S.S., and Heck, A.J. (2012). A small novel A-kinase anchoring protein (AKAP) that localizes specifically protein kinase A-regulatory subunit I (PKA-RI) to the plasma membrane. J Biol Chem 287, 43789-797.

Burton, K.A., Johnson, B.D., Hausken, Z.E., Westenbroek, R.E., Idzerda, R.L., Scheuer, T., Scott, J.D., Catterall, W.A., and McKnight, G.S. (1997). Type II regulatory subunits are not required for the anchoring-dependent modulation of Ca2+ channel phosphorylation by cAMP-dependent protein kinase. Proceedings of the National Academy of Sciences 94, 11067-072.

Buxton, I.L., and Brunton, L.L. (1983). Compartments of cyclic AMP and protein kinase in mammalian cardiomyocytes. J Biol Chem 258, 10233.

Cadd, G.G., Uhler, M.D., and McKnight, G.S. (1990). Holoenzymes of cAMP-dependent protein kinase containing the neural form of type I regulatory subunit have an increased sensitivity to cyclic nucleotides. Journal of Biological Chemistry 265, 19502-06.

Carr, D.W., Stofko-Hahn, R.E., Fraser, I.D., Bishop, S.M., Acott, T.S., Brennan, R.G., and Scott, J.D. (1991). Interaction of the regulatory subunit (RII) of cAMP-dependent protein kinase with RII-anchoring proteins occurs through an amphipathic helix binding motif. Journal of Biological Chemistry 266, 14188-192.

Carr, D.W., Stofko-Hahn, R.E., Fraser, I.D., Cone, R.D., and Scott, J.D. (1992). Localization of the cAMP-dependent protein kinase to the postsynaptic densities by A-kinase anchoring proteins. Characterization of AKAP 79. Journal of Biological Chemistry 267, 16816-823.

Carr, S.A., Biemann, K., Shoji, S., Parmelee, D.C., and Titani, K. (1982). n-Tetradecanoyl is the NH2-terminal blocking group of the catalytic subunit of cyclic AMP-dependent protein kinase from bovine cardiac muscle. Proc Natl Acad Sci U S A 79, 6128-131.

Castro, L.R., Gervasi, N., Guiot, E., Cavellini, L., Nikolaev, V.O., Paupardin-Tritsch, D., and Vincent, P. (2010). Type 4 phosphodiesterase plays different integrating roles in different cellular domains in pyramidal cortical neurons. J Neurosci 30, 6143-151.

Chen, Q., Lin, R.Y., and Rubin, C.S. (1997). Organelle-specific targeting of protein kinase AII (PKAII). Molecular and in situ characterization of murine A kinase anchor proteins that recruit regulatory subunits of PKAII to the cytoplasmic surface of mitochondria. J Biol Chem 272, 15247-257.

Chen, C., Nakamura, T., and Koutalos, Y. (1999). Cyclic AMP diffusion coefficient in frog olfactory cilia. Biophysical journal *76*, 2861-67.

Chen, Y., Yu, F.H., Surmeier, D.J., Scheuer, T., and Catterall, W.A. (2006). Neuromodulation of Na+ channel slow inactivation via cAMP-dependent protein kinase and protein kinase C. Neuron 49, 409-420.

Cheng, X., Ma, Y., Moore, M., Hemmings, B.A., and Taylor, S.S. (1998). Phosphorylation and activation of cAMP-dependent protein kinase by

phosphoinositide-dependent protein kinase. Proc Natl Acad Sci U S A *95*, 9849.

Choi, J., Ko, J., Park, E., Lee, J.R., Yoon, J., Lim, S., and Kim, E. (2002). Phosphorylation of stargazin by protein kinase A regulates its interaction with PSD-95. J Biol Chem *277*, 12359-363.

Clegg, C.H., Ran, W., Uhler, M.D., and McKnight, G.S. (1989). A mutation in the catalytic subunit of protein kinase A prevents myristylation but does not inhibit biological phosphorylation. J Biol Chem *264*, 20140-46.

Coghlan, V.M., Perrino, B.A., Howard, M., Langeberg, L.K., Hicks, J.B., Gallatin, W.M., and Scott, J.D. (1995). Association of protein kinase A and protein phosphatase 2B with a common anchoring protein. Science *267*, 108-111.

Cohen, P. (2002). The origins of protein phosphorylation. Nature cell biology *4*, E127-130.

Colledge, M., Dean, R.A., Scott, G.K., Langeberg, L.K., Huganir, R.L., and Scott, J.D. (2000). Targeting of PKA to glutamate receptors through a MAGUK-AKAP complex. Neuron *27*, 107-119.

Cooper, D.M., Mons, N., and Karpen, J.W. (1995). Adenylyl cyclases and the interaction between calcium and cAMP signalling. Nature *374*, 421-24.

Das, R., Esposito, V., Abu-Abed, M., Anand, G.S., Taylor, S.S., and Melacini, G. (2007). cAMP activation of PKA defines an ancient signaling mechanism. Proceedings of the National Academy of Sciences *104*, 93-98.

Davare, M.A., Avdonin, V., Hall, D.D., Peden, E.M., Burette, A., Weinberg, R.J., Horne, M.C., Hoshi, T., and Hell, J.W. (2001). A beta2 adrenergic receptor signaling complex assembled with the Ca2+ channel Cav1.2. Science *293*, 98-101.

Davare, M.A., Dong, F., Rubin, C.S., and Hell, J.W. (1999). The A-kinase anchor protein MAP2B and cAMP-dependent protein kinase are associated with class C L-type calcium channels in neurons. J Biol Chem *274*, 30280.

Dell'Acqua, M.L., Smith, K.E., Gorski, J.A., Horne, E.A., Gibson, E.S., and Gomez, L.L. (2006). Regulation of neuronal PKA signaling through AKAP targeting dynamics. Eur J Cell Biol *85*, 627-633.

Depry, C., Allen, M.D., and Zhang, J. (2011). Visualization of PKA phosphorylation in plasma membrane microdomains. Mol Biosyst *7*, 52-58.

DiPilato, L.M., Cheng, X., and Zhang, J. (2004). Fluorescent indicators of cAMP and Epac activation reveal differential dynamics of cAMP signaling within discrete subcellular compartments. Proc Natl Acad Sci U S A *101*, 16513-18.

Dodge-Kafka, K.L., Soughayer, J., Pare, G.C., Carlisle Michel, J.J., Langeberg, L.K., Kapiloff, M.S., and Scott, J.D. (2005). The protein kinase A anchoring protein mAKAP coordinates two integrated cAMP effector pathways. Nature *437*, 574-78.

Drobizhev, M., Makarov, N.S., Tillo, S.E., Hughes, T.E., and Rebane, A. (2011). Two-photon absorption properties of fluorescent proteins. Nat Methods *8*, 393-99.

Durocher, D., Henckel, J., Fersht, A.R., and Jackson, S.P. (1999). The FHA domain is a modular phosphopeptide recognition motif. Mol Cell *4*, 387-394.

Durocher, D., Taylor, I.A., Sarbassova, D., Haire, L.F., Westcott, S.L., Jackson, S.P., Smerdon, S.J., and Yaffe, M.B. (2000). The molecular basis of FHA domain: phosphopeptide binding specificity and implications for phospho-dependent signaling mechanisms. Mol Cell *6*, 1169-182.

Esteban, J.A., Shi, S.H., Wilson, C., Nuriya, M., Huganir, R.L., and Malinow, R. (2003). PKA phosphorylation of AMPA receptor subunits controls synaptic trafficking underlying plasticity. Nat Neurosci 6, 136-143.

Ferguson, S.M., Eskenazi, D., Ishikawa, M., Wanat, M.J., Phillips, P.E., Dong, Y., Roth, B.L., and Neumaier, J.F. (2011). Transient neuronal inhibition reveals opposing roles of indirect and direct pathways in sensitization. Nature neuroscience 14, 22-24.

Few, W.P., Scheuer, T., and Catterall, W.A. (2007). Dopamine modulation of neuronal Na(+) channels requires binding of A kinase-anchoring protein 15 and PKA by a modified leucine zipper motif. Proc Natl Acad Sci U S A 104, 5187-192.

Francis, S.H., and Corbin, J.D. (1994). Structure and function of cyclic nucleotide-dependent protein kinases. Annual Review of Physiology 56, 237-272.

Frey, U., Huang, Y.Y., and Kandel, E.R. (1993). Effects of cAMP stimulate a late stage of LTP in hippocampal CA1 neurons. Science 260, 1661-64.

Fukuda, M., Gotoh, I., Gotoh, Y., and Nishida, E. (1996). Cytoplasmic localization of mitogen-activated protein kinase kinase directed by its NH2-terminal, leucine-rich short amino acid sequence, which acts as a nuclear export signal. Journal of Biological Chemistry 271, 20024-28.

Gaffarogullari, E.C., Masterson, L.R., Metcalfe, E.E., Traaseth, N.J., Balatri, E., Musa, M.M., Mullen, D., Distefano, M.D., and Veglia, G. (2011). A myristoyl/phosphoserine switch controls cAMP-dependent protein kinase association to membranes. J Mol Biol 411, 823-836.

Ganesan, S., Ameer-Beg, S.M., Ng, T.T.C., Vojnovic, B., and Wouters, F.S. (2006). A dark yellow fluorescent protein (YFP)-based Resonance Energy-Accepting Chromoprotein (REACh) for Förster resonance energy transfer with GFP. Proc Natl Acad Sci U S A 103, 4089.

Gangal, M., Clifford, T., Deich, J., Cheng, X., Taylor, S.S., and Johnson, D.A. (1999). Mobilization of the A-kinase N-myristate through an isoform-specific intermolecular switch. Proc Natl Acad Sci U S A 96, 12394-99.

Gervasi, N., Hepp, R., Tricoire, L., Zhang, J., Lambolez, B., Paupardin-Tritsch, D., and Vincent, P. (2007). Dynamics of protein kinase A signaling at the membrane, in the cytosol, and in the nucleus of neurons in mouse brain slices. J Neurosci 27, 2744-750.

Gervasi, N., Tchénio, P., and Preat, T. (2010). PKA dynamics in a Drosophila learning center: coincidence detection by rutabaga adenylylyl cyclase and spatial regulation by dunce phosphodiesterase. Neuron 65, 516-529.

Gill, G.N., and Garren, L.D. (1971). Role of the receptor in the mechanism of action of adenosine 3 : 5 -cyclic monophosphate. Proceedings of the National Academy of Sciences 68, 786-790.

Glantz, S.B., Li, Y., and Rubin, C.S. (1993). Characterization of distinct tethering and intracellular targeting domains in AKAP75, a protein that links cAMP-dependent protein kinase II beta to the cytoskeleton. J Biol Chem 268, 12796-2804.

Gold, M.G., Lygren, B., Dokurno, P., Hoshi, N., McConnachie, G., Taskén, K., Carlson, C.R., Scott, J.D., and Barford, D. (2006). Molecular basis of AKAP specificity for PKA regulatory subunits. Mol Cell 24, 383-395.

Gold, M.G., Stengel, F., Nygren, P.J., Weisbrod, C.R., Bruce, J.E., Robinson, C.V., Barford, D., and Scott, J.D. (2011). Architecture and dynamics of an A-kinase

anchoring protein 79 (AKAP79) signaling complex. Proceedings of the National Academy of Sciences *108*, 6426-431

Goldsmith, B.A., and Abrams, T.W. (1992). cAMP modulates multiple K+ currents, increasing spike duration and excitability in Aplysia sensory neurons. Proc Natl Acad Sci U S A 89, 11481-85.

Hancock, J.F., Magee, A.I., Childs, J.E., and Marshall, C.J. (1989). All< i> ras proteins are polyisoprenylated but only some are palmitoylated. Cell 57, 1167-177.

Hanoune, J., and Defer, N. (2001). Regulation and role of adenylyl cyclase isoforms. Annual review of pharmacology and toxicology *41*, 145-174.

Harris, K.M., and Stevens, J.K. (1989). Dendritic spines of CA 1 pyramidal cells in the rat hippocampus: serial electron microscopy with reference to their biophysical characteristics. The Journal of neuroscience 9, 2982-997.

Hempel, C.M., Vincent, P., Adams, S.R., Tsien, R.Y., and Selverston, A.I. (1996). Spatio-temporal dynamics of cyclic AMP signals in an intact neural circuit. Nature 384, 166-69.

Herberg, F.W., Taylor, S.S., and Dostmann, W.R. (1996). Active site mutations define the pathway for the cooperative activation of cAMP-dependent protein kinase. Biochemistry 35, 2934-942.

Hidaka, H., and Kobayashi, R. (1992). Pharmacology of protein kinase inhibitors. Annual review of pharmacology and toxicology 32, 377-397.

Howe, D. (2002). Molecular and Behavioral Effects of a Null Mutation in All PKA Cβ Isoforms. Molecular and Cellular Neuroscience 20, 515-524.

Huang, L.J.-S., and Taylor, S.S. (1998). Dissecting cAMP Binding Domain A in the RIα Subunit of cAMP-dependent Protein Kinase DISTINCT SUBSITES FOR RECOGNITION OF cAMP AND THE CATALYTIC SUBUNIT. Journal of Biological Chemistry 273, 26739-746.

Iyer, G.H., Moore, M.J., and Taylor, S.S. (2005). Consequences of lysine 72 mutation on the phosphorylation and activation state of cAMP-dependent kinase. J Biol Chem *280*, 8800-07.

Johnson, D.A., Akamine, P., Radzio-Andzelm, E., Madhusudan, and and Taylor, S.S. (2001). Dynamics of cAMP-dependent protein kinase. Chemical Reviews 101, 2243-270.

Joiner, M.L., Lisé, M.F., Yuen, E.Y., Kam, A.Y., Zhang, M., Hall, D.D., Malik, Z.A., Qian, H., Chen, Y., et al. (2010). Assembly of a beta2-adrenergic receptor--GluR1 signalling complex for localized cAMP signalling. EMBO J 29, 482-495.

Kasai, H., and Petersen, O.H. (1994). Spatial dynamics of second messengers: IP3 and cAMP as long-range and associative messengers. Trends Neurosci 17, 95-101.

Kim, C., Xuong, N.H., and Taylor, S.S. (2005). Crystal structure of a complex between the catalytic and regulatory (RIα) subunits of PKA. Science 307, 690.

Kim, M., Park, A.J., Havekes, R., Chay, A., Guercio, L.A., Oliveira, R.F., Abel, T., and Blackwell, K.T. (2011). Colocalization of protein kinase A with adenylylyl cyclase enhances protein kinase A phosphorylation during induction of long-lasting long-term-potentiation. PLoS Comput Biol 7, e1002084.

Kinderman, F.S., Kim, C., von Daake, S., Ma, Y., Pham, B.Q., Spraggon, G., Xuong, N.H., Jennings, P.A., and Taylor, S.S. (2006). A dynamic mechanism for AKAP binding to RII isoforms of cAMP-

dependent protein kinase. Mol Cell 24, 397-408.

Kinderman, F.S., Kim, C., von Daake, S., Ma, Y., Pham, B.Q., Spraggon, G., Xuong, N.H., Jennings, P.A., and Taylor, S.S. (2006). A dynamic mechanism for AKAP binding to RII isoforms of cAMP-dependent protein kinase. Mol Cell 24, 397-408.

Kogure, T., Kawano, H., Abe, Y., and Miyawaki, A. (2008). Fluorescence imaging using a fluorescent protein with a large Stokes shift. Methods 45, 223-26.

Kopperud, R., Christensen, A.E., Kjarland, E., Viste, K., Kleivdal, H., and Døskeland, S.O. (2002). Formation of inactive cAMP-saturated holoenzyme of cAMP-dependent protein kinase under physiological conditions. J Biol Chem 277, 13443-48.

Kuo, J.F., and Greengard, P. (1969). Cyclic nucleotide-dependent protein kinases, IV. Widespread occurrence of adenosine 3 , 5 -monophosphate-dependent protein kinase in various tissues and phyla of the animal kingdom. Proceedings of the National Academy of Sciences 64, 1349-355.

Lakowicz, J.R. (2007). Principles of fluorescence spectroscopy (Springer).

Lancaster, B., Hu, H., Gibb, B., and Storm, J.F. (2006). Kinetics of ion channel modulation by cAMP in rat hippocampal neurones. J Physiol 576, 403-417.

Lohmann, S.M., DeCamilli, P., Einig, I., and Walter, U. (1984). High-affinity binding of the regulatory subunit (RII) of cAMP-dependent protein kinase to microtubule-associated and other cellular proteins. Proc Natl Acad Sci U S A 81, 6723.

Madison, D.V., and Nicoll, R.A. (1986). Cyclic adenosine 3',5'-monophosphate mediates beta-receptor actions of noradrenaline in rat hippocampal pyramidal cells. J Physiol 372, 245-259.

Miyawaki, A. (2011). Development of probes for cellular functions using fluorescent proteins and fluorescence resonance energy transfer. Annu Rev Biochem 80, 357-373.

Mumby, S.M., Heukeroth, R.O., Gordon, J.I., and Gilman, A.G. (1990). G-protein alpha-subunit expression, myristoylation, and membrane association in COS cells. Proceedings of the National Academy of Sciences 87, 728-732.

Murakoshi, H., Lee, S.J., and Yasuda, R. (2008). Highly sensitive and quantitative FRET-FLIM imaging in single dendritic spines using improved non-radiative YFP. Brain Cell Biol 36, 31-42.

Neves, S.R., and Iyengar, R. (2009). Models of spatially restricted biochemical reaction systems. J Biol Chem *284*, 5445-49.

Newlon, M.G., Roy, M., Morikis, D., Carr, D.W., Westphal, R., Scott, J.D., and Jennings, P.A. (2001). A novel mechanism of PKA anchoring revealed by solution structures of anchoring complexes. The EMBO journal 20, 1651-662.

Oliveira, R.F., Kim, M., and Blackwell, K.T. (2012). Subcellular location of PKA controls striatal plasticity: stochastic simulations in spiny dendrites. PLoS Comput Biol 8, e1002383.

Oliveira, R.F., Terrin, A., Di Benedetto, G., Cannon, R.C., Koh, W., Kim, M., Zaccolo, M., and Blackwell, K.T. (2010). The role of type 4 phosphodiesterases in generating microdomains of cAMP: large scale stochastic simulations. PLoS One 5, e11725.

Patterson, G.H., and Lippincott-Schwartz, J. (2002). A photoactivatable GFP for selective photolabeling of proteins and cells. Science 297, 1873-77.

Pedarzani, P., and Storm, J.F. (1993). PKA mediates the effects of monoamine transmitters on the K+ current underlying

the slow spike frequency adaptation in hippocampal neurons. Neuron 11, 1023-035.

Pologruto, T.A., Sabatini, B.L., and Svoboda, K. (2003). ScanImage: flexible software for operating laser scanning microscopes. Biomed. Eng. Online 2, 13.

Posner, J.B., Stern, R., and Krebs, E.G. (1965). Effects of electrical stimulation and epinephrine on muscle phosphorylase, phosphorylase b kinase, and adenosine 3', 5'-phosphate. Journal of Biological Chemistry 240, 982-85.

Reinhart, P.H., Chung, S., Martin, B.L., Brautigan, D.L., and Levitan, I.B. (1991). Modulation of calcium-activated potassium channels from rat brain by protein kinase A and phosphatase 2A. The Journal of neuroscience 11, 1627-635.

Rich, T.C., Fagan, K.A., Nakata, H., Schaack, J., Cooper, D.M., and Karpen, J.W. (2000). Cyclic nucleotide-gated channels colocalize with adenylylyl cyclase in regions of restricted cAMP diffusion. J Gen Physiol 116, 147-161.

Rich, T.C., Fagan, K.A., Tse, T.E., Schaack, J., Cooper, D.M., and Karpen, J.W. (2001). A uniform extracellular stimulus triggers distinct cAMP signals in different compartments of a simple cell. Proc Natl Acad Sci U S A 98, 13049-054.

Rich, T.C., Webb, K.J., and Leavesley, S.J. (2014). Can we decipher the information content contained within cyclic nucleotide signals? J Gen Physiol 143, 17-27.

Rizzo M. A., Springer G. H., Granada B., & Piston D. W. (2004). Nat Biotechnol. In An improved cyan fluorescent protein variant useful for FRET.. United States: [UNKNOWN REFERENCE TYPE]

Rosenmund, C., Carr, D.W., Bergeson, S.E., Nilaver, G., Scott, J.D., and Westbrook, G.L. (1994). Anchoring of protein kinase A is required for modulation of AMPA/kainate receptors on hippocampal neurons. Nature 368, 853-56.

Sabatini, B.L., Oertner, T.G., and Svoboda, K. (2002). The life cycle of Ca(2+) ions in dendritic spines. Neuron 33, 439-452.

Sastri, M., Barraclough, D.M., Carmichael, P.T., and Taylor, S.S. (2005). A-kinase-interacting protein localizes protein kinase A in the nucleus. Proc Natl Acad Sci U S A 102, 349-354.

Saucerman, J.J., Zhang, J., Martin, J.C., Peng, L.X., Stenbit, A.E., Tsien, R.Y., and McCulloch, A.D. (2006). Systems analysis of PKA-mediated phosphorylation gradients in live cardiac myocytes. Proceedings of the National Academy of Sciences 103, 12923-28.

Shaner, N.C., Lin, M.Z., McKeown, M.R., Steinbach, P.A., Hazelwood, K.L., Davidson, M.W., and Tsien, R.Y. (2008). Improving the photostability of bright monomeric orange and red fluorescent proteins. Nat Methods 5, 545-551.

Shaner, N.C., Steinbach, P.A., and Tsien, R.Y. (2005). A guide to choosing fluorescent proteins. Nat Methods 2, 905-09.

Ska lhegg, B.S., Huang, Y., Su, T., Idzerda, R.L., McKnight, G.S., and Burton, K.A. (2002). Mutation of the Cα subunit of PKA leads to growth retardation and sperm dysfunction. Molecular Endocrinology 16, 630-39.

Smith, F.D., Reichow, S.L., Esseltine, J.L., Shi, D., Langeberg, L.K., Scott, J.D., and Gonen, T. (2013). Intrinsic disorder within an AKAP-protein kinase A complex guides local substrate phosphorylation. Elife 2

Soderling, T.R., Hickenbottom, J.P., Reimann, E.M., Hunkeler, F.L., Walsh, D.A., and Krebs, E.G. (1970). Inactivation of glycogen synthetase and activation of phosphorylase kinase by muscle adenosine 3', 5'-monophosphate-dependent protein

kinases. Journal of Biological Chemistry 245, 6317-328.

Steinberg, R.A., Cauthron, R.D., Symcox, M.M., and Shuntoh, H. (1993). Autoactivation of catalytic (C alpha) subunit of cyclic AMP-dependent protein kinase by phosphorylation of threonine 197. Mol Cell Biol 13, 2332-341.

Struppe, J., Komives, E.A., Taylor, S.S., and Vold, R.R. (1998). 2H NMR studies of a myristoylated peptide in neutral and acidic phospholipid bicelles. Biochemistry 37, 15523-27.

Svoboda, K., Tank, D.W., and Denk, W. (1996). Direct measurement of coupling between dendritic spines and shafts. Science 272, 716-19.

Taylor, S.S., Kim, C., Vigil, D., Haste, N.M., Yang, J., Wu, J., and Anand, G.S. (2005). Dynamics of signaling by PKA. Biochim Biophys Acta 1754, 25-37.

Taylor, S.S., Zhang, P., Steichen, J.M., Keshwani, M.M., and Kornev, A.P. (2013). PKA: Lessons learned after twenty years. Biochimica et Biophysica Acta (BBA)-Proteins and Proteomics 1834, 1271-78.

Tewson, P., Westenberg, M., Zhao, Y., Campbell, R.E., Quinn, A.M., and Hughes, T.E. (2012). Simultaneous detection of Ca2+ and diacylglycerol signaling in living cells. PLoS One 7, e42791.

Tillo, S.E., Hughes, T.E., Makarov, N.S., Rebane, A., and Drobizhev, M. (2010). A new approach to dual-color two-photon microscopy with fluorescent proteins. BMC Biotechnol 10, 6.

Towler, D.A., Gordon, J.I., Adams, S.P., and Glaser, L. (1988). The biology and enzymology of eukaryotic protein acylation. Annu Rev Biochem 57, 69-97.

Trotter, K.W., Fraser, I.D., Scott, G.K., Stutts, M.J., Scott, J.D., and Milgram, S.L. (1999). Alternative splicing regulates the subcellular localization of A-kinase anchoring protein 18 isoforms. The Journal of cell biology 147, 1481-492.

Tzingounis, A.V., Kobayashi, M., Takamatsu, K., and Nicoll, R.A. (2007). Hippocalcin gates the calcium activation of the slow afterhyperpolarization in hippocampal pyramidal cells. Neuron 53, 487-493.

Uhler, M.D., Chrivia, J.C., and McKnight, G.S. (1986). Evidence for a second isoform of the catalytic subunit of cAMP-dependent protein kinase. Journal of Biological Chemistry 261, 15360-63.

Vaandrager, A.B., Ehlert, E.M., Jarchau, T., Lohmann, S.M., and de Jonge, H.R. (1996). N-terminal myristoylation is required for membrane localization of cGMP-dependent protein kinase type II. J Biol Chem 271, 7025-29.

Vaandrager, A.B., Smolenski, A., Tilly, B.C., Houtsmuller, A.B., Ehlert, E.M., Bot, A.G., Edixhoven, M., Boomaars, W.E., Lohmann, S.M., and de Jonge, H.R. (1998). Membrane targeting of cGMP-dependent protein kinase is required for cystic fibrosis transmembrane conductance regulator Cl-channel activation. Proc Natl Acad Sci U S A 95, 1466-471.

Valentin, G., Verheggen, C., Piolot, T., Neel, H., Coppey-Moisan, M., and Bertrand, E. (2005). Photoconversion of YFP into a CFP-like species during acceptor photobleaching FRET experiments. Nat Methods 2, 801-1.

Ventra, C., Porcellini, A., Feliciello, A., Gallo, A., Paolillo, M., Mele, E., Avvedimento, V.E., and Schettini, G. (1996). The differential response of protein kinase A to cyclic AMP in discrete brain areas correlates with the abundance of regulatory subunit II. J Neurochem 66, 1752-761.

Vigil, D., Blumenthal, D.K., Taylor, S.S., and Trewhella, J. (2006). Solution scattering reveals large differences in the global structures of type II protein kinase A isoforms. J Mol Biol *357*, 880-89.

Vigil, D., Lin, J.H., Sotriffer, C.A., Pennypacker, J.K., McCammon, J.A., and Taylor, S.S. (2006). A simple electrostatic switch important in the activation of type I protein kinase A by cyclic AMP. Protein Sci 15, 113-121.

Walsh, D.A., Perkins, J.P., and Krebs, E.G. (1968). An adenosine 3',5'-monophosphate-dependant protein kinase from rabbit skeletal muscle. J Biol Chem 243, 3763-65.

Wilson, C.J., Groves, P.M., Kitai, S.T., and Linder, J.C. (1983). Three-dimensional structure of dendritic spines in the rat neostriatum. The Journal of Neuroscience 3, 383-88.

Wong, W., and Scott, J.D. (2004). AKAP signalling complexes: focal points in space and time. Nat Rev Mol Cell Biol 5, 959-970.

Yang, J., Ten Eyck, L.F., Xuong, N.H., and Taylor, S.S. (2004). Crystal structure of a cAMP-dependent protein kinase mutant at 1.26 Å: New insights into the catalytic mechanism. J Mol Biol 336, 473-487.

Yasuda, R., Harvey, C.D., Zhong, H., Sobczyk, A., van Aelst, L., and Svoboda, K. (2006). Supersensitive Ras activation in dendrites and spines revealed by two-photon fluorescence lifetime imaging. Nat Neurosci 9, 283-291.

Yonemoto, W., McGlone, M.L., and Taylor, S.S. (1993). N-myristylation of the catalytic subunit of cAMP-dependent protein kinase conveys structural stability. J Biol Chem 268, 2348-352.

Zaccolo, M., De Giorgi, F., Cho, C.Y., Feng, L., Knapp, T., Negulescu, P.A., Taylor, S.S., Tsien, R.Y., and Pozzan, T. (1999). A genetically encoded, fluorescent indicator for cyclic AMP in living cells. Nature Cell Biology 2, 25-29.

Zaccolo, M., Di Benedetto, G., Lissandron, V., Mancuso, L., Terrin, A., and Zamparo, I. (2006). Restricted diffusion of a freely diffusible second messenger: mechanisms underlying compartmentalized cAMP signalling. Biochem Soc Trans 34, 495-97.

Zacharias, D.A., Violin, J.D., Newton, A.C., and Tsien, R.Y. (2002). Partitioning of lipid-modified monomeric GFPs into membrane microdomains of live cells. Science 296, 913-16.

Zhang, J., Hupfeld, C.J., Taylor, S.S., Olefsky, J.M., and Tsien, R.Y. (2005). Insulin disrupts beta-adrenergic signalling to protein kinase A in adipocytes. Nature 437, 569-573.

Zhang, J., Ma, Y., Taylor, S.S., and Tsien, R.Y. (2001). Genetically encoded reporters of protein kinase A phosphorylation reveal impact of substrate tethering. Proc Natl Acad Sci U S A 98, 14997-15002.

Zhang, P., Smith-Nguyen, E.V., Keshwani, M.M., Deal, M.S., Kornev, A.P., and Taylor, S.S. (2012). Structure and allostery of the PKA RIIβ tetrameric holoenzyme. Science 335, 712-16.

Zhao, Y., Araki, S., Wu, J., Teramoto, T., Chang, Y.F., Nakano, M., Abdelfattah, A.S., Fujiwara, M., Ishihara, T., et al. (2011). An expanded palette of genetically encoded Ca^{2+} indicators. Science 333, 1888-891.

Zheng, J., Knighton, D.R., Xuong, N.H., Taylor, S.S., Sowadski, J.M., and Ten Eyck, L.F. (1993). Crystal structures of the myristylated catalytic subunit of cAMP-dependent protein kinase reveal open and closed conformations. Protein Sci 2, 1559-573.

Zhong, H., Lai, J., and Yau, K.-W. (2003). Selective heteromeric assembly of cyclic

nucleotide-gated channels. Proceedings of the National Academy of Sciences 100, 5509-513.

Zhong, H., Sia, G.M., Sato, T.R., Gray, N.W., Mao, T., Khuchua, Z., Huganir, R.L., and Svoboda, K. (2009). Subcellular dynamics of type II PKA in neurons. Neuron 62, 363-374.

Zhou, J., and Adams, J.A. (1997). Participation of ADP dissociation in the rate-determining step in cAMP-dependent protein kinase. Biochemistry 36, 15733-38.